SECURITY MARKING

The classified or limited status of this report applies to each page, unless otherwise marked.
Separate page printouts MUST be marked accordingly.

THIS DOCUMENT CONTAINS INFORMATION AFFECTING THE NATIONAL DEFENSE OF THE UNITED STATES WITHIN THE MEANING OF THE ESPIONAGE LAWS, TITLE 18, U.S.C., SECTIONS 793 AND 794. THE TRANSMISSION OR THE REVELATION OF ITS CONTENTS IN ANY MANNER TO AN UNAUTHORIZED PERSON IS PROHIBITED BY LAW.

NOTICE: When government or other drawings, specifications or other data are used for any purpose other than in connection with a definitely related government procurement operation, the U. S. Government thereby incurs no responsibility, nor any obligation whatsoever; and the fact that the Government may have formulated, furnished, or in any way supplied the said drawings, specifications, or other data is not to be regarded by implication or otherwise as in any manner licensing the holder or any other person or corporation, or conveying any rights or permission to manufacture, use or sell any patented invention that may in any way be related thereto.

DASA 1652

IITRI

SYNTHESIS OF ROCK HUGONIOTS

by

R. S. Dennen

IIT Research Institute

DASA 1652

SYNTHESIS OF ROCK HUGONIOTS

Prepared for:

DEFENSE ATOMIC SUPPORT AGENCY
WASHINGTON, D.C. 20301

Sponsored by: Advanced Research Projects Agency

By: R. S. Dennen
IIT Research Institute

IITRI Project No. T6056

Contract Number:	DA49-146-XZ-237
Contract Expiration Date:	30 April 1965
ARPA Order Number:	172
Project Code Number:	8100
Amount of Contract:	$105,874.00
Project Scientist:	R. S. Dennen
Phone Number:	225-9630 (Area Code 312), Ext. 2224

FOREWORD

This final report on IITRI Project T6056 "Determination of Hugoniots of Rocks from the Hugoniots of Their Mineral Constituents" describes studies conducted for the Defense Atomic Support Agency under Contract DA-49-146-XZ-237. This work was accomplished during the period 30 June 1963 through 31 March 1965.

The IITRI Project team comprised D. Baker, R. Blumenthal, J. Daley, C. Christenson, R. Dennen (Project Engineer), J. Gershon, S. Pernic, and M. Terra.

Special acknowledgments are due Dr. E. Olsen, Curator for Minerals at the Museum of Natural History, Chicago, Ill., for several helpful discussions and for providing several mineral samples used in the experiments; to Drs. Chabai and Bass of the Sandia Corporation; and to Dr. G. R. Fowles of the Stanford Research Institute for helpful discussions.

The very helpful technical and administrative aid and understanding of Major B. M. Carswell is especially acknowledged. Major Carswell was the technical monitor during the major part of this program.

Respectfully submitted,

IIT RESEARCH INSTITUTE

Robert S. Dennen

Robert S. Dennen
Research Engineer and
Group Leader
Explosion Mechanics and
Rheology

Approved:

T. H. Schiffman, Assistant Director
Geophysics Research

ABSTRACT

Methods of obtaining the Hugoniot equation of state were investigated. Several of these, employing high explosive devices, were used to obtain Hugoniot data for mineral samples common to many igneous rocks. Hugoniot data were found for orthoclase, oligoclase, labradorite and olivine in the pressure range from 50 to 300 kilobars. Analytical synthesis models were constructed and used to determine the synthesized Hugoniot equations of state for granodiorite, gabbro and dunite. These compared favorably with existing Hugoniot data for similar materials. Methods were also developed and used to predict, roughly, Hugoniot curves for other geological composites for which no experimental data are presently available. These materials included syenite, quartzdiorite, diorite, olivine diabase, and diabase. Estimates of temperatures along the Hugoniots and along several selected unloading adiabats were calculated for several minerals and igneous rocks.

CONTENTS

FIGURES

FIGURES (Cont.)

FIGURES (Cont.)

TABLES

TABLES (Cont.)

I INTRODUCTION

In many applications, knowledge of the dynamic equation of state, or Hugoniot, of a material is required. Various laboratory and field experiments have been devised to determine the Hugoniot of a particular material. These experiments are, in general, costly and time-consuming, while the range of materials of interest is, in some cases, extensive. This is especially true where geological materials are involved. These exist in nature in almost endless variety depending only on the relative abundance of the constituents of the material. Although many geological materials, which have been and will be of interest, differ only slightly in mineral content, it has been customary to investigate each composite separately. Thus, previous Hugoniot information on similar materials has been utilized, at best, only in a qualitative way.

One aim of this program was to determine the feasibility of utilizing known constituent Hugoniot data to determine analytically the Hugoniots of composites made up largely of these constituents. Consideration was given to one class of geological materials, the igneous rocks. The Hugoniots of several igneous rocks have been previously determined. In addition, a few of the mineral constituents common to several rocks have been investigated.

Before this synthesis method could be studied, it was necessary to obtain Hugoniot information for several additional

minerals. Orthoclase, Labradorite, Oligoclase, Clivine and Biotite were investigated in this program. This choice was based on the abundance of these minerals in many igneous rocks and on their structural similarity to other minerals occurring in rocks for which Hugoniot information is presently known or anticipated.

Many factors other than the mineral content of an igneous rock might influence its Hugoniot. These include grain size and orientation of the constituent minerals, water content, and porosity. The way in which each of these factors affects the response of the composite to dynamic loading would form the basis of an ultimate synthesis theory. The application of such a theory would greatly reduce the effort involved in composite Hugoniot determination. In application, it would be necessary only to measure the necessary factors and apply the analytical expression relating them to the Hugoniot of the composite.

In this investigation, the synthesized Hugoniots were based on the measured or assumed mineral content only. Although, for the mineral data used in the synthesis, Hugoniot data were available for several crystal orientations, only an average Hugoniot was used for each mineral. Even with this simplified model the results are very promising. Unfortunately, for several of the composites for which Hugoniot measurements have been made, little is known about the mineral content. Future experiments will have to be performed on composites of carefully controlled or measured structure and petrography.

Within the framework of the simplified synthesis model, two methods were used to calculate composite Hugoniots. The first was direct application of the Hugoniots of the known constituent minerals to determine the Hugoniot of the composite. In the second, "indirect," method both known mineral data and known composite data were used to increase the number of "known" minerals. These minerals were then used to expand composite calculations to those containing relatively large amounts of minerals for which experimental Hugoniots are not yet available. Composites for which these "implied" Hugoniots were calculated are syenite, quartzdiorite, diorite, olivinediabase, and diabase. These Hugoniot data are considered to be of more value for illustrative purposes than for use in calculations requiring exact Hugoniots for these materials. This indirect synthesis illustrates a method by which a maximum number of Hugoniots can be calculated from a minimum number of experimentally determined Hugoniots.

An attempt was made to use only single crystals of minerals in the Hugoniot determinations. This was not possible for olivine. Although the igneous rocks are made up of polycrystals of the minerals, these are not always in random orientation and it seems desirable to have single crystal data for several orientations. Such data can then be averaged, as was done here, or used in a more complete theory where crystal orientation is considered to be a factor.

Many of the minerals obtained in single crystal form were found to have relatively large variations in density. Because

of this variation, it was decided to perform the shock experiments on only a small number of single crystals of each type, making up all required samples from these few. This procedure often imposed the condition of carrying out the experiments on very small samples. It was necessary to examine some of the experimental techniques previously used and some variations of these techniques to determine the feasibility of each for the intended application. This examination formed one of the three major phases of this investigation.

The other two phases were devoted to the experimental determination of the mineral Hugoniots and the synthesis of composite Hugoniots from these results. Discussions of the results and methods used in each of these phases constitute the major sections of this report. The final section summarizes the major results of the study and briefly outlines the future requirements and outlook for Hugoniot synthesis.

II METHODS OF HUGONIOT DETERMINATION

A. Hugoniot Description

1. Shock Wave Equations

The dynamic loading process gives rise to the dynamic equation of state, or Hugoniot, of a material. In dynamic loading, different regions of the material are at different stress levels and have correspondingly different values of density and temperature. For this reason, although local thermodynamic equilibrium is supposed to exist, the whole sample is not in equilibrium. Each region of local equilibrium and, therefore, uniform temperature, pressure, and density corresponds closely, in the absence of shear forces, to a state in hydrostatic compression. As a result, not only does the Hugoniot give basic information regarding the shock loading process but, in addition, relates to the fundamental properties of materials.

In Figure 1, the shock-loading process is compared with a similar static loading process; both represent cases of uniaxial strain, i.e., strain occurring only in the axial, 1, or loading direction, all other strains being equal to zero. As is seen in the static case, Figure 1(a), the whole sample is in a state of equilibrium. The stressed element shown in the insert is the same throughout the sample. In the dynamic case, Figure 1(b), the loading device causes a shock wave to be transmitted. In this case the sample is separated into two different equilibrium regions. The region to the right of the shock wave discontinuity has not yet been compressed. The Hugoniot relates the values of stress σ_{11} to strain ε or specific volume V in the shocked

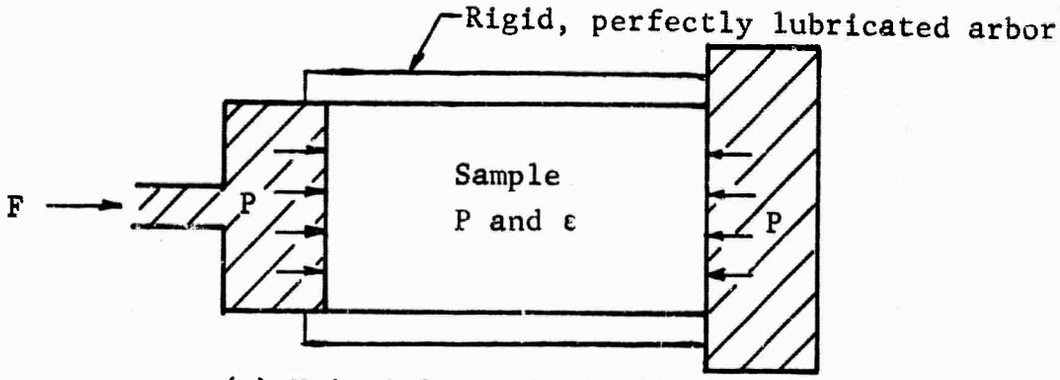

(a) Uniaxial static loading

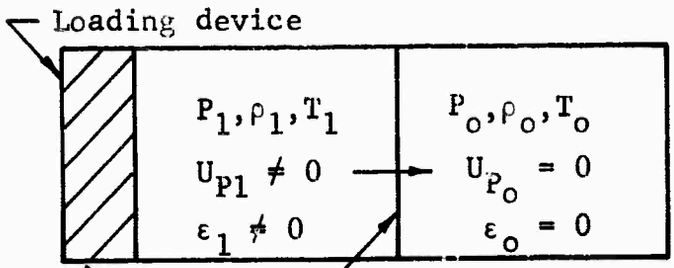

(b) Uniaxial shock loading

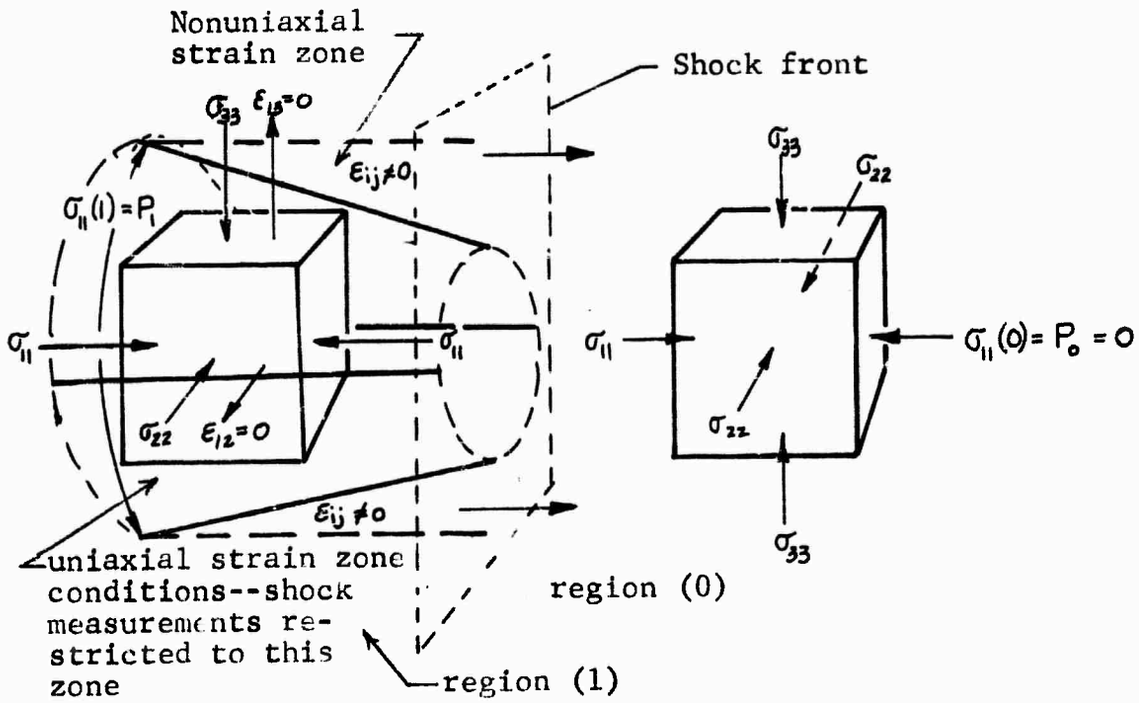

(c) Stress-strain elements in shock compression zones

Figure 1 Comparison of Static and Dynamic Loading Conditions

state to those in the initial state. It refers only to these end states and gives no information on the loading path between these end states. If the stress, σ_{11}, and temperature, T, behind the shock wave corresponded to those of the hypothetical static configuration, the elements of stress and strain in both would be equal.

For some materials for which a thermodynamic equation of state is available, e.g., a perfect gas, the Hugoniot may be derived. For solids, there is no general equation of state that may be used in such a derivation and the Hugoniot is usually not represented in an analytical form. There are, however, general shock wave equations which apply to all materials. These equations include only the stress, σ_{11}, in the shock propagation direction and the uniaxial strain in that direction. The stress in this direction is referred to as the pressure. For very high stresses, which might cause the solid to liquify, the diagonal stress elements are equal to the pressure.

Regardless of the stress level, the correct interpretation is that the pressure P is considered equal to the diagonal stress tensor element in the direction of the one dimensional strain. In the experiments described, the configuration is such that all measurements are made in the one dimensional region (Figure 1(c)).

Conservation of mass and momentum across the shock wave require that

$$\rho_o U_s = \rho_1 (U_s - U_{P1}) \qquad \text{(Conservation of mass)} \qquad (1)$$

$$P_o + \rho_o U_s^2 = P_1 + \rho_1 (U_s - U_{P1})^2 \qquad \text{(Conservation of momentum)} \qquad (2)$$

where

U_s = the shock velocity

U_{P1} = the particle velocity behind the shock wave

P_o = initial pressure

ρ_o = initial density.

The pressure behind the shock wave,

$$P_1 = \rho_o U_s U_{P1} + P_o \, . \tag{3}$$

In most cases of interest here, the shock compression is of the order of at least several thousand atmospheres so that the ambient pressure or initial pressure of about one atmosphere can be neglected. Then,

$$P_1 = \rho_o U_s U_{P1} \tag{4}$$

From the definition of strain,

$$\varepsilon = \frac{V_o - V}{V_o} = \frac{\rho - \rho_o}{\rho} = 1 - \frac{\rho_o}{\rho}$$

where V is the specific volume, and equation (1),

$$\varepsilon_1 = 1 - \frac{\rho_o}{\rho_1} = \frac{U_{P1}}{U_s} \tag{5}$$

so that the dynamic stress and strain, P_1 and ε_1, can be determined from U_s and U_p, the variables usually directly or indirectly measured in shock wave experiments. From equations (4) and (5), these velocities can be related to the dynamic material properties occurring behind a single shock wave:

$$U_s = \sqrt{\frac{P_1}{\rho_o \varepsilon_1}} \, , \tag{6}$$

$$U_P = \sqrt{\frac{P_1 \varepsilon_1}{\rho_o}} \quad . \tag{7}$$

Thus, by measuring any two of the four variables occurring in equations (1) and (3), the other two may be uniquely determined. The Hugoniot generally refers to any representation of two of these variables, though most often it refers to the pressure-density states.

Up to this point, as shown in Figure 1(b), only a single shock wave was considered. For various combinations of material properties and shock-loading pressures, two or more shock waves may result (Ref. 1). In such cases, an element of material is successively loaded by several shock waves. To determine the final state after the last loading shock wave the equations of mass and momentum may also be successively applied. Equations analogous to (4) and (5) but for N waves are

$$P_N = P_{N-1} + \frac{\rho_o (U_{SN} - U_{P,N-1})(U_{PN} - U_{P,N-1})}{1 - \varepsilon_{N-1}} \tag{8}$$

$$1 - \varepsilon_N = \prod_{i=1}^{i=N} \frac{(U_{Si} - U_{Pi})}{(U_{Si} - U_{P,i-1})} \quad . \tag{9}$$

To calculate the stress P_N and strain ε_N, it is necessary to measure the shock velocities of, and particle velocities behind, these N waves. Such instrumentation techniques become quite involved and analysis becomes especially difficult where N is large and samples are too short to obtain the necessary readings prior to the occurrence of shock reflections.

Both dynamic yield points and material phase changes occurring below the shock-loaded high pressure state may cause multiple shock systems. In these experiments on single crystals, it was anticipated that both might be experienced and, therefore, consideration was given to instrumentation systems capable of yielding the required information.

It is often necessary to deal with only two waves, a precursor having the velocity of a longitudinal acoustic wave (Ref. 1), and a plastic wave U_{S2} whose velocity is dependent on the pressure P_2. In this case, equations (8) and (9) become

$$P_2 = P_1 + \frac{P_o(U_{S2} - U_{P1})(U_{P2} - U_{P1})}{1 - U_{P1}/C} \tag{10}$$

$$\varepsilon_2 = 1 - \frac{(C - U_{P1})(U_{S2} - U_{P2})}{C(U_{S2} - U_{P1})} \tag{11}$$

where U_{S1} the shock velocity is taken as C the acoustic velocity and P_1 is the dynamic yield pressure.

The Hugoniot for a material which would be expected to yield a two-wave system is shown in Figure 2(a). For such a material shocked to a pressure P_2, the resulting pressure pulse is shown in Figure 2(b) and the regions of various instantaneous pressures in Figure 2(c).

As in a one-wave system, the wave and particle velocities are found from equations (10) and (11) to be functions of the slope and area under the P-ε Hugoniot curve. Equations analogous to (5) and (6) for a two-wave system are:

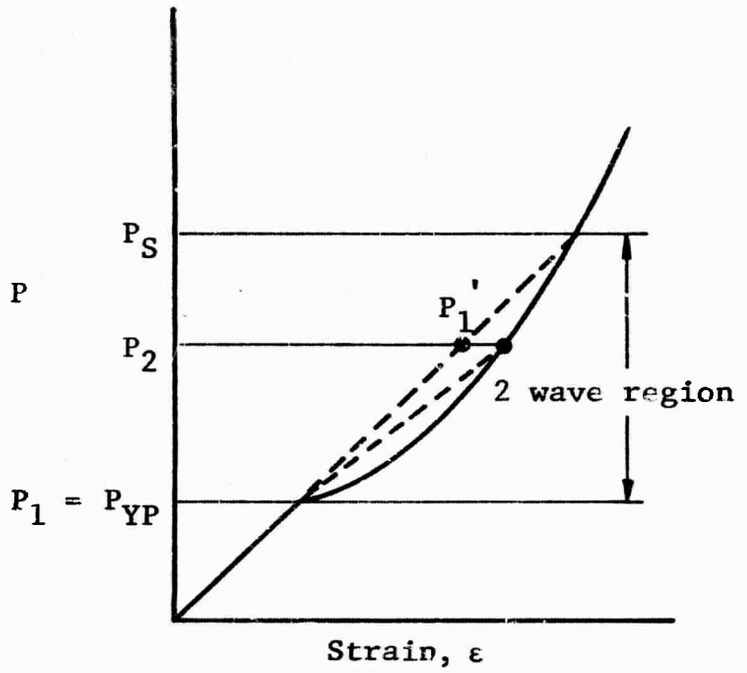

(a) Stress-strain curve

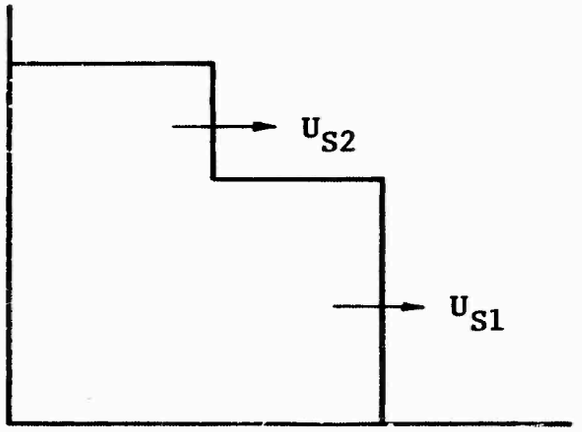

(b) Pressure pulse

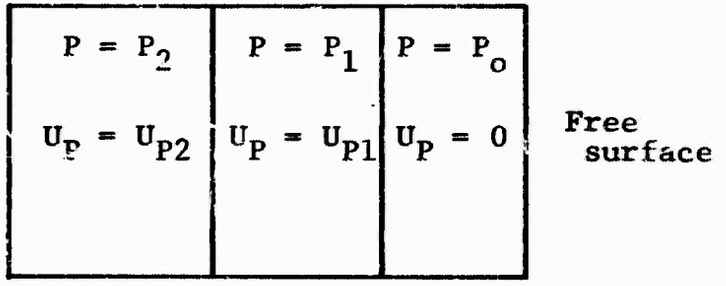

(c) Sample

Figure 2 Sample with Yield Point in Stress-Strain Curve (a) Shown Transmitting Two Shock Waves of Velocities U_{S1} and U_{S2} (b) Yielding Three Pressure Regions in Sample (c)

$$U_{S2} = \sqrt{\frac{P_2 - P_1}{\rho_o(\varepsilon_2 - \varepsilon_1)}}\,(1 - \varepsilon_1) + \left(U_{P1} = \sqrt{\frac{P_1\varepsilon_1}{\rho_o}}\right);$$

where U_{P1} is the particle velocity behind the first or precursor wave. The precursor wave transmitting the pressure, $P_1 = P_{YP}$, travels at a higher velocity than U_{S2}. As the second wave arrives at a point in the material, the pressure at that point is raised from P_1 to P_2. The final particle velocity behind U_{S2} is greater than U_{P1}.

$$U_{P2} - U_{P1} = \sqrt{\frac{(P_2 - P_1)(\varepsilon_2 - \varepsilon_1)}{\rho_o}}$$

It may be seen that the velocity of the second wave U_{S2} is equal to the precursor for $P_2 \geq P_S$ and $P_2 \leq P_{YP}$. Therefore, for this material, only shock pressures between P_{YP} and P_S give rise to two-wave systems.

For such a two-wave system, it would be necessary to measure the shock velocities of both waves C and U_{S2} and the particle velocities U_{P1} and U_{P2} behind each wave. From this information, two Hugoniot states are determined;

$$(P_1, \varepsilon_1) \text{ and } (P_2, \varepsilon_2)$$

where $P_1 = \rho_o C U_{P1}$ is the dynamic yield pressure and $\varepsilon_1 = U_{P1}/C$ is the strain at the yield point. P_2 and ε_2 refer to the high pressure state behind the second wave. For such a material the complete Hugoniot would be found from several shock experiments at different final pressures P_2. In each experiment the values of P_1 and ε_1 would be expected to be the same. Recently it has

been pointed out, however, that stress relaxation effects can cause an initially higher apparent yield point P_1' (Ref. 2), decaying gradually to the dynamic yield pressure P_1. When these effects are present, the measured value of the precursor wave velocity could depend on the sample length. Furthermore, studies of the equation of state of snow (Ref. 3) indicate that the value of the dynamic yield point is not independent of the value of the final pressure, but increases with P_2. Both the determination of constituents' Hugoniots and the derivation of an ultimate synthesis model would be complicated by these features, if significant.

2. Analytical Form of Hugoniot

A Hugoniot with a single discontinuity at P_1 is adequate to describe many materials. For a large number of materials, the Hugoniot is adequately represented by a simpler curve in (P,ε) coordinates, one in which P_1 is sufficiently small that it may be neglected. The Hugoniot then has the appearance of that in Figure 3(a). These materials may always be loaded by a single shock wave (Ref. 1). For a large number of materials, the experimentally determined variables of particle velocity and shock velocity associated with this single wave are linearly related (Ref. 4), as Figure 3(b) shows. The complete Hugoniot is then described by only two states, and the shape of the Hugoniot in the (P,ε) plane is fixed by the slope and intercept of the (U_S,U_P) curve. The resulting Hugoniot equation is

$$P = \frac{\rho_o C^2 \varepsilon}{(1 - S\varepsilon)^2} \quad . \tag{12}$$

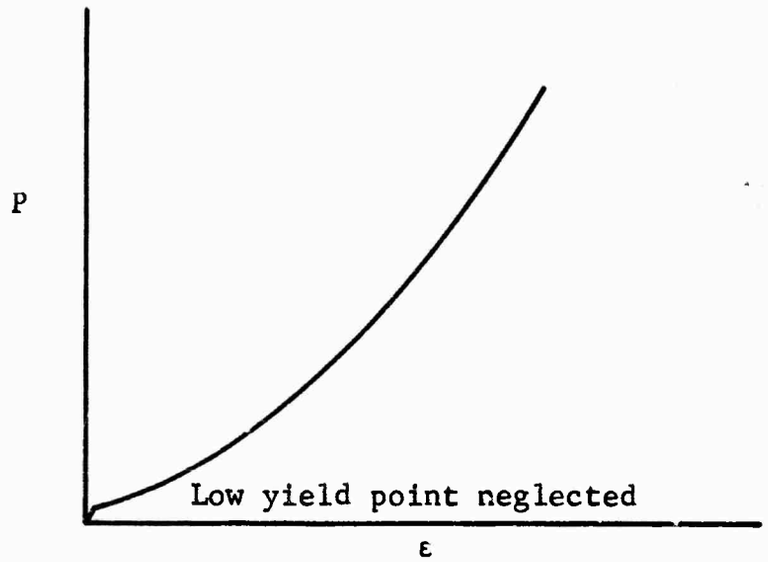

(a) Material with negligible yield pressure

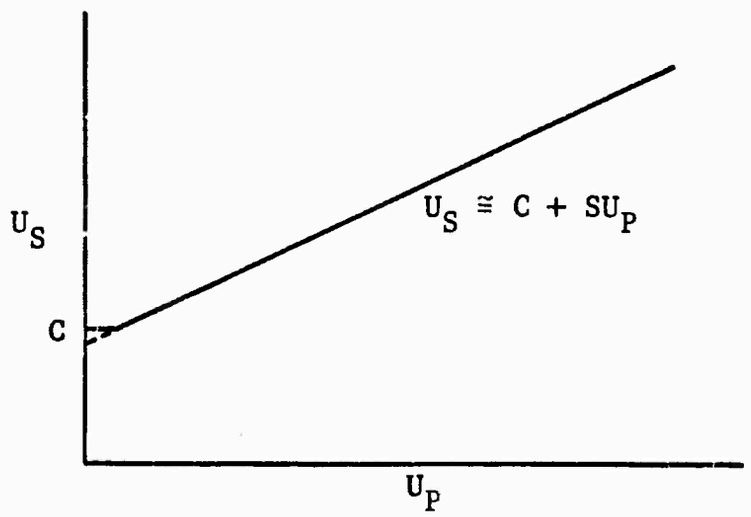

(b) Linear (U_S, U_P) plot

Figure 3 Material Characterized by a Single Shock Wave (a) and Represented by a Linear Velocity Relationship (b)

The value of the intercept C may be approximated by the bulk sound speed, yielding

$$P = \frac{\varepsilon}{\beta_o(1 - S\varepsilon)^2} \tag{13}$$

where $C = \sqrt{\frac{1}{\beta_o \rho_o}}$.

If the bulk compressibility β_o is known, as it often is, and if the linear relationship between U_S and U_P pertains, it is necessary only to determine the value of S to obtain a useful description of the (P,ε) states occurring in shock compression.

There is at present, however, no theoretical justification for the linear (U_S,U_P) relationship, even for those metals in which it has been found to exist. Therefore, presently, S may be found only experimentally. For many metals, however, the S-values lie within fairly narrow limits. Using the data of reference 4 an average value of slope of about 1.42 is within 15 per cent of the experimentally determined value of S for over 80 per cent of the metals satisfied by the linear (U_S,U_P) relationship. These relatively narrow limits suggest that appropriate values of S might be found for other classes of materials. Furthermore, even for materials not representable by a single straight line on the (U_S,U_P) curve, there are indications that a series of straight lines would be applicable (Ref. 5,6).

Several minerals are believed to be in this category, i.e., requiring only two lines, one below the yield point ($S = 0$), and one above the yield point ($S > 0$). At present, however, there is insufficient mineral data to determine the value or existence of a suitable average S.

Equation (13) suggests that, to a rough approximation, the Hugoniots for which an average S exists depend significantly only on the compressibility. Since, in the present synthesis method, the (P,ε) or (P,V) states of the constituents are required, it was desired to further investigate the significance of β_o in describing the known metal Hugoniots.

Rather than applying equation (13) directly with a particular value of S, another empirical procedure was adopted. The metal Hugoniot data of reference 4 were replotted against the zero pressure compressibility as listed in references 7 and 8 for several values of the strain for metals described by the linear (U_S,U_P) relationships. These curves, shown in Figure 4, were used to generate semiempirical Hugoniot data by picking the appropriate value of the compressibility for a metal and simply reading the pressures for each of the isostrain curves of Figure 4. These are compared with the (P,ε) states for several metals investigated in reference 4 in Figure 5.

Since we are, in reality, only comparing the derived (P,V) states with the original data from which they were derived, the fairly good agreement is not startling. What is more interesting is the importance of β_o as a single parameter describing the (P,V) states for this class of materials. The scatter in the Figure 4 data indicates that a single slope S is not exact in describing all of these metals.

Other Materials

Unsuccessful attempts were made to use the curves of Figure 4 to generate Hugoniot data for several geological materials. Because many geological composites have bilinear (U_S,U_P) relationships

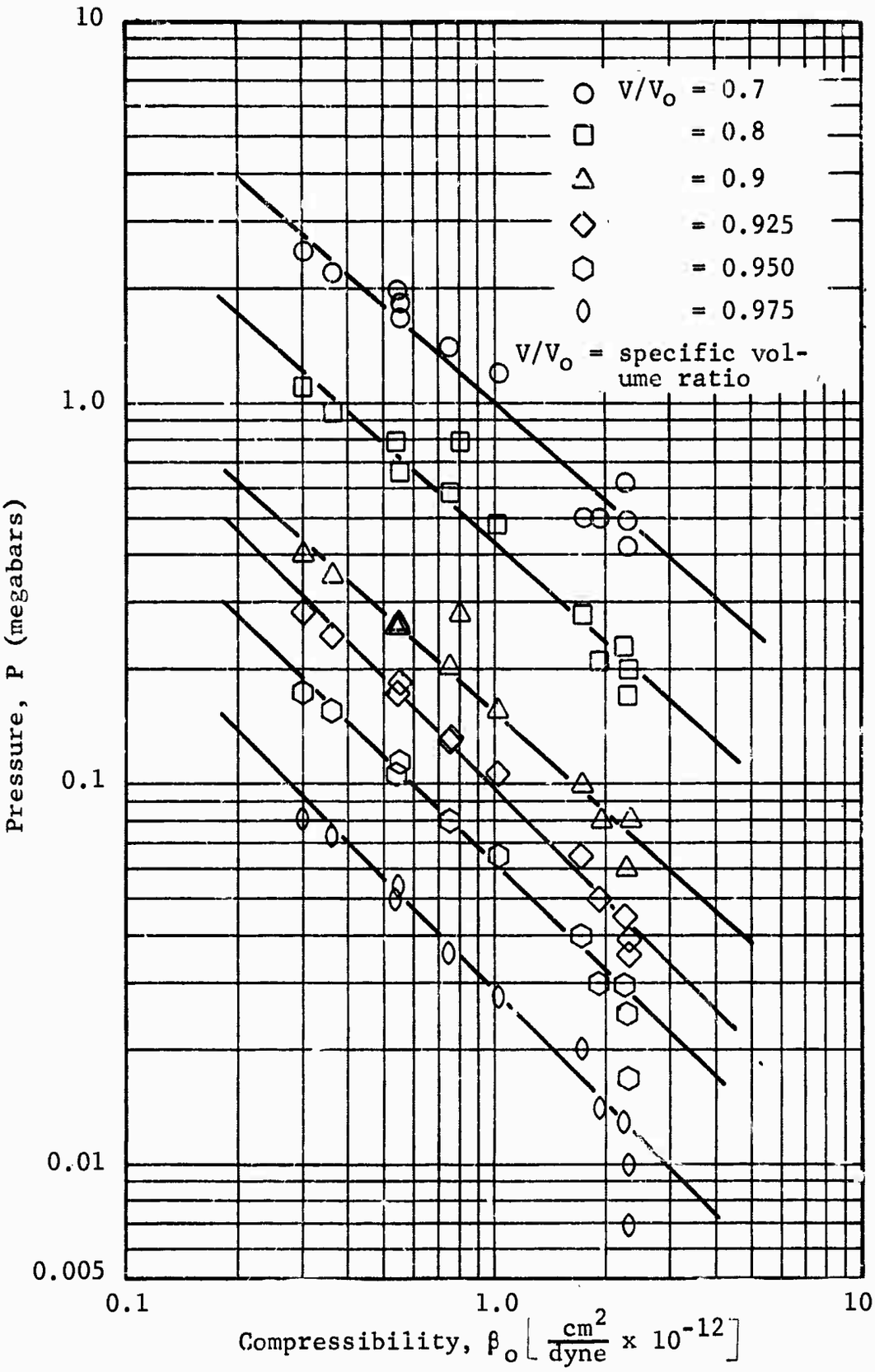

Figure 4 Pressure As a Function of Low Pressure Compressibility for Various Shock-Compressed Metals (Ref. 4)

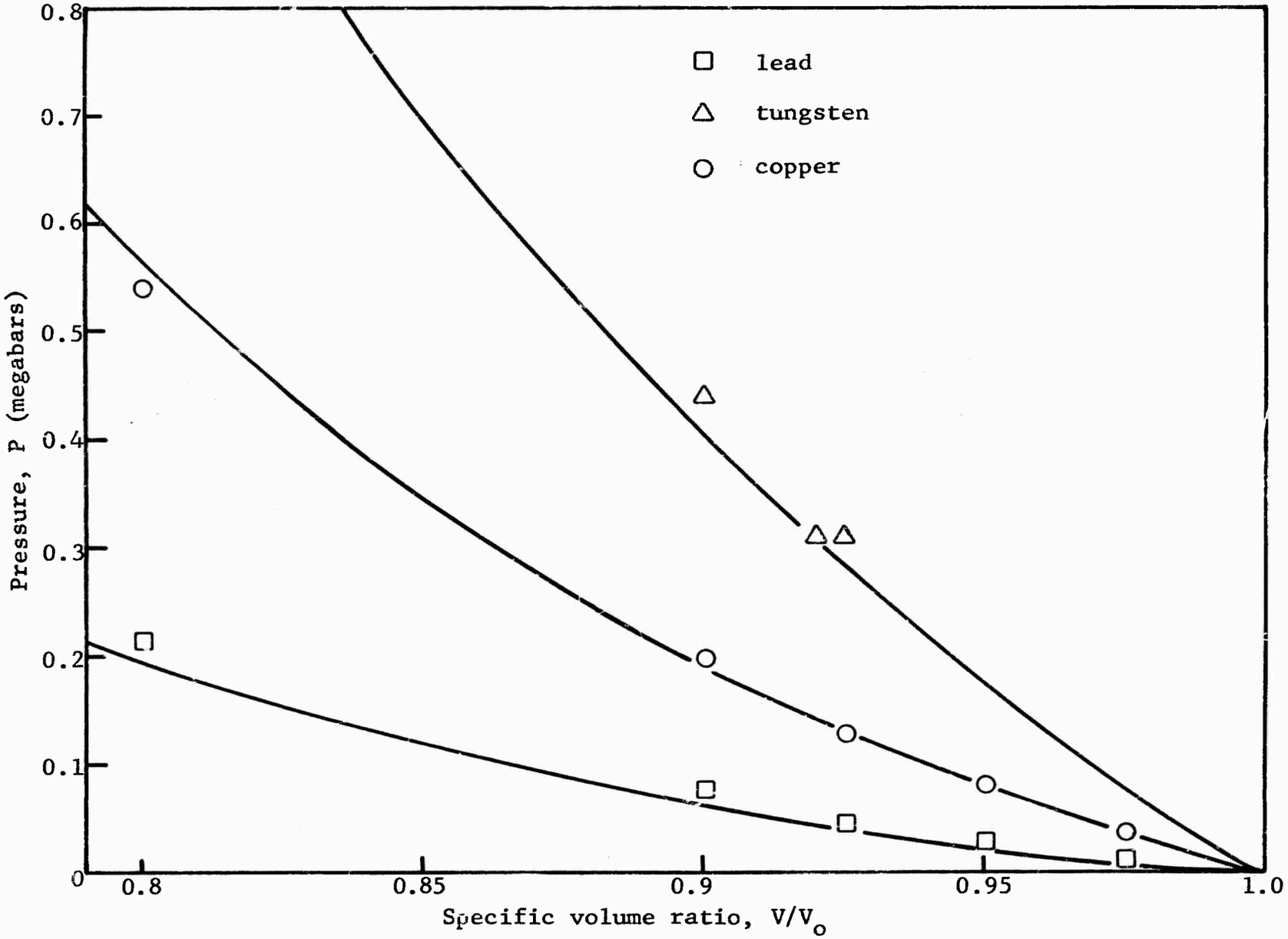

Figure 5 Comparison of Hugoniot Data (Ref. 4) and Hugoniot Based on Average Log P, Log β_o Plot of Figure 4

(Ref. 5,6,9,10), the S-values associated with the higher pressure states reached by a single shock wave are concentrated at values around 1.6 with a somewhat wider spread than for the metals (Ref. 10). Interestingly, the value of S for air, for which the Hugoniot is analytically derivable, converges to

$$\frac{\gamma+1}{2}, \quad \text{where } \gamma = C_p/C_V = 1.4$$

for high pressure states. Similarly, for a monatomic perfect gas, S converges to 1.33, while, for a more complicated perfect gas, S is lower yet always greater than 1. An average linear fit using the analytical curve of reference 11 gives a value of ~1.6 for water. A large fraction of the materials for which Hugoniot data are known have S-values within the range of 1 to 1.67. Although the analytically derived Hugoniot for a perfect gas could not be expected to apply to other materials, the implied significance of γ is notable.

B. Experimental Hugoniot Determination

The experimental work in this program was divided into two phases. The first phase was directed toward an examination of various experimental techniques to determine those best suited for use with the samples of interest. The second phase was devoted to determining the Hugoniots for the minerals, utilizing the results of the earlier experimental work. The results of both phases and the resulting mineral Hugoniot data are discussed in this section.

The minerals of interest were some of the major constituents of several igneous rocks. Those investigated were orthoclase,

oligoclase, labradorite and olivine. Certain peculiarities of the feldspar group made the complete separation of these phases impossible. These peculiarities are associated with the apparent existence of a very weak precursor wave. Shock wave experiments of an exploratory nature were required and performed during the entire period of the investigation. The resulting interrelationship between the two phases makes it convenient to discuss both phases together. The only exception is the following brief discussion of some of the early experiments that were entirely of an exploratory nature.

Before embarking on a detailed discussion of the shock experiments, it is necessary to consider the relationships between the measurable variables and the desired information to be derived from these variables. Although many references concerning these relationships are available in the literature, it is desirable to re-emphasize some of that work for certain aspects of the present problem.

1. Shock State Determination

The shock equations discussed earlier indicate the requirement to measure the shock and particle velocity behind each wave in order to determine the shock states or Hugoniot. The instrumentation schemes used here are capable of furnishing information on free surface motion only. Electrically conducting pins and piezoelectric crystals (Ref. 12,13) have been used to indicate the time-of-arrival of a conducting surface at a new location: Changes in light reflectance with time of a mirror placed at the free surface of the sample have been used to measure the free

surface velocity (Ref. 14,15,16). It has been shown that the free surface velocity is a good approximation to twice the particle velocity for metals (Ref. 16). Free use has been made of this free surface approximation for all of the optical records. Pins and crystals placed at or near a free surface have been used to indicate shock wave arrival time and, thus, shock wave velocity. Two basic types of experiments were used: the impedance match solution incorporating the electrical instrumentation and the velocity method incorporating optical instrumentation. In several experiments both instrumentations were included.

Impedance-Match Method

The impedance matching method depends on the existence of known Hugoniot data, both loading and unloading, for one or more witness materials (Ref. 17). In addition, this method can be used only for single-wave loading conditions. A possible sample configuration is shown in Figure 6(a). Here a witness material of the same material as the buffer plate is affixed to, or machined as part of, the plate. The sample material is also affixed to the buffer plate. From readings of the times of motion of the three free surfaces, i.e., the shock arrival times t_c at the buffer sample interface, t_w at the witness material free surface, and t_s at the sample free surface, the transit times and shock velocities through the buffer plate and sample are determined. From the known Hugoniot of the witness material, the pressure P and particle velocity U_p are known, as Figure 6(b) shows. For the sample material, the slope on the (P,U_p) plot is known from the measured shock velocity in the sample. From equation (4),

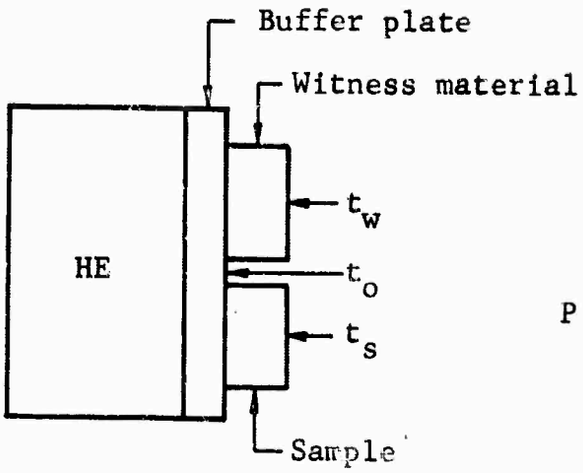

(a) Experimental configuration

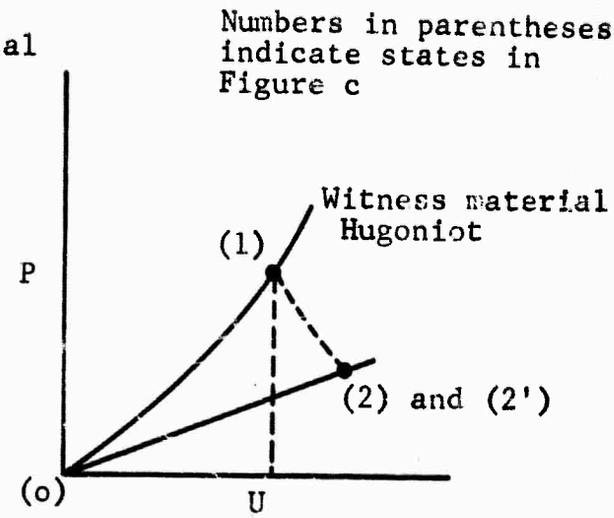

(b) Impedance matching solution

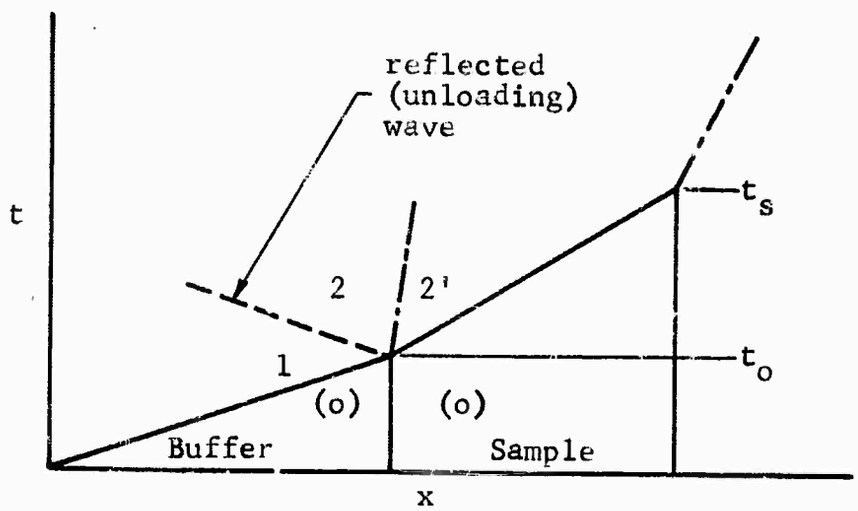

(c) t-x diagram

Figure 6 Schematic of Experimental Configuration (a) Suitable for Impedance Matching Solution (b) Based on Continuity of Pressure-Material Velocity States (2,2') Shown in t-x Diagram of (c)

$$\frac{P}{U_P} = \rho_o U_s \quad . \tag{14}$$

Since the normal pressure and material velocity are continuous across the sample buffer interface, the pressure velocity states in regions 2 and 2' of Figure 6(c) are the same. The state (2) of Figure 6(c) represents the state behind the reflected wave. The slope of equation (14) must then intersect the locus of possible reflected states in the buffer material. Since the buffer material is usually of higher impedance, $\rho_o U_s$, than the sample material, these possible states represent the unloading adiabat from the initial state (1), i.e., the dashed line in Figure 6(b). In this work, the unloading adiabat has been taken as the mirror reflection of the known loading curve of the buffer and witness material (either aluminum or brass).

One advantage of this method is that the free surface approximation is not required because it is not necessary to measure the known particle velocity in the sample. The attending disadvantages are that the location of state (1) from shock velocity measurements alone is difficult. It also may be argued that the assumption regarding the unloading path in the buffer material is more severe than the assumption of the validity of the free surface approximation (Ref. 18). Because of these difficulties, several experiments combining the impedance method with optical methods were run in addition to the series using pins alone.

Velocity Method

In the velocity method, the shock and particle velocity associated with each wave must be known. For materials compressed

by a single wave, only two velocities are required: For more complicated materials where there are two or more waves, the optical methods of Fowles (Ref. 14) and Wackerle (Ref. 15) are particularly suited as they are capable of furnishing a continuous history of the free surface motion. In our experiments, the optical methods were restricted to several variations of the inclined mirror method of Fowles (Ref. 14). Some laboratory simulation experiments were made, however, using the wire method of Wackerly (Ref. 15). (These experiments are discussed in Appendix A.) Although a few experiments were run using crystals and pins to measure the free surface velocity, optical methods were found more suitable to the samples of interest.

In all experiments in which a measurement of the free surface velocity was made, use of the free surface approximation was required to obtain the necessary particle velocity. A more subtle approximation is also implied in all Hugoniot methods utilizing free surface motion measurements. In Figure 7, a schematic of a typical inclined mirror experiment is shown. Light from an intense HE light source is reflected from the mirrors mounted as shown. The reflected light from the mirrors passes through the slit of a rotating mirror camera* and is focussed on the film plane. The view through the slit (Figure 7(b)) is recorded on the film where position is proportional to time. Figure 7(c) shows an idealized record. As the shock-accelerated free surface engages the reflecting surfaces of the mirrors, the reflected light intensity

*Beckman-Whitley Model 189 with special telescopic lens and streak attachments.

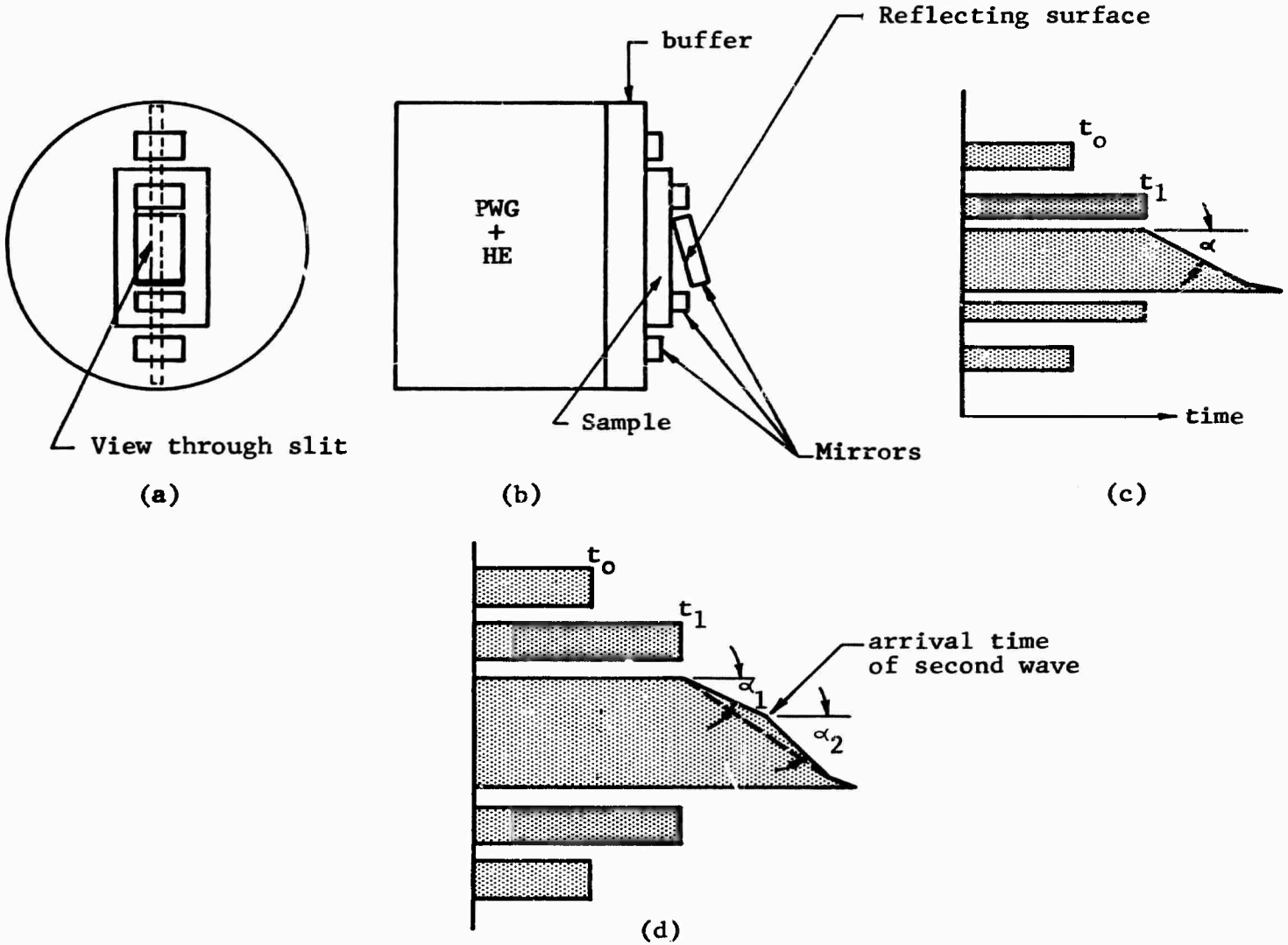

Figure 7 Experimental Configuration for Velocity Method Using Mirror Method (a) and (b), Showing Idealized Film Record for Single Wave (c) and Double Wave (d) Systems

changes (usually reduced) and the times of these are recorded. The flat mirrors, located on the buffer plate and sample free surfaces, give the shock time-of-arrival. The reflectance as a function of time of the inclined mirror indicates the free surface velocity of the sample. If there is only one wave, the velocity angle α is a constant. For a material shocked above its yield point in a stress region where it is compressed by two waves, a record as shown in Figure 7(d) might be expected. At time t_2, the pressure reaches the mirror-sample interface and accelerates the rate of reflectance change.

This shock wave configuration is shown in Figure 8. Here we consider a t-x diagram for a condition yielding an elastic precursor and a slower plastic wave. In Figure 8(a), the simple case is considered. Here, no interactions are taken into account. The free surface being observed is simply presumed to be accelerated, impulsively with the arrival of each wave. These velocities are related to the dynamic yield point P_{YP} and the final pressure P_f by the equations set down earlier. Using pins in such an experiment would require two arrays of pins, one for each free surface velocity.

A more detailed view of the situation is that of Figure 8(b). Here it is seen that the plastic wave, in fact, never does reach the free surface. Instead, succeeding free-surface accelerations are caused by the reverberating elastic wave. While, according to the theory, the final free-surface velocity is approximately twice the material velocity in region (2) behind the plastic wave, the transition to the final free-surface velocity is not abrupt.

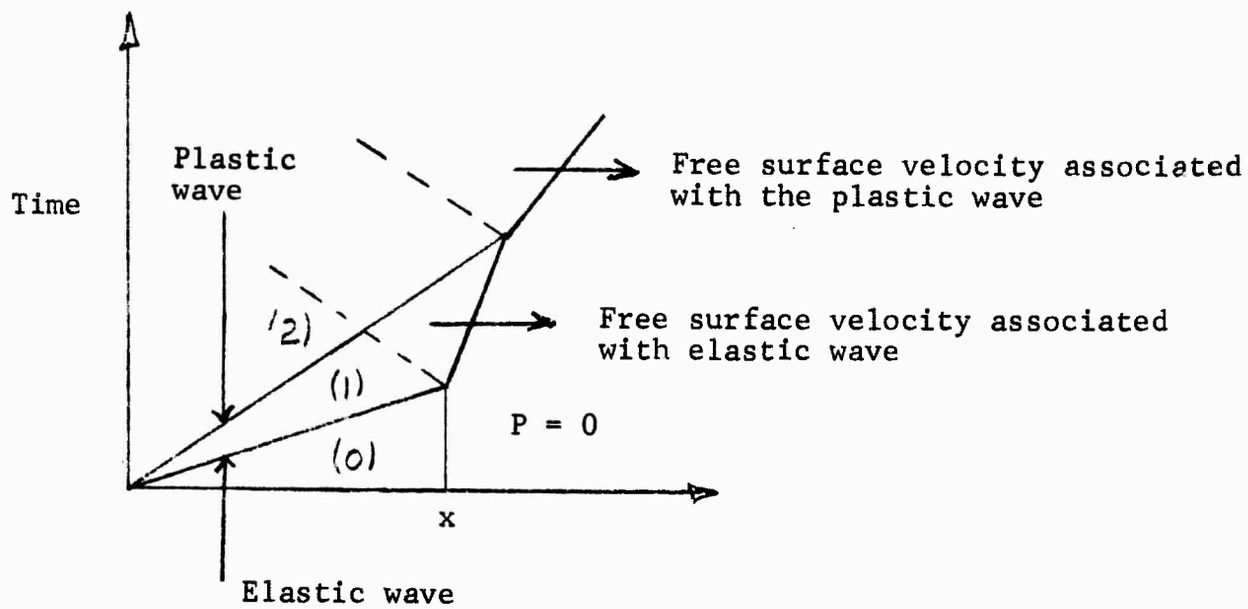

Figure 8(a) Simple Double Shock System Involving No Interactions

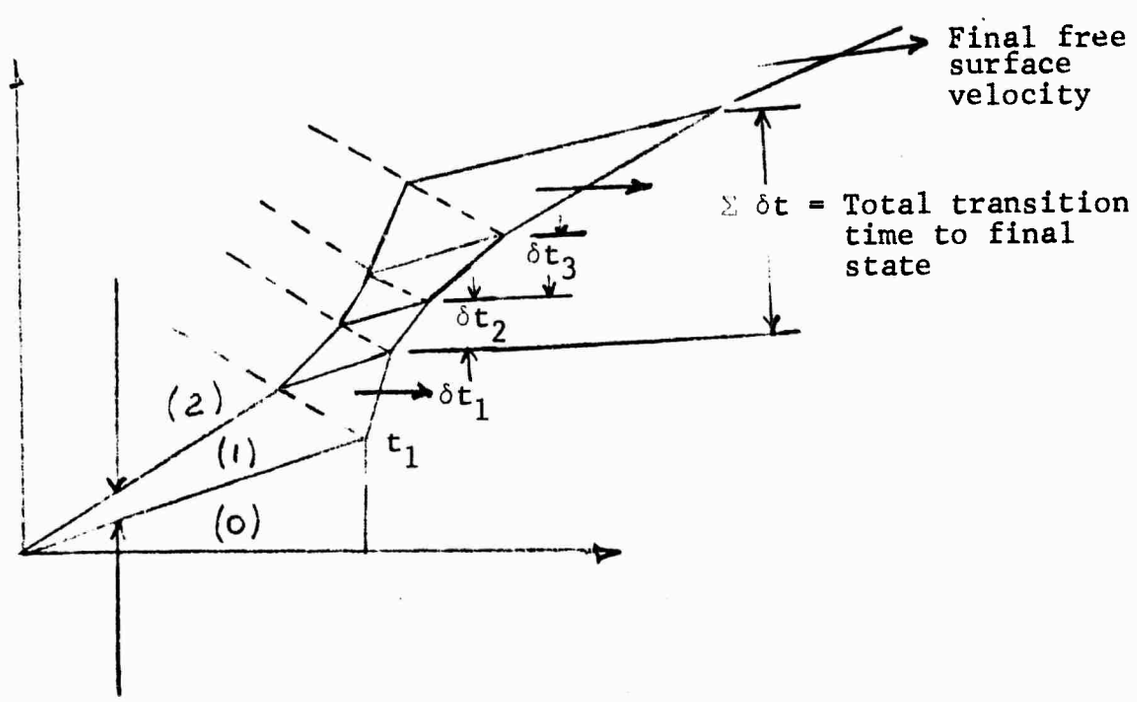

Figure 8(b) More Detailed Shock System Showing Shock Wave Reverberations and Transition Time to Final State

It occurs over a series of jumps of 2n times the particle velocity in region (1), where n is the n^{th} increment of free-surface acceleration. The time period between successive accelerations is dependent on the properties of the sample material as these affect the ratio of the elastic precursor to the plastic wave velocity. These have been worked out for several cases and are listed in Table I. The sum of these times is the total transition

Table I

TRANSITION TIMES ASSOCIATED WITH SHOCK TRANSITIONS

$R = U_e/U_P$ (μsec)	P_{YP} (kbars)	$\frac{\delta t_1}{t_1}$	$\frac{\delta t_2}{t_1}$	$\frac{\delta t_3}{t_1}$	$\frac{\delta t_4}{t_1}$	$\sum_{e=2}^{4} \frac{\delta t_e}{t_1}$
0.5	50	0.75	0.48	0.48	1.722	1.682
0.75	50	0.32	0.116	0.046	0.055	0.217
0.5	25	0.71	0.25	0.285	0.156	0.70
0.75	25	0.3	0.07	0.02	0.011	0.101

time necessary for the free surface velocity to be an indication of the plastic pressure. Since we are interested only in the transition time for the initial free surface velocity to the final free surface velocity, $\delta t_1/t_1$ cannot be included in this sum. It is necessary, therefore, in some cases, to require that the instrumentation technique be capable of extremely good time resolution in order to observe free surface velocity changes. In fact, the simpler situation depicted in Figure 8(a) only approximately applies in cases where the time period δt is small compared with

t_1, the time required for transit of the first wave across the sample. For an intermediate case where τ is too large to neglect, a time resolution of at least 0.1 μsec is required. A transit time t_1 of between 0.5 and 1.0 μsec is typical in these experiments.

The details discussed here have not yet been experimentally observed with sufficient accuracy for complete analysis. An attempt to observe these details requires very high camera speeds--such speeds must be consistent with the ultimate time resolution prescribed by the slit width. In addition high camera speed results in very small angles α_i in Figure 7(c) and 7(d). These small angles make it very difficult to determine the time t_2.

Consideration of these details, therefore, indicates that the transition time between the free surface velocity associated with an elastic precursor (and characterized by the angle α_1 of Figure 7(d)) and the free surface velocity associated with the final plastic state (and characterized by the angle α_2 of Figure 7(d)) cannot be a unique time t_2. Rather, this transition must be spread over a period of time, as indicated in Figure 8(b) (i.e., $\Sigma\delta t$). Then, a rounded record like that of the dashed line in Figure 7(d) might be expected.

Almost all records for the feldspars appeared either rounded as in Figure 7(d) or straight as in Figure 7(c). Certain other peculiarities discussed in the next section led to a decision to treat the records as if they were the result of compression by a single shock wave.

One difficulty in attempting to analyze these records is the fact that any observed rounding may be the result of material

properties. Consider, for example, a material characterized by the Hugoniot of Figure 9(a). Such a material shocked by a flat-topped pressure pulse of amplitude P_2 would cause the transmittal of a pressure pulse of the type shown in Figure 9(b). Because of the dispersive nature of this material, the pressure pulse would change shape with time as shown in Figure 9(b), the lower amplitude portions of the wave traveling at higher velocities than the higher amplitude portions. The arrival of such a wave at a free surface would cause the gradual acceleration of the free surface rather than the abrupt acceleration often associated with a sharp yield point. This gradual acceleration would cause a streak record of an inclined mirror to have a rounded appearance, which, in many cases, would be difficult to distinguish from the rounding caused by shock reverberations at the free surface.

Records of this type are discussed in the next section. In general, however, while such records may be analyzed graphically, a computer solution to the problem is considered much more amenable for the records of interest here. The short times associated with any curvature make a graphical solution too crude. Unfortunately, no such analysis was possible on any records in which curvature was noticed or suspected.

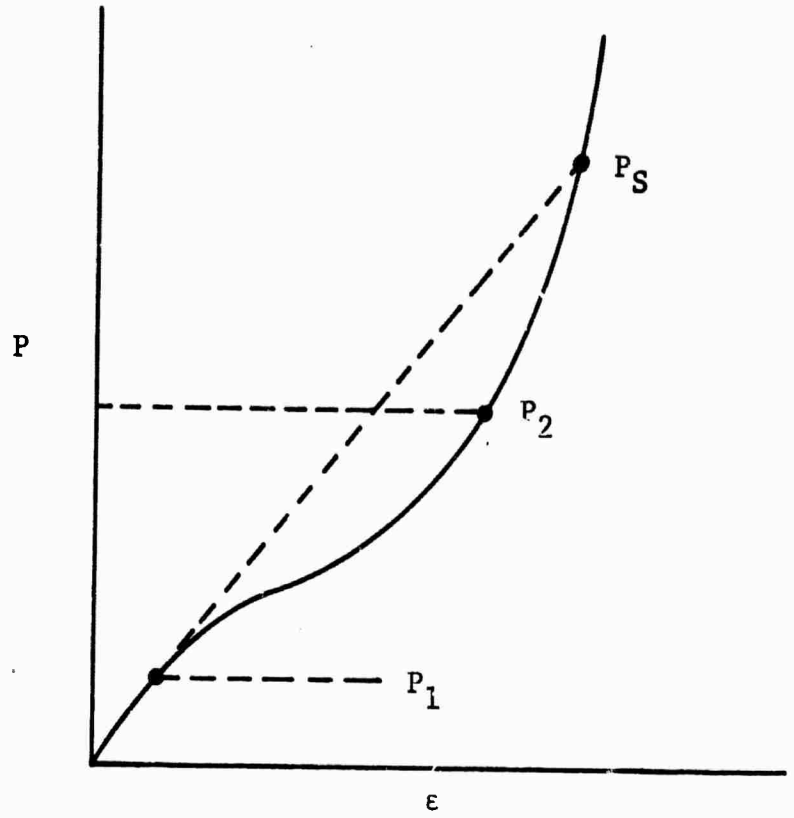

(a) Hypothetical Hugoniot of material that would cause compression fan

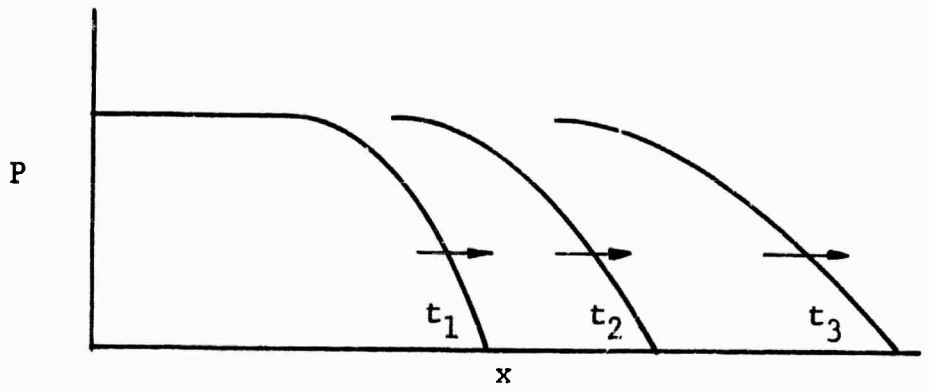

(b) Transmitted pressure pulse associated with a compression fan

Figure 9 Material Properties Leading to Compression Fan of Shock Waves Resulting in Continuous Change in Free Surface Velocity

III SHOCK WAVE EXPERIMENTS

In the experimental portion of this program, 60 experiments were run. About one-third of these were primarily exploratory and not intended for obtaining Hugoniot data. Many, however, incorporated mineral samples. These earlier experiments were used to investigate the effect of various optical parameters, such as optical configuration, slit width, light intensity, mirror configuration and magnification. In addition, in many, electrical time-of-arrival indicators were also used and comparisons between piezoelectric crystals and pins were made.

As a result of these preliminary experiments, several modifications to the existing optical system were decided upon. These involved the construction of a new lens system and a modified slit arrangement. As an alternative to carrying out additional experiments of a purely exploratory nature, a laboratory optical mock-up was set up and used to compare the wire technique of Wackerle (Ref. 15) with the inclined mirror technique for various free surface motions. The results of this investigation indicated that the differences in sensitivity of the two methods to changes in free surface motion did not warrant the additional effort involved in providing the reflecting surface necessary for the wire method. Consequently, only the inclined mirror optical method was used in the high pressure experiments.

These mock-up experiments, as well as preliminary high pressure experiments on the minerals, indicated the degree of difficulty that might be encountered in locating any times associated with the arrival of a second or plastic wave in yielding materials

(Figure 7). The results of a brief study to determine the effect of arbitrarily choosing such transition times are discussed. The major data-gathering high-pressure experiments were divided into several series involving different combinations of optical and electrical configurations.

A. Inclined Mirror Experiments

This series of experiments utilized the mirror configuration shown in Figure 10. A 4-in. plane-wave generator in direct contact with a 4-in.-diam by 1/2-in.-thick aluminum buffer plate was used as the shock wave driver. The first experiment in this series, using the mirror configuration shown in Figure 10(a), indicated the presence of a very low amplitude precursor wave. There was no measurable free surface velocity associated with this wave, as may be seen in Figure 11, so that the pressure level transmitted by this wave was considered negligibly small. This inference indicated that the impedance match solution discussed might be applicable to the minerals of interest here. Consequently, several additional experiments were carried out using this mirror configuration but incorporating witness materials in place of a second mineral sample. The impedance match solution indicated that the hypothesis of the existence of the low-pressure wave was correct but, in addition, these records showed that there was, in fact, some very slight free surface velocity imparted <u>after</u> the arrival of the weak precursor. This "rounding" in the record was attributed to the reverberations of the precursor between the free surface of the sample and the high pressure wave. This phenomenon was considered in the discussion of Figure 7.

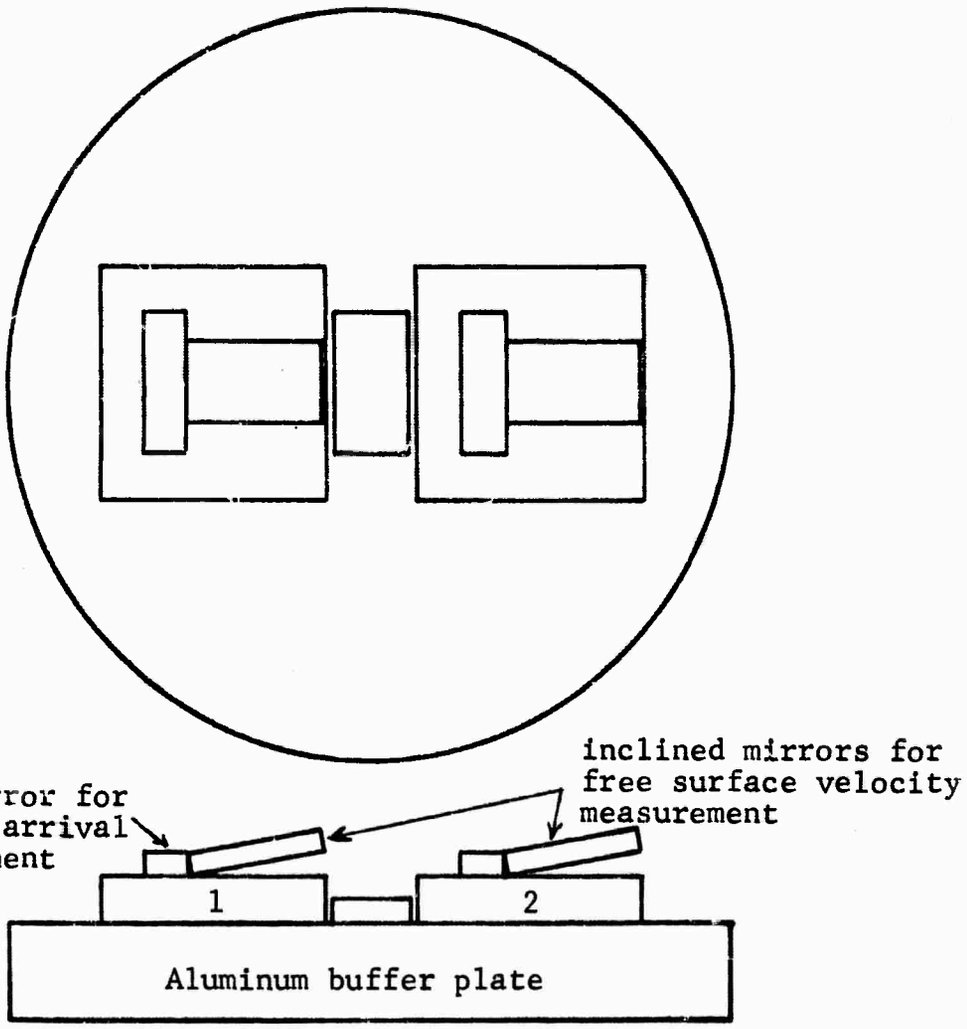

Shot	Sample 1	Sample 2	Explosive
14	Oligoclase	Orthoclase	PWG(P-40)
16-17	Oligoclase	Al	PWG(P-40)
18-19	Labradorite	Al	PWG(P-40)

Figure 10(a) Mirror Configuration Used for Shock and Particle Velocity Determination for Listed Feldspar Experiments

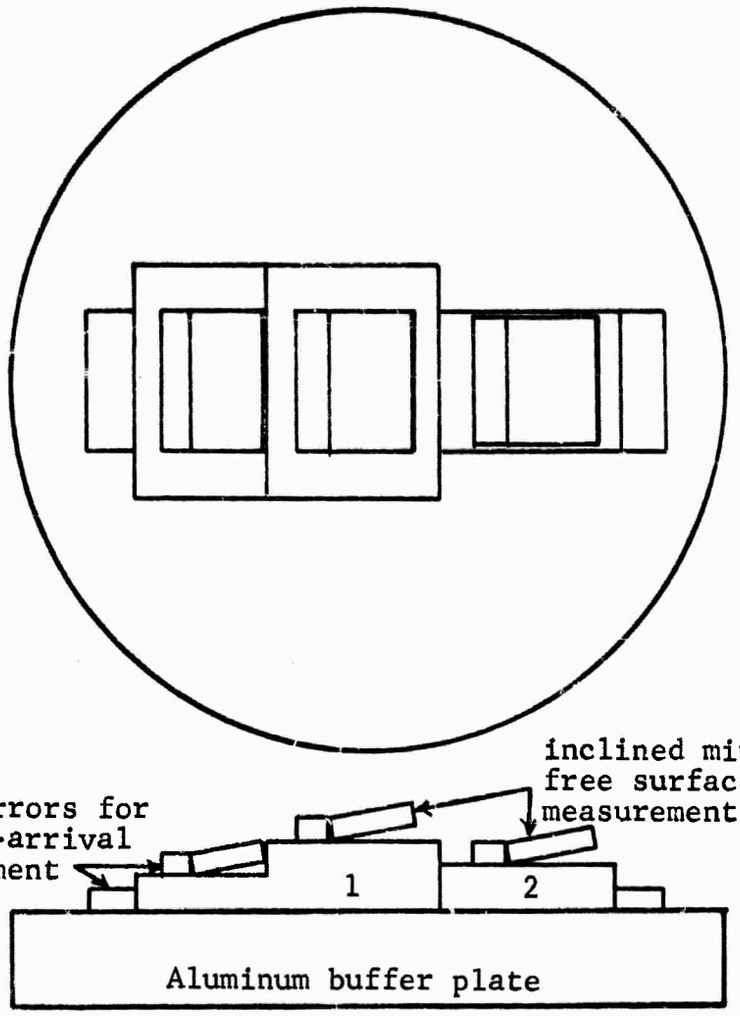

Shot	Sample 1	Sample 2	Explosive
20-21	Oligoclase	Al	PWG(P-40)
22*	Oligoclase	--	PWG(P-40)

*large flat mirrors only

Figure 10(b) Mirror Configuration Used for Shock and Particle Velocity Determination for Listed Feldspar Experiments

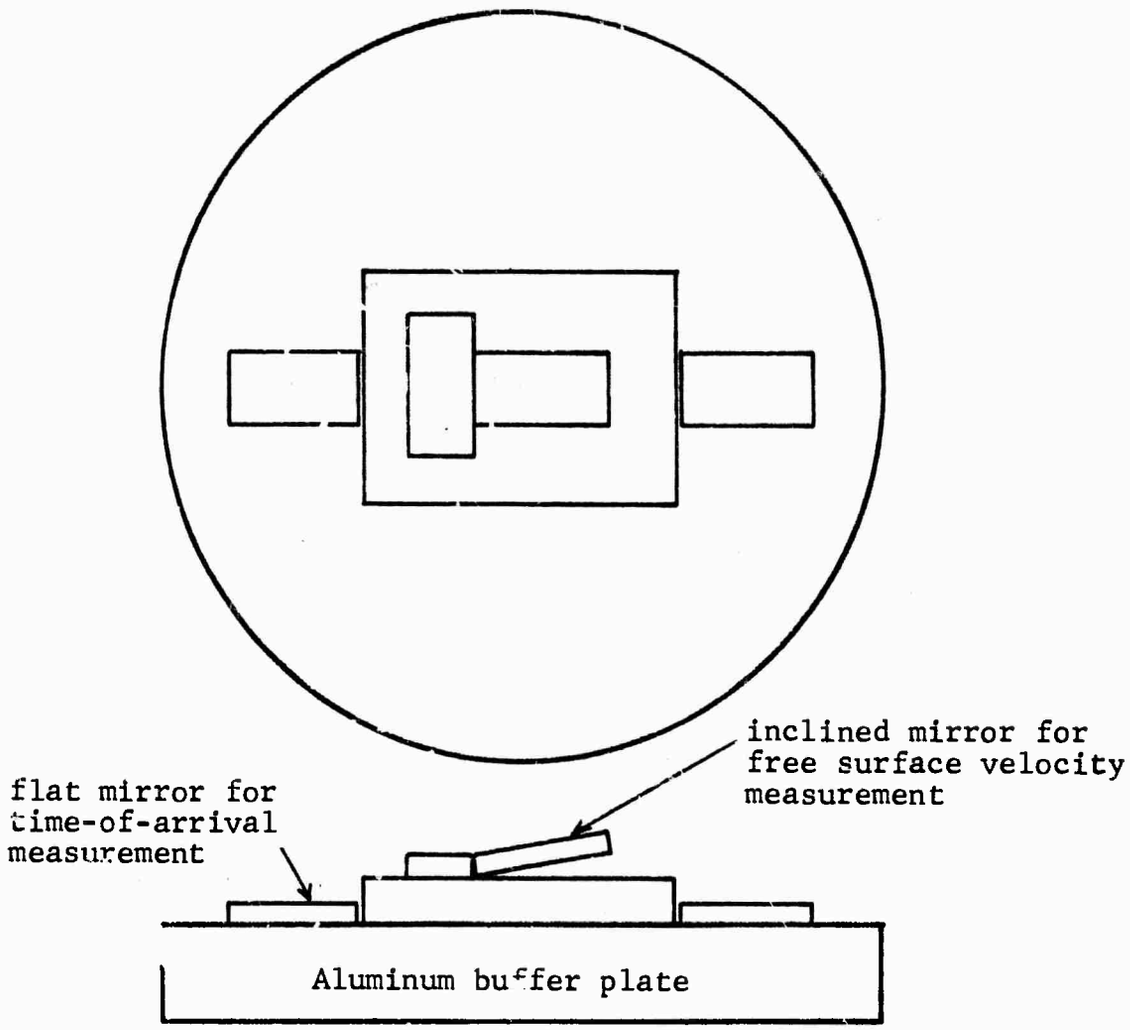

Shot	Sample	Explosive
24	Aluminum	PWG (P-40)
25	Labradorite	PWG (P-40)
26	Oligoclase	PWG (P-40)
27	Labradorite	PWG + 2-in.PBX*
28	Oligoclase	PWG + 2-in.PBX*
29-30	Orthoclase	PWG + 2-in.PBX*
31-32	Orthoclase	PWG + 2-in.PBX*
33-39	(see Table II)	(see Table II)

*2-in.PBX refers to use of a 2 x 4-in.-diam slab of PBX used with PWG (P-40 plane wave generator)

Figure 10(c) Mirror Configuration Used for Shock and Particle Velocity Determination for Listed Feldspar Experiments

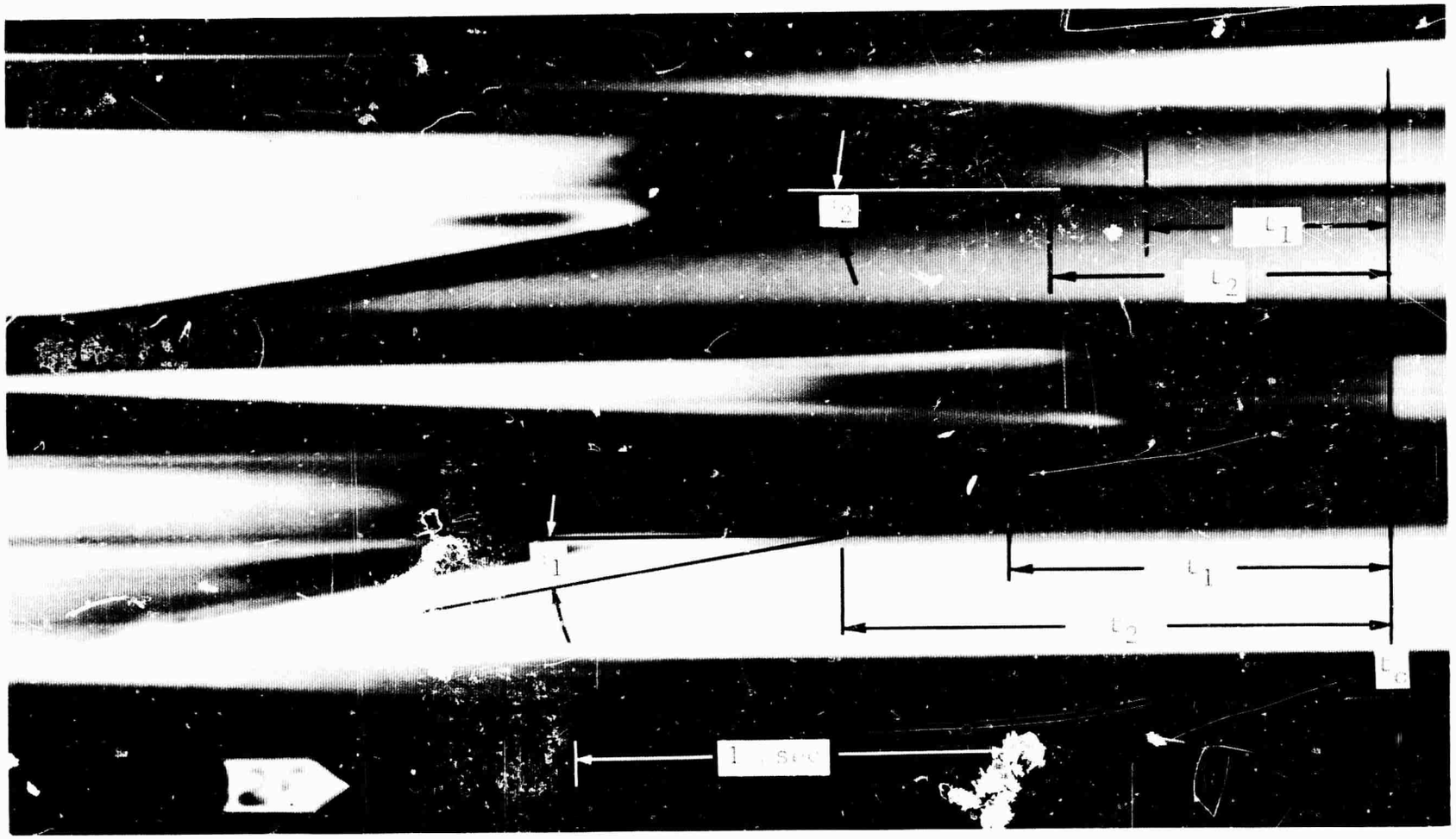

Figure 11 Sample Record Showing Arrival of Shock Wave at Buffer Plate Free Surface t_o, Transit Times of Precursor Waves Δt_1, 2nd Shock Waves Δt_2 and Free Surface Angles α_1 for Orthoclase (Lower) and Oligoclase (Upper)

Because of the surprisingly high velocity of the precursor wave (greater than 7mm/μsec) in the oligoclase sample, the configuration was modified to that shown in Figure 10(b). It was then possible to measure two values for the precursor velocity. The unexpected result, as shown in Table II, is that rather than showing a reduction, the average value of the precursor velocity over the second portion of the sample is higher than that over the first portion.

In addition, there was no indication of any unloading from the explosive. It was decided, therefore, that the driver system using a plane-wave generator as the only explosive was a fairly good system for our purposes.

The next series of experiments utilized the mirror/sample configuration of Figure 10(c). In this series, relatively large flat mirrors were used in an effort to determine the planarity and times associated with the wave system. A sample record is shown in Figure 12. The results of these experiments are also listed in Table II. For several experiments, two wave velocities are shown but only the particle velocity associated with the second wave has been listed. The pressure and strain are calculated from equations (4) and (5).

The same optical configuration was used in an additional series of experiments that incorporated piezoelectric crystal transducers of the type described in reference 12. These gages are shown in place on a sample in Figure 13. It was desired to compare the shock velocities derived from these gage readings with those obtained from the mirrors.

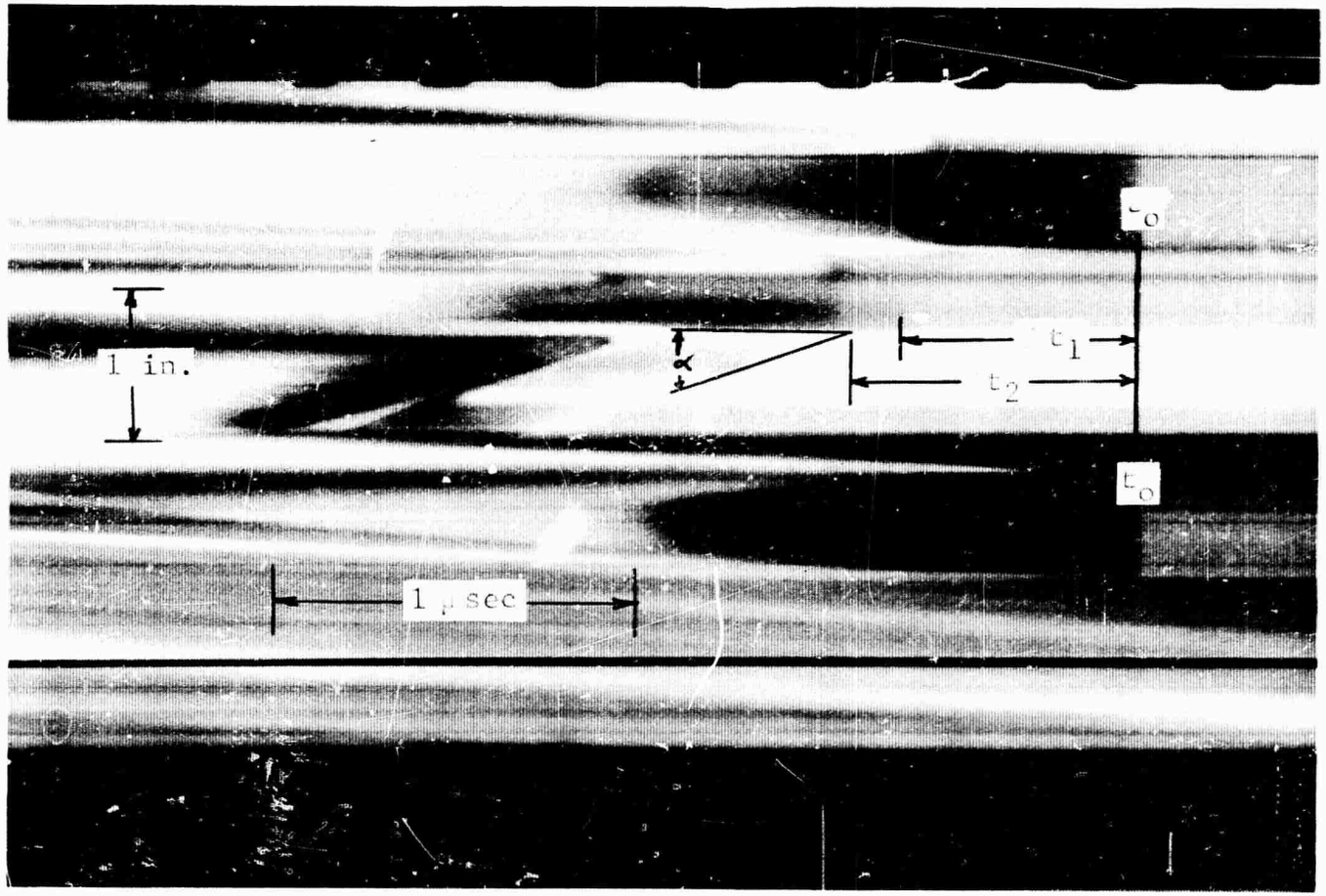

Figure 12 Sample Record of Configuration Shown in Figure 10(c) Showing Arrival Time of Shock Wave of Flat Mirrors t_o, Transit Times of Precursor and 2nd Shock Waves Δt_1 and Δt_2, and Free Surface Angle α

Table II

RESULTS OF SHOCK WAVE EXPERIMENTS ON FELDSPARS
(ORTHOCLASE, OLIGOCLASE, AND LABRADORITE)

Exp. No.	Material	Crystal Direction	Density (gm/cc)	Explosive PWE	Explosive HE	Configuration Opt.	Configuration Elect.	Sample Length (in.)
14	Orthoclase	C	2.57	P-40	--	Fig 10a	--	0.253
14	Oligoclase	C	2.65	P-40	--	Fig 10a	--	0.182
15	Labradorite	C	2.71	P-40	--	Fig 10a	--	0.265
15	Labradorite	C	2.71	P-40	--	Fig 10a	--	0.265
16	Oligoclase	C	2.65	P-40	--	Fig 10a	--	0.179
17	Oligoclase	C	2.65	P-40	--	Fig 10a	--	0.182
18	Labradorite	C	2.71	P-40	--	Fig 10a	--	0.219
19	Labradorite	C	2.71	P-40	--	Fig 10a	--	0.371
20	Oligoclase	C	2.65	P-40	--	Fig 10b	--	0.370
20	Oligoclase	C	2.65	P-40	--	Fig 10b	--	0.186
21	Oligoclase	C	2.65	P-40	--	Fig 10b	--	0.373
21	Oligoclase	C	2.65	P-40	--	Fig 10b	--	0.191
22	Oligoclase	C	2.65	P-40	--	Fig 10b*	--	0.413
22	Oligoclase	C	2.65	P-40	--	Fig 10b*	--	0.178
25	Labradorite	C	2.71	P-40	--	Fig 10c	--	0.175
26	Oligoclase	C	2.65	P-40	PBX	Fig 10c	--	0.180
27	Labradorite	C	2.71	P-40	PBX	Fig 10c	--	0.182
28	Oligoclase	C	2.65	P-40		Fig 10c	--	0.181
30	Orthoclase	B	2.57	P-40	PBX	Fig 10c	--	0.225
32	Orthoclase	B	2.57	P-40		Fig 10c	--	0.251
33	Orthoclase	C	2.57	P-40		Fig 10c	cryst	0.250
34	Oligoclase	C	2.65	P-40		Fig 10c	cryst	0.250
35	Orthoclase	C	2.57	P-40	PBX	Fig 10c	cryst	0.250
36	Oligoclase	C	2.65	P-40	PBX	Fig 10c	cryst	0.250
37	Labradorite	C	2.71	P-40		Fig 10c	cryst	0.250
38	Labradorite	C	2.71	P-40	PBX	Fig 10c	cryst	0.250
39	Labradorite	C	2.71	P-40		Fig 10c	cryst	0.250
40	Labradorite	C	2.71	P-40		Fig 16a	cryst	0.250
41	Oligoclase	C	2.65	P-40		Fig 16a	--	0.250
42	Oligoclase	C	2.65	P-40	PBX	Fig 16a	--	0.250
43	Labradorite	P	2.71	P-40		Fig 16a	--	0.250
44	Labradorite	P	2.71	P-40	PBX	Fig 16a	--	0.250
49	Oligoclase	C	2.65	P-60		Fig 18	pin	0.250
50	Oligoclase	C	2.65	P-60		Fig 18	pin	0.250
50	Oligoclase	P	2.65	P-60		Fig 18	pin	0.250

*flat mirrors only

**nonplanar shock wave

+questionable record

++based on crystal reading

‡rounded--no definite 2nd wave

Table II (Cont.)

Shock Wave Transit Times (μsec) Optical		Elect	Shock Velocities (mm/μ sec)		Particle Velocities (mm/μsec) Optical		Elect	Pressure P (kilobars)	Strain ε
Δt_1	Δt_2	Δt	1st U_{S1}	2nd U_{S2}	1st U_{P1}	2nd U_{P2}	Est. U_P		
.935	1.23	--	7.02	5.32	0‡			102	.141
.585	.873	--	7.9	5.91	0‡	.86		135	.145
.965	1.22	--	6.99	5.51	0‡	.60		89	.109
.965	1.22	--	6.99	5.51	0‡	.60		89	.109
	.82	--		5.55		.70		103	.126
	.78	--		5.92		.68		107	.115
.87	1.11	--	6.40	5.05	0	.76		104	.15
1.29	1.61	--	7.30	5.85	0	.63		100	.108
1.40	1.83	--	6.7	5.15	0	.78		107	.151
.72	.90	--	6.56	5.25	0	.78		108	.148
1.31	1.7	--	7.25	5.60	0	.74		110	.132
	.84	--		5.80		.74		114	.127
1.47		--	7.1	--	--				
.646		--	7.0	--	--				
.695	.92	--	6.4**	4.84	0‡	.77		101	.159
.754	1.06	--	6.08+	4.32	0‡	.795		(91)	(.184)
	.83	--		5.57		1.78		269	.320
.645	.782	--	7.15	5.89	0‡	1.83		286	3.12
.87	1.31	--	6.60	4.36	0‡	.77		86	.176
.84	1.17	--	7.60	5.45	0‡	1.50		210	.275
--	--	1.2		5.30			.74	101	.140
.9	1.2	.92	7.09	5.30	0‡	.59	.47	83	.111
1.0	1.2	1.02	6.20++	5.30	0	1.60	1.77	255	.258
.836	1.05	.88	7.59	6.05	0	1.78	1.52	286	.294
1.05	1.33	1.26	6.05	5.04++	0	.69	.55	94	.137
.932	1.07	.89	6.82	5.95	0	1.39		224	.234
	1.03	1.03		6.10		.76	.52	126	.125
1.04	1.3	1.04	6.07	4.88	0‡	.62	.57	82	.127
1.02	1.34		6.24	4.75‡	0‡	.77		127	.123
--	--			5.96		1.88		296	.32
--	--		6.32		0‡	.74		127	.117
--	--			5.02		1.57		214	.314
	1.14	1.00	7.52	5.58	0‡	.86	.63	135	.145
	.964	1.02	9.91	6.20‡	0‡	1.08	.93	177	.174
	1.27	1 11		5.65		.97	.78	145	.172

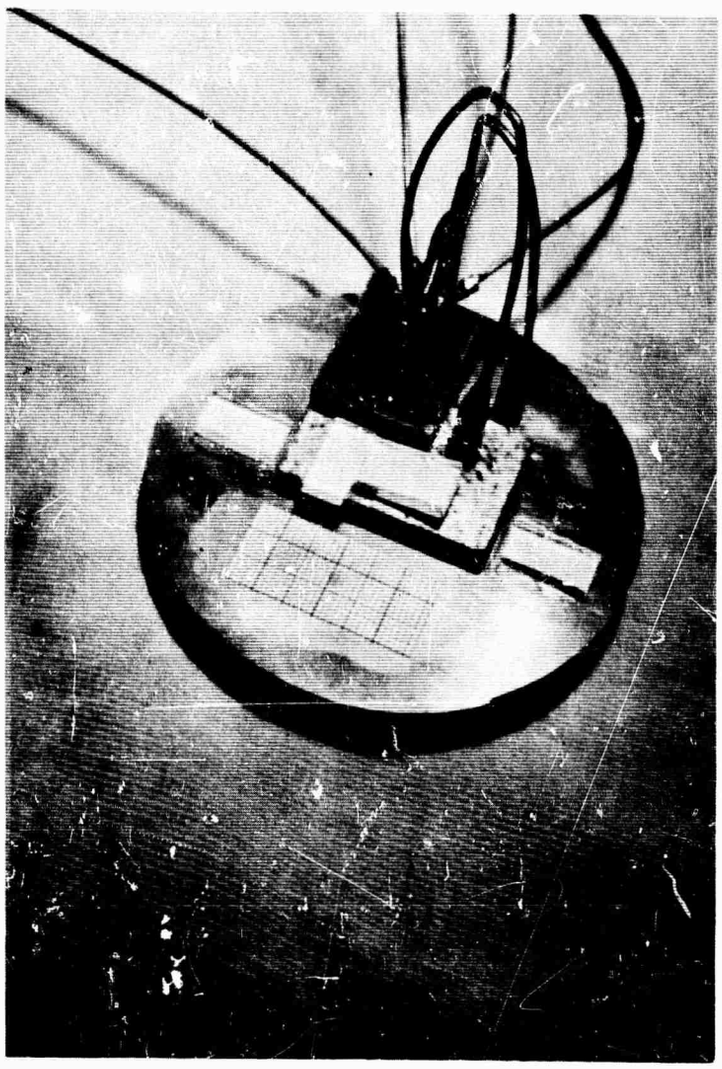

Figure 13 Experimental Configuration Showing Electrical and Optical Instrumentation

The sample is from a single crystal of orthoclase. Microcline particles are also seen.

As Table II shows, these velocities do not generally coincide but the crystals seem to indicate the arrival of the plastic wave and not the precursor. A record showing the times associated with both readings is shown in Figure 14. The times are normalized to the arrival of the shock wave at the free surface of the buffer plate.

It was hoped that the crystal gage readings might indicate the arrival of both the elastic and plastic waves. As may be seen from the sample record of the crystals (Figure 15), the gage becomes inoperative immediately after the first indication. This lends support to the view that the precursor wave is quite weak. Although it might be concluded that a higher amplitude elastic wave might also break the crystal gage, the closer correlation of crystal signal to the plastic wave is contrary to such a conclusion.

In an effort to further investigate the amplitude and velocity of the precursor wave, a series of experiments utilizing the optical configuration shown in Figure 16(a) was run. A slight modification is shown in Figure 16(b). The elastic wave velocities derived from these records show considerable variation for a given sample, but appear to be constant throughout the width of the sample. For both oligoclase and labradorite, the high-pressure shots showed a lower precursor velocity than the low pressure shots. As is noted in Figures 10 and 16, the higher pressures were obtained by adding a 2-in. slab of PBX between the plane wave generator and the buffer plate. A record from one of these, Figure 17, shows the constancy of the velocity of the first wave through the sample. This record is especially interesting because

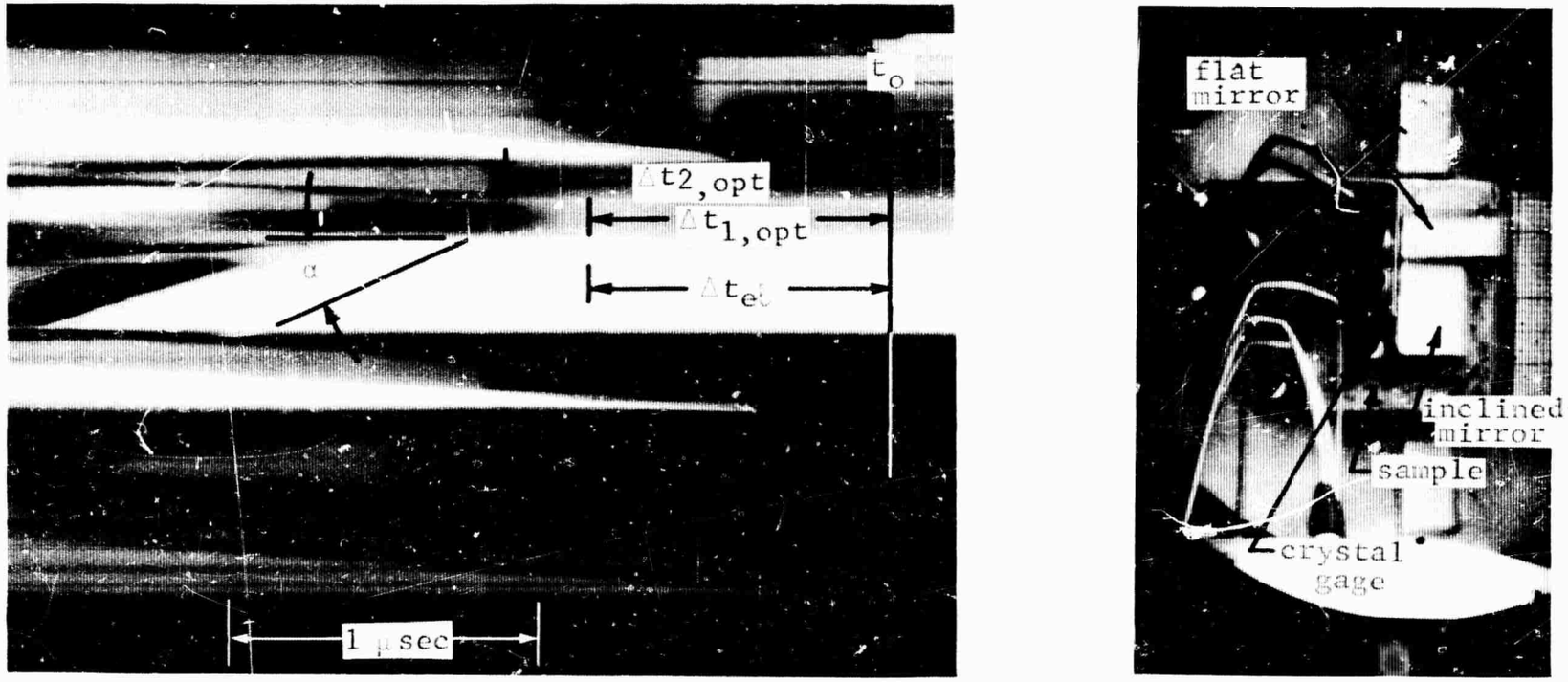

(a) (b)

Figure 14 Streak Record (a) from Mirror Configuration of Figure 10(c) for Sample of Orthoclase, Showing Shock Transit Times Measured Optically, Δt_{opt}, and Electrically, Δt_{el}, and Free Surface Velocity Angle, α; and (b) Model before Firing As Viewed in Static Frame of Rotating Mirror Camera

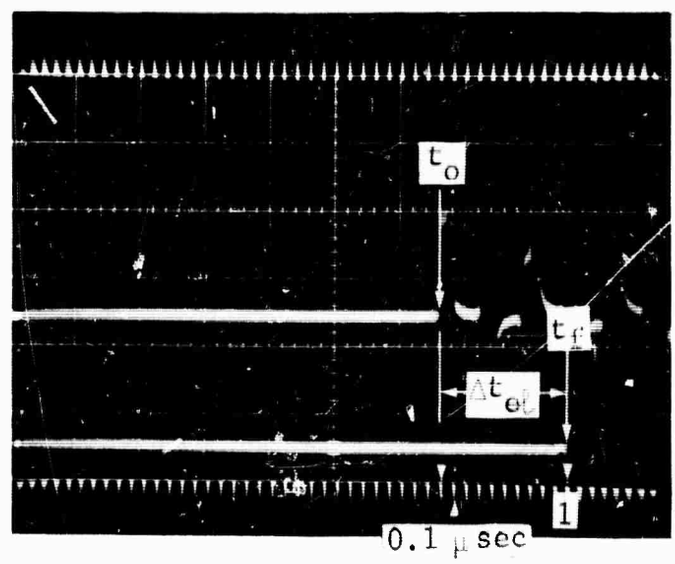

Figure 15 Oscilloscope Trace of Crystal Readings of Time-of-Arrival of Shock Wave at Buffer Plate Free Surface, t_o, and Sample Free Surface, t_f

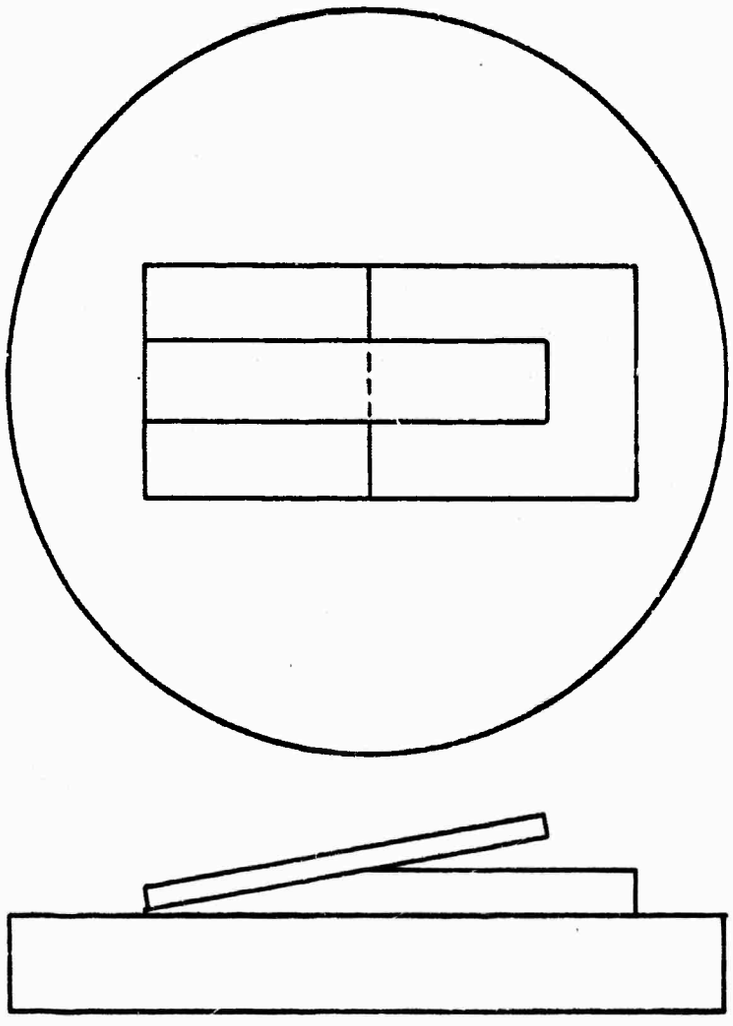

Shot	Sample	Explosive
40	Labradorite	PWG(P-40)
41	Oligoclase	PWG
42	Oligoclase	PWG + 4-in. PBX

Figure 16(a) Mirror Configuration Used for Shock and Particle Velocity Determination for Listed Feldspar Experiments

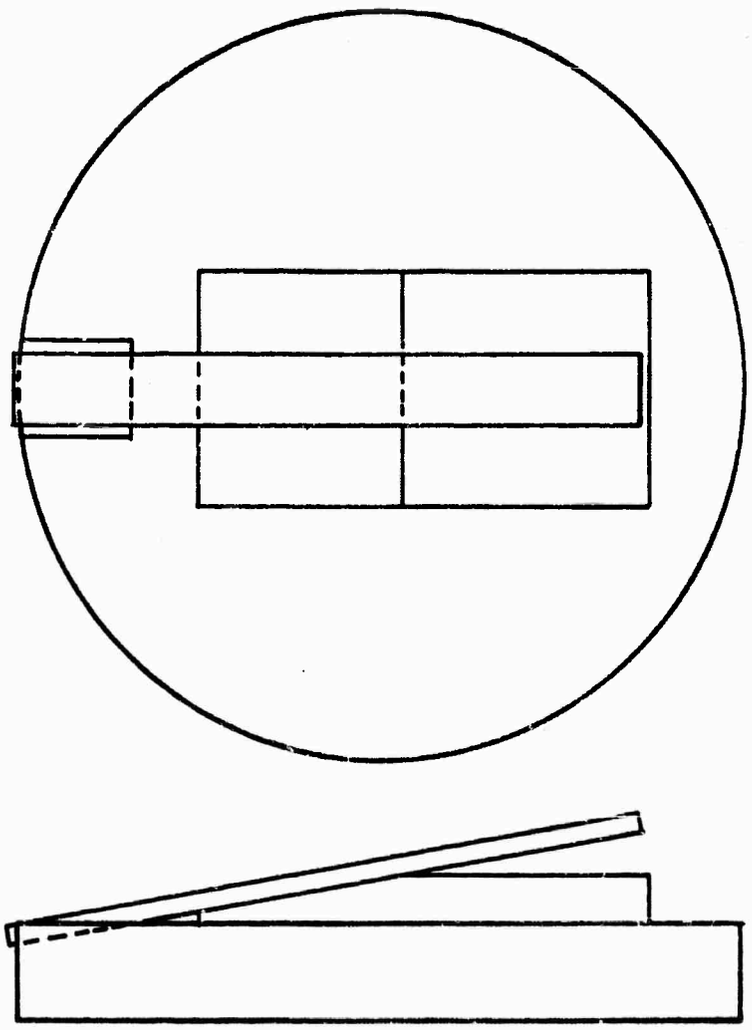

Shot	Sample	Explosive
43	Labradorite	PWG (P-40)
44	Labradorite	PWG + 4-in. PBX

Figure 16(b) Mirror Configuration Used for Shock and Particle Velocity Determination for Listed Feldspar Experiments

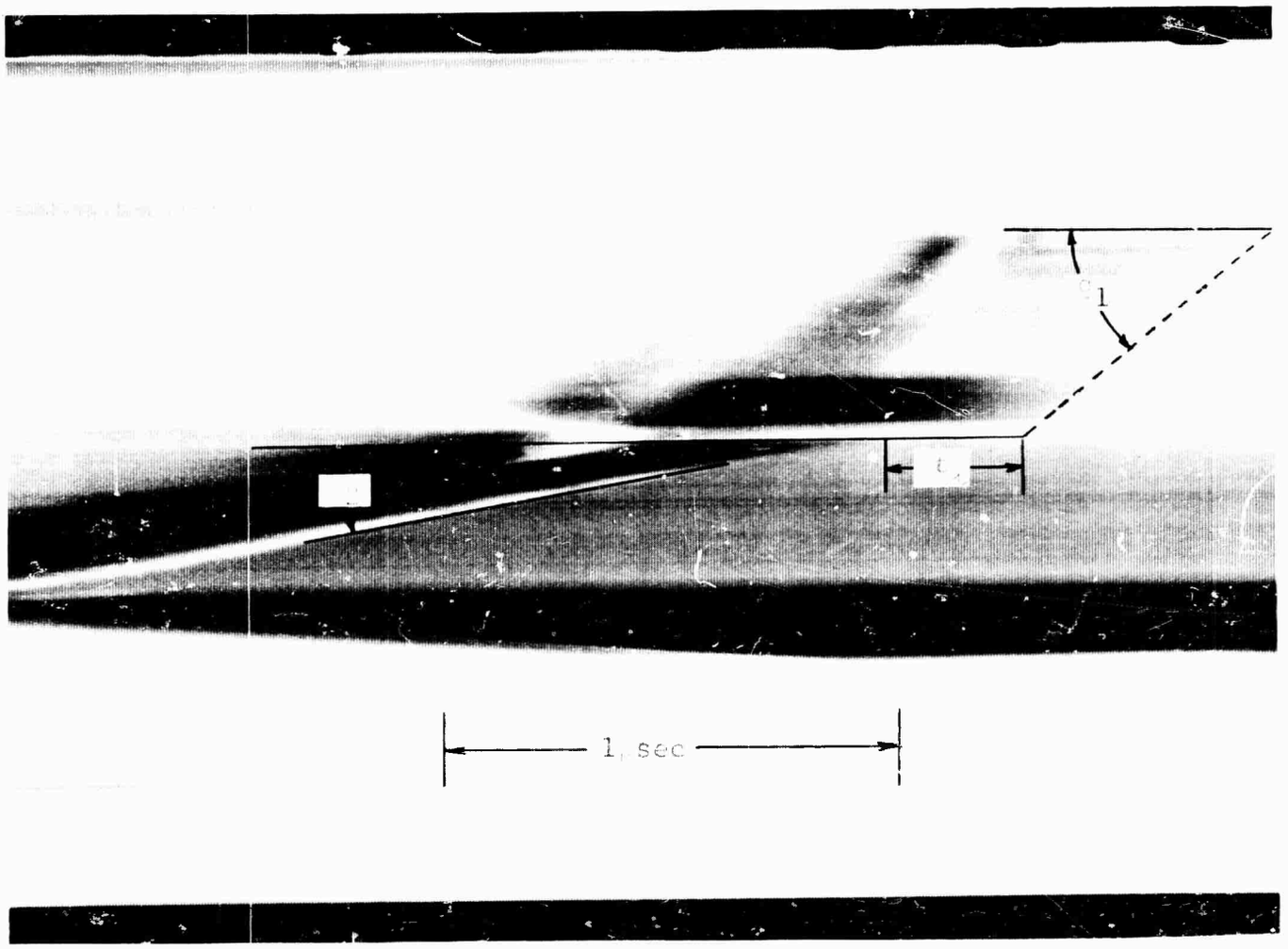

Figure 17 Sample Record oi Configuration 16(a) Showing Precursor Shock Velocity Angle α_1, Free Surface Velocity Angle α_2, and Lag Time Δt_ℓ between Arrival of Precursor and the Motion of the Free Surface

it shows the time lag between the arrival of the first wave and the acceleration of the free surface wave. Furthermore, it is seen that the acceleration of the free surface is not abrupt but is quite gradual. This indicates that the motion is due to a series of waves generated either from shock reverberations between the free surface and a later plastic wave or as a result of a Hugoniot curve rounded in the vicinity of its dynamic yield point.

B. Pin Experiments

All experiments described thus far utilized mirror reflection techniques. The results of these experiments have shown large sample-to-sample anomalies. Nevertheless, these experiments have been valuable in gaining insight into the wave structure generated in these feldspars. As a result of these experiments, it was tentatively concluded that the high-pressure Hugoniot states may be treated as if they are attained by shock compression from a single shock wave.

As a result of this conclusion, two additional sets of experiments were run. In the first set, the mirror configuration shown in Figure 18 was combined with the pin closure switches shown in Figure 19. The results of this series are shown in Table II. The shock arrival times coincide roughly with the motion of the sample's free surface, as shown in Figure 20.

The second set of experiments was based entirely on the impedance matching method and utilized electrical closure pins only. In this set of experiments, 6-in. plane wave generators were used with various explosives and driver plates to impart a series of loading conditions to the samples. A sample

it shows the time lag between the arrival of the first wave and the acceleration of the free surface wave. Furthermore, it is seen that the acceleration of the free surface is not abrupt but is quite gradual. This indicates that the motion is due to a series of waves generated either from shock reverberations between the free surface and a later plastic wave or as a result of a Hugoniot curve rounded in the vicinity of its dynamic yield point.

B. Pin Experiments

All experiments described thus far utilized mirror reflection techniques. The results of these experiments have shown large sample-to-sample anomalies. Nevertheless, these experiments have been valuable in gaining insight into the wave structure generated in these fe spars. As a result of these experiments, it was tentatively concluded that the high-pressure Hugoniot states may be treated as if they are attained by shock compression from a single shock wave.

As a result of this conclusion, two additional sets of experiments were run. In the first set, the mirror configuration shown in Figure 18 was combined with the pin closure switches shown in Figure 19. The results of this series are shown in Table II. The shock arrival times coincide roughly with the motion of the sample's free surface, as shown in Figure 20.

The second set of experiments was based entirely on the impedance matching method and utilized electrical closure pins only. In this set of experiments, 6-in. plane wave generators were used with various explosives and driver plates to impart a series of loading conditions to the samples. A sample

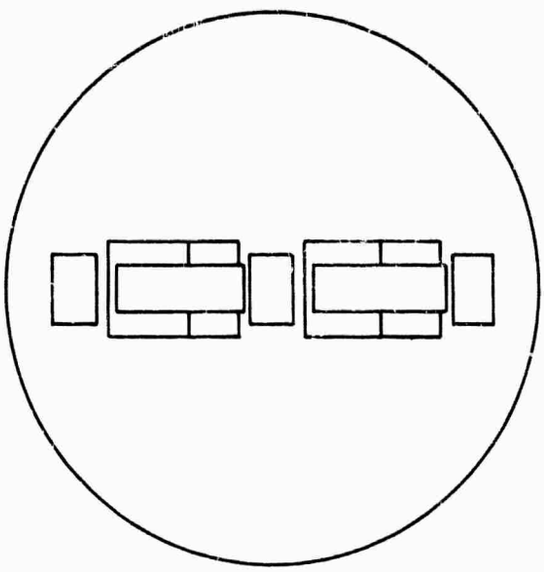

Shot	Sample	Explosive
49	Oligoclase-C dir/Aluminum	PWG(P-60)*
50	Oligoclase-C dir/Oligoclase-P dir	PWG(P-60)*

*6-in.-diam plane wave generator

Figure 18 Mirror Configuration Used for Shock and Particle Velocity Determination for Listed Feldspar Experiments

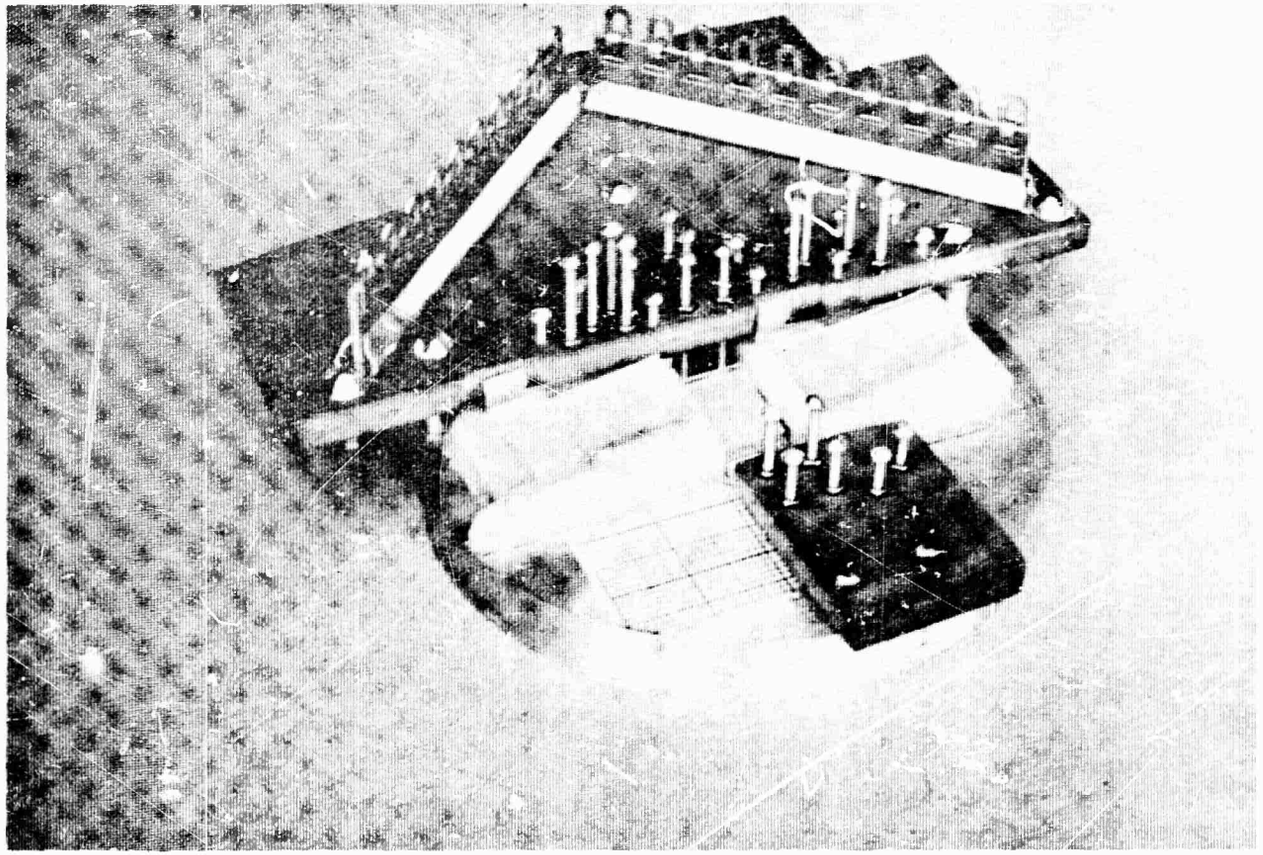

Figure 19 Test Specimen Using Both Mirrors and Pin Probes (Two Samples)

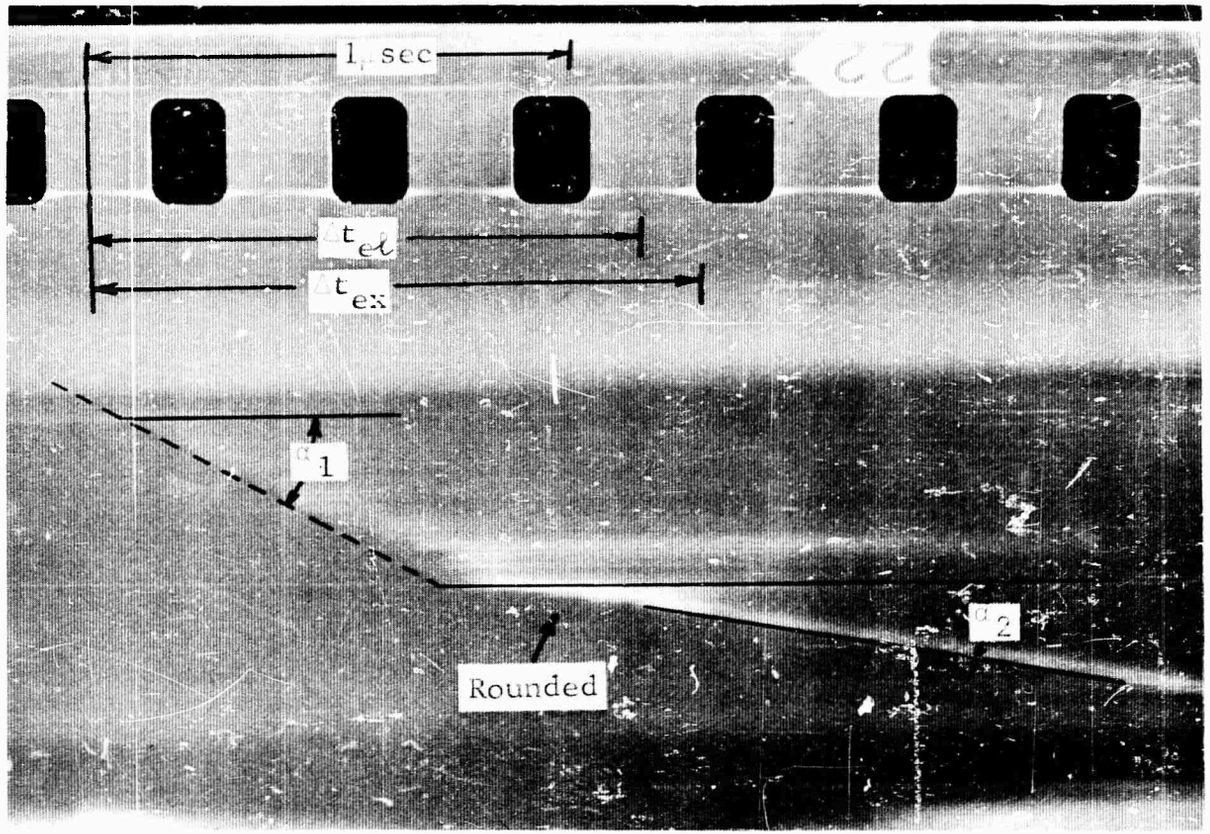

Figure 20 Sample Record of Configuration 18 Showing Precursor and 2nd Wave Velocity Angles α_1 and α_2, the Transit Times Measured from Electrical Pins Δt_{el} and Calculated from Velocity Angle Δt_{ex} (Note rounded appearance of free surface motion)

configuration is shown in Figure 21. In each experiment, five mineral samples were mounted in five pie-shaped segments of equal size. In addition, in each segment two witness materials, brass and aluminum, were mounted. Pin switches set just off the free surface were set to close at the time of free surface motion. Pin closure caused a condenser to discharge through a resistor and the associated voltage signal was displayed on an oscilloscope. On each oscilloscope trace, there were four signal inputs; one each from pins located to measure free surface motions of the mineral sample, the two witness materials and the buffer plate. The pin locations are shown in Figure 22; an oscilloscope trace is shown in Figure 23. The pertinent times are indicated by the sharp change in amplitude of the signal. Fairly good time resolution is made possible by a sweep speed of 0.5 cm per μsec and the signal generator trace located above and below each trace.

The various minerals of interest and several samples of granite were distributed among the eight experiments of this series so that each sample was subjected to a variety of stress levels. In Table III the samples included on each shot are listed as is the explosive and buffer configuration.

All of the minerals of interest were included in this series of experiments. Samples of orthoclase, labradorite, and oligoclase were cut and shock-loaded in two directions (referred to as B and C directions). These orientations are described in the next section. Single-crystal samples of olivine were not available for experiments so it was necessary to use polycrystalline or "isotropic" samples. A few samples of biotite were also included in this series. We were able to cut biotite only in one

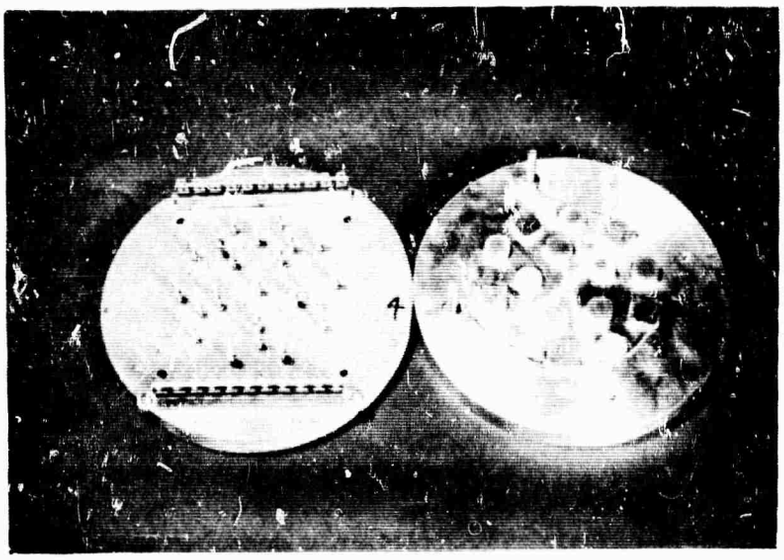

(a) Open View

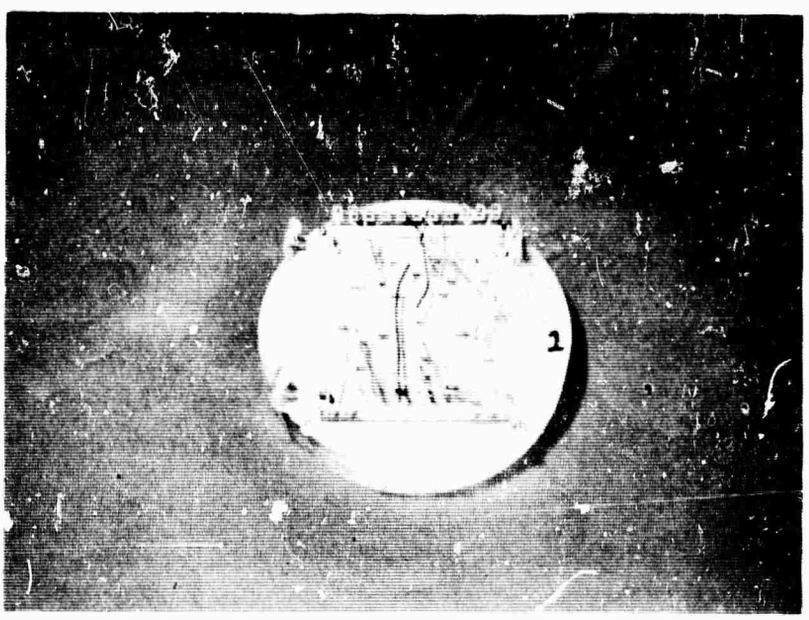

(b) Closed View

Figure 21 Configurations Snowing Mineral Samples (Square), Witness Materials (Round) in Open View (a) and Pins with Connections in Closed View (b)

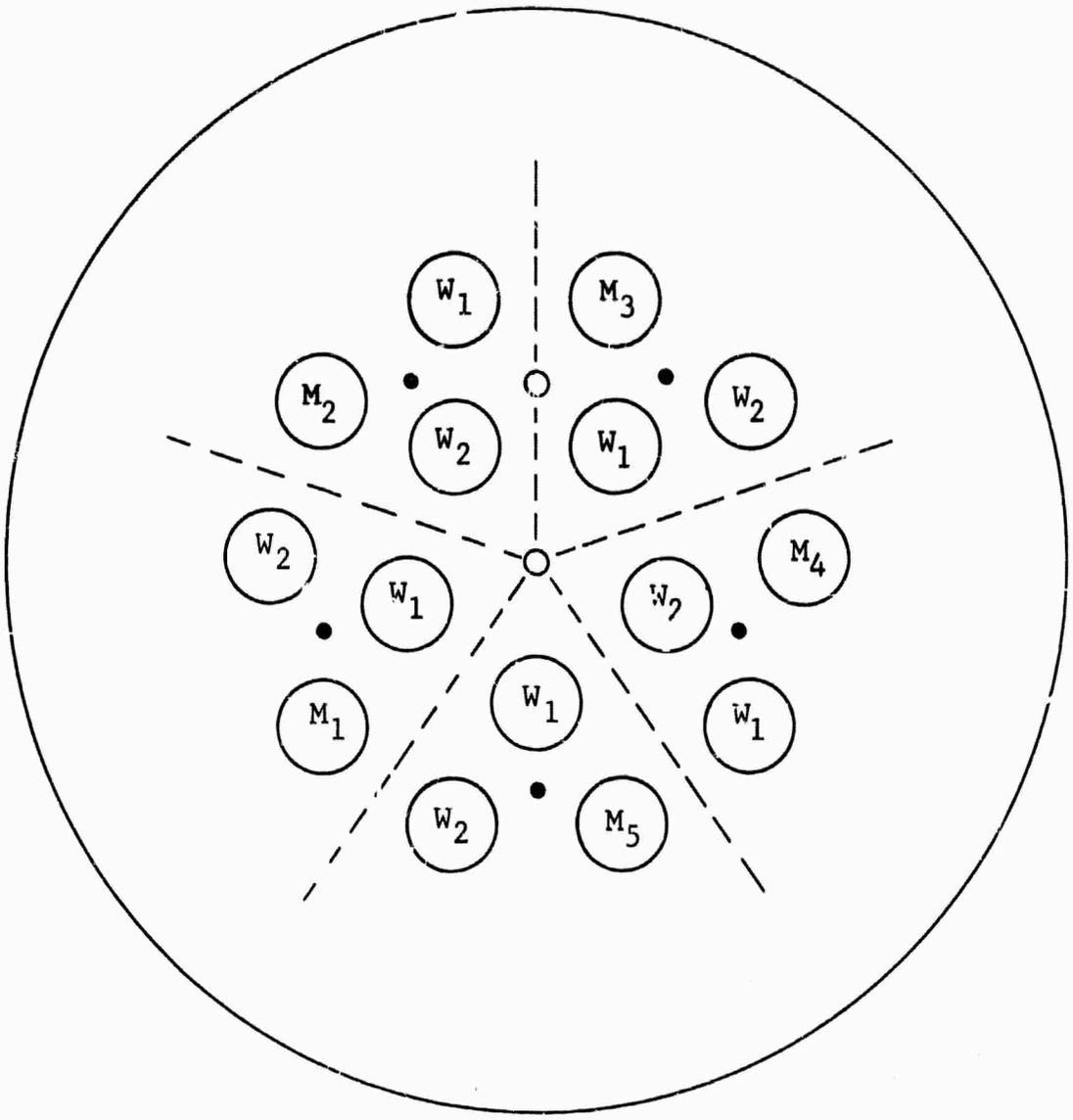

(a) Mineral and witness material locations

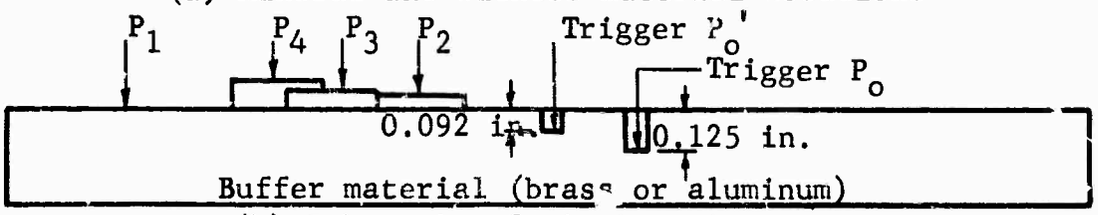

(b) Schematic of pin locations
P_o and P_o' trigger locations
P_1 buffer free surface
P_2-P_4 0.092 in. Al, 0.125 in. mineral, 0.155 in. brass free surface

Figure 22 Sample Configuration for Pin Experiments Showing Mineral and Witness (M_i and W_i) Material Locations (a) and Pin Locations P_i for One Segment and One Oscilloscope Trace

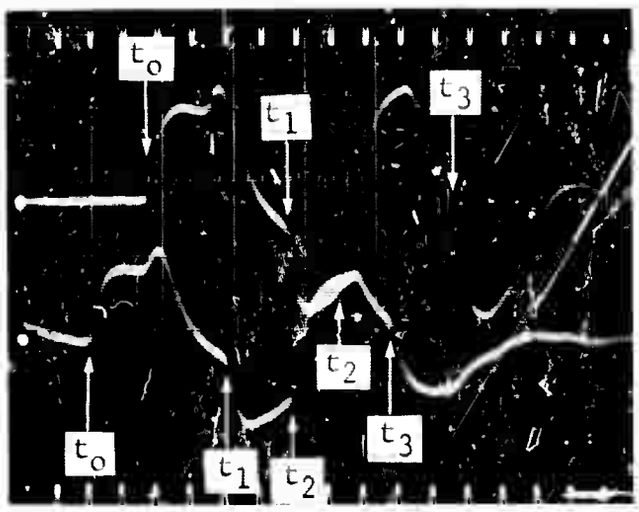

Figure 23 Oscilloscope Trace from Pin Instrumentation of Figure 22, Showing Times of Arrival at Buffer Plate Free Surface, t_o, at Aluminum Free Surface, t_1; at Mineral Free Surface t_2 and at Brass Free Surface, t_3 (Sweep speed 0.2 μsec/cm. Time marks are at intervals of 0.1 μsec)

Table III

SAMPLES INCLUDED IN PIN EXPERIMENTS

Shot No.	Explosive	Buffer Plate Material (0.500 in.)	Mineral Included in Shot								
			Orthoclase-C	Orthoclase-B	Oligoclase-C	Oligoclase-P	Labradorite-C	Labradorite-P	Olivine	Biotite	Granite
1	PWG	Al	X	X	X	X					X
2	P-60	Brass	X				X	X	X		X
3	P-60	Al		X	X	X	X			X	
4	P-60	Brass	X	X					X	X	X
5	P-60	Brass			X	X	X	X	X		
6	P-60	Al*	X		X				X	X	X
7	P-60	Al		X		X	X	X	X		
8	P-60	Brass	X		X		X		X		X

*0.125-in. Al flyer plate used; no data

direction. Thus, including several samples of granite, this series included nine sample types. The results are listed in Table IV.

C. Summary of Experimental Results

The Hugoniot data for the feldspars are subject to some interpretation. The elastic precursor of low amplitude is followed by plastic loading to the final state. The optical records indicate that, in some cases, the plastic loading is accomplished by a single shock wave while, in others, the plastic loading is accomplished by a compression fan. Schematics of these optical records are shown in Figure 24. In Figure 24(a) the elastic wave would be of very low amplitude and could be neglected with little error. The sample is essentially loaded by the plastic wave arriving at t_2. In Figure 24(b) there is evidence of a second elastic wave at t' and a plastic wave at t_2.

The location of t' and t_2 is very difficult and these records are in some cases indistinguishable from Figure 24(a) and (c). In Figure 24(c), there is evidence of shock loading by a compression fan. Because of the apparent zero free-surface velocity in Figure 24(c), records of this type were analyzed on the basis of a single loading wave. Interpretations of these records on the basis of a loading fan would require the type of analysis indicated in Appendix B, where a gradually increasing loading history is treated as if a series of plastic waves causes the loading. Although such an interpretation of all of the optical records, Figure 24(a), (b) and (c), might cause considerable changes in the final results, no such analysis has yet been attempted. Each

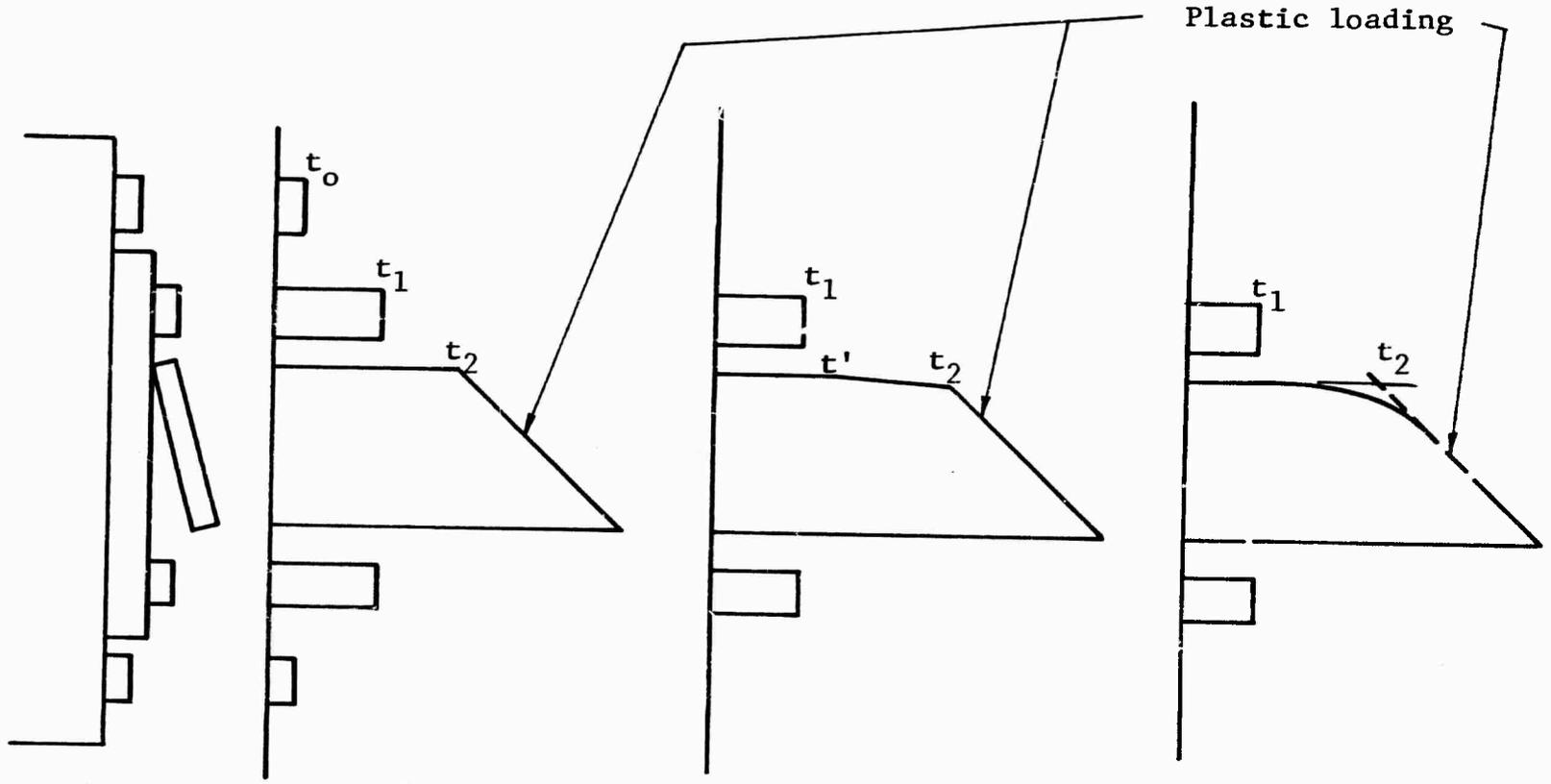

Configuration

(a) Record of sample with very low pressure precursor

(b) Record showing arrival of a second low pressure wave at t'

(c) Rounded record attributable to compression fan or elastic wave reverberations

Figure 24 Schematic Representation of Rotating Mirror Streak Records Occurring in Experiments on Feldspars

Table IV

RESULTS OF PIN EXPERIMENTS ON MINERALS (CONFIGURATION SHOWN IN FIGURE 22)

Exp. No.	Material	Crystal Direction (Fig. 29)	Density (gm/cc)	Explosive PWE	Explosive HE	Buffer Material	Sample Length (in.)	Shock Velocity (mm/μsec) Buffer	Shock Velocity (mm/μsec) Sample	Pressure (Kilobars)	Strain ε
1	Orthoclase	C	2.59	P-60	--	Al	0.128	6.70	6.22	173	0.171
2	Orthoclase	C	2.60	P-60	--	Brass	0.126	4.32	6.62	82	0.073
4	Orthoclase	C	2.59	P-60	2"B*	Brass	0.126	4.37	5.79	83	0.095
8	Orthoclase	C	2.59	P-60	4"B**	Brass	0.126	4.95	5.76	170	0.198
1	Orthoclase	B	2.58	P-60	--	Al	0.128	5.80	5.88	61	0.068
3	Orthoclase	B	2.60	P-60	--	Al	0.125	4.32	5.23	90	0.101
4	Orthoclase	B	2.59	P-60	2"B	Brass	0.126	4.90	5.22	146	0.209
7	Orthoclase	B	2.58	P-60	4"B	Al	0.125	7.38	5.80	248	0.284
1	Oligoclase	C	2.66	P-60	--	Al	0.126	6.21	6.01	111	0.115
3	Oligoclase	C	2.67	P-60	--	Brass	0.125	4.22	5.81	64	0.069
5	Oligoclase	C	2.67	P-60	2"B	Brass	0.125	4.84	6.30	164	0.155
8	Oligoclase	C	2.65	P-60	4"B	Brass	0.125	4.84	5.74	151	0.174
1	Oligoclase	P	2.66	P-60	--	Al	0.126	6.39	6.13	132	0.132
3	Oligoclase	P	2.67	P-60	--	Al	0.125	4.34	5.20	74	0.102
5	Oligoclase	P	2.68	P-60	2"B	Brass	0.125	5.15	5.96	208	0.220
7	Oligoclase	P	2.68	P-60	4"B	Al	0.125	8.00	5.64	326	0.386
2	Labradorite	C	2.74	P-60	--	Brass	0.125	4.22	5.35	60	0.077
3	Labradorite	C	2.72	P-60	--	Brass	0.126	4.49	5.59	102	0.120
5	Labradorite	C	2.72	P-60	2"B	Brass	0.126	4.84	5.78	156	0.171
7	Labradorite	C	2.72	P-60	4"B	Al	0.125	8.14	5.55	351	0.418
8	Labradorite	C	2.71	P-60	4"B	Brass	0.125	5.25	5.65	228	0.265
2	Labradorite	P	2.74	P-60	--	Brass	0.125	4.32	5.54	78	0.092
5	Labradorite	P	2.73	P-60	2"B	Brass	0.125	5.15	6.20	217	0.208
7	Labradorite	P	2.74	P-60	4"B	Al	0.125	7.16	5.84	230	0.247
2	Olivine+	polycryst.	3.24	P-60	--	Brass	0.126	4.59	5.55	126	0.126
4	Olivine	polycryst.	3.22	P-60	2"B	Brass	0.124	4.90	6.38	201	0.152
5	Olivine	polycryst.	3.21	P-60	2"B	Brass	0.126	5.10	7.20	262	0.158
7	Olivine	polycryst.	3.22	P-60	4"B	Al	0.125	6.95	7.15	246	0.151
8	Olivine	polycryst.	3.26	P-60	4"B	Brass	0.126	5.03	6.24	222	0.180
3	Biotite++	--	3.11	P-60	--	Brass	0.0425	4.54	1.77	48	0.492
4	Biotite	--	3.17	P-60	2"B	Brass	0.0430	4.78	2.24	78	0.580

*2-in.-thick, 6-in.-diam comp B
**4-in.-thick, 6-in.-diam comp B
+Only polycrystalline samples were used
++Shock propagation direction was perpendicular to cleavage plane

of the records was considered as if one plastic wave arriving at t_2 resulted in the final state manifested in the final free surface velocity. This interpretation was consistent with the impedance match (the pin) experiments valid only for single wave sample loading.

At first it was anticipated that the double shock wave system ordinarily associated with a Hugoniot with a sharp yield point would lead to a sharp discontinuity in the observed free-surface velocity. As mentioned in the discussion of Table I, the sharpness of the transition is a function of the separation between the two waves. In any case, some rounding, associated with the elastic wave reverberations, would be expected. This rounding was especially apparent in the record of Figure 17. For the same configuration, a slower camera speed would tend to give the impression of a sharp discontinuity. On the other hand, a higher camera speed combined with greater light intensity and perhaps a narrower slit width might enhance the time resolution to the point where the reverberation details are apparent. Neither extreme was obtained in this study.

The methods of analysis adopted for the reduction of the optical records are admittedly a practical compromise between the rather arbitrary choice of an intermediate arrival time for the plastic wave and the more general graphical iteration shown in Appendix B. The choice of the arrival time of the plastic wave between the two extremes, the arrival time of the elastic wave and the time at which the final free surface velocity is achieved, has profound influence on the calculated yield point. The

graphical method was attempted on several records where rounding was noticed. Even the graphical method was unsatisfactory for the times and free surface velocities involved here. A simple computer calculation would be best but was not attempted on these records.

1. Hugoniot Curves

The results of the optical and combination optical and electrical experiments (Table II) and of the pin experiments (Table IV) are combined into the Hugoniot curves plotted in pressure-strain coordinates in Figures 25, 26, 27 and 28. In these figures data are listed for two crystal orientations. These orientations are the same as those listed in Figures 10 and 16 and Tables II, III, and IV.

In the Hugoniot curves for orthoclase, labradorite and olivine, a yield point is depicted. The location of this yield point has been inferred from only one record thus far. The method of analysis described obviously precludes the possibility of such yield-point determination. Nevertheless, Hugoniot data for composites made up of these minerals, notably granite (Ref.9, 10, 12), indicate the presence of a yield point at about 50 kilobars. The yield points for orthoclase, labradorite and olivine are based on a rough approximation using the hydrostatic compressibility data of Bridgman (Ref. 19) and the low pressure shear data of reference 20.

All of the synthesis work was based on the experimental Hugoniots of Figures 25, 26, 27 and 28. It is hoped that a more complete future analysis of the data could be based on a

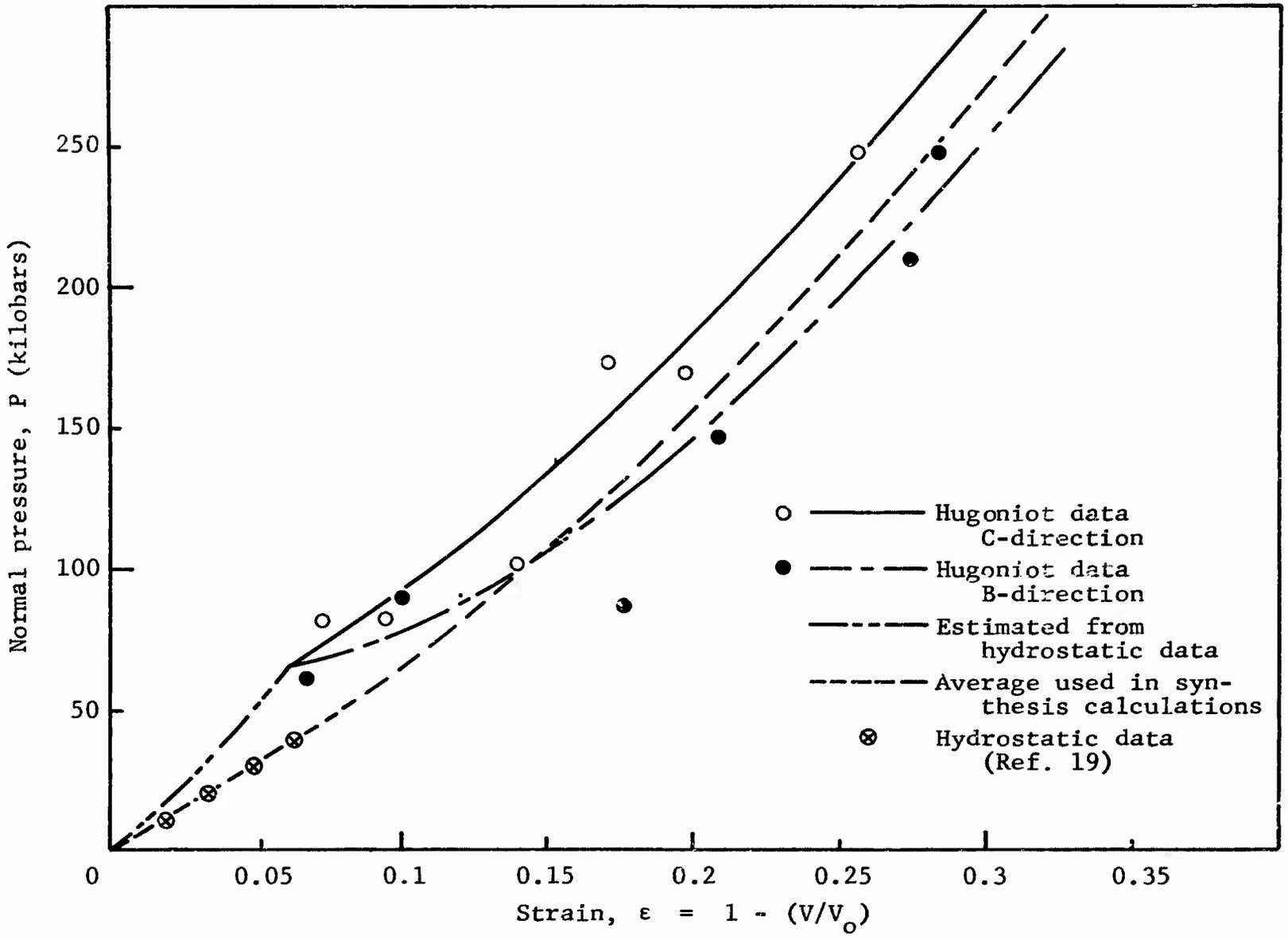

Figure 25 Hugoniot Curve for Orthoclase Showing Average Used in Synthesis Calculations

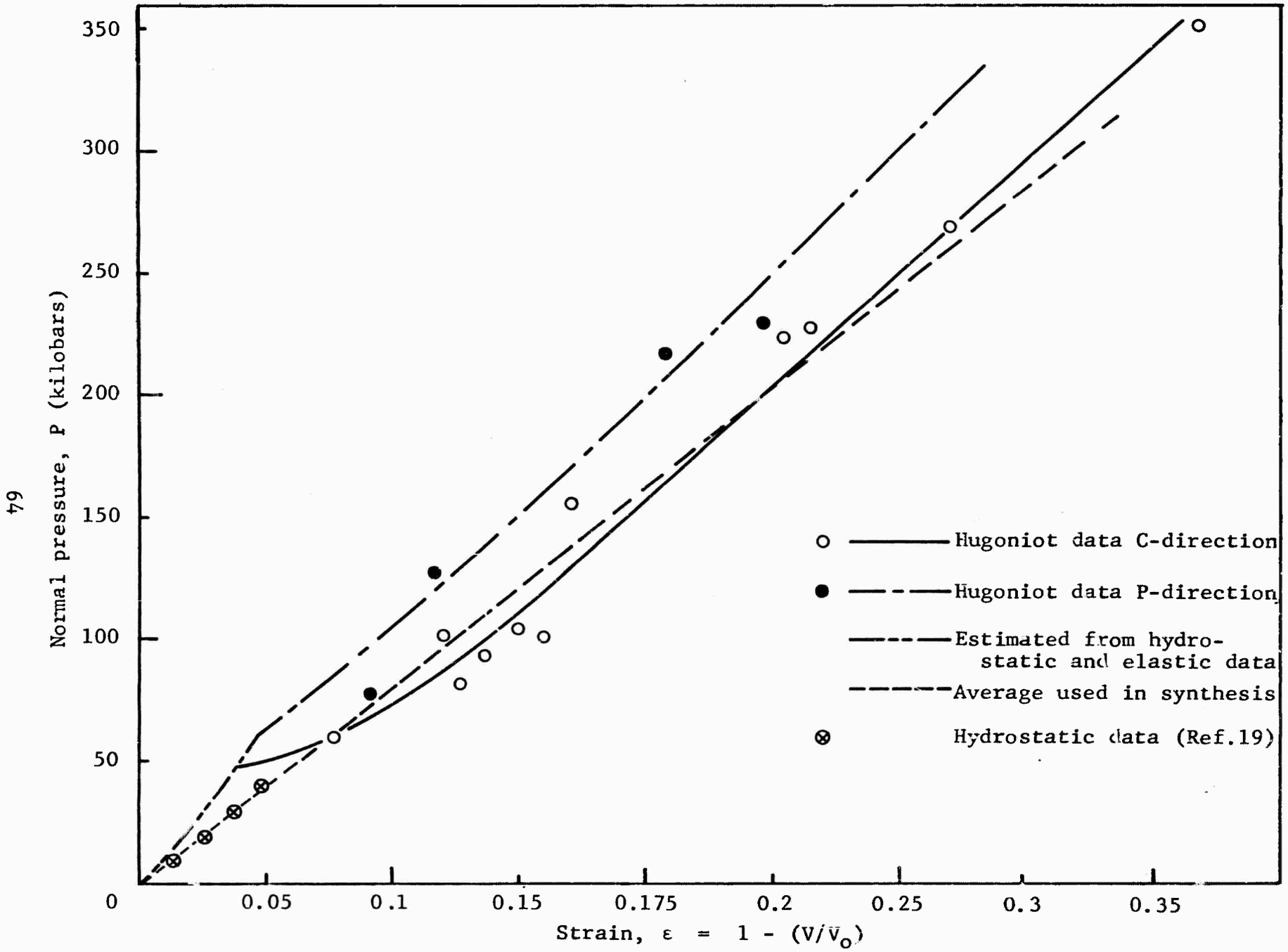

Figure 26. Hugoniot Curve for Labradorite Showing Average Used in Synthesis Calculations

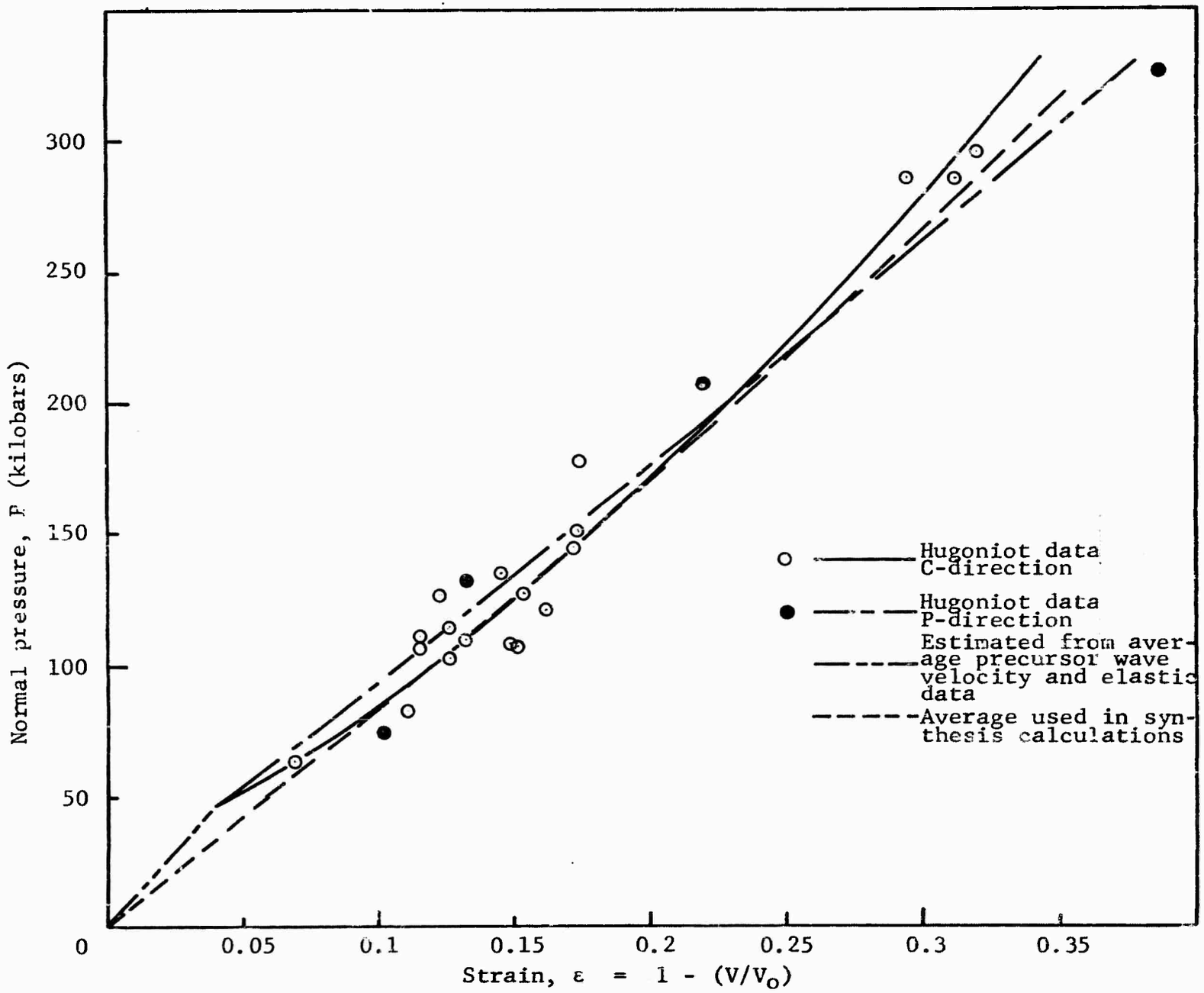

Figure 27 Hugoniot Curve for Oligoclase Showing Average Used in Synthesis Calculations

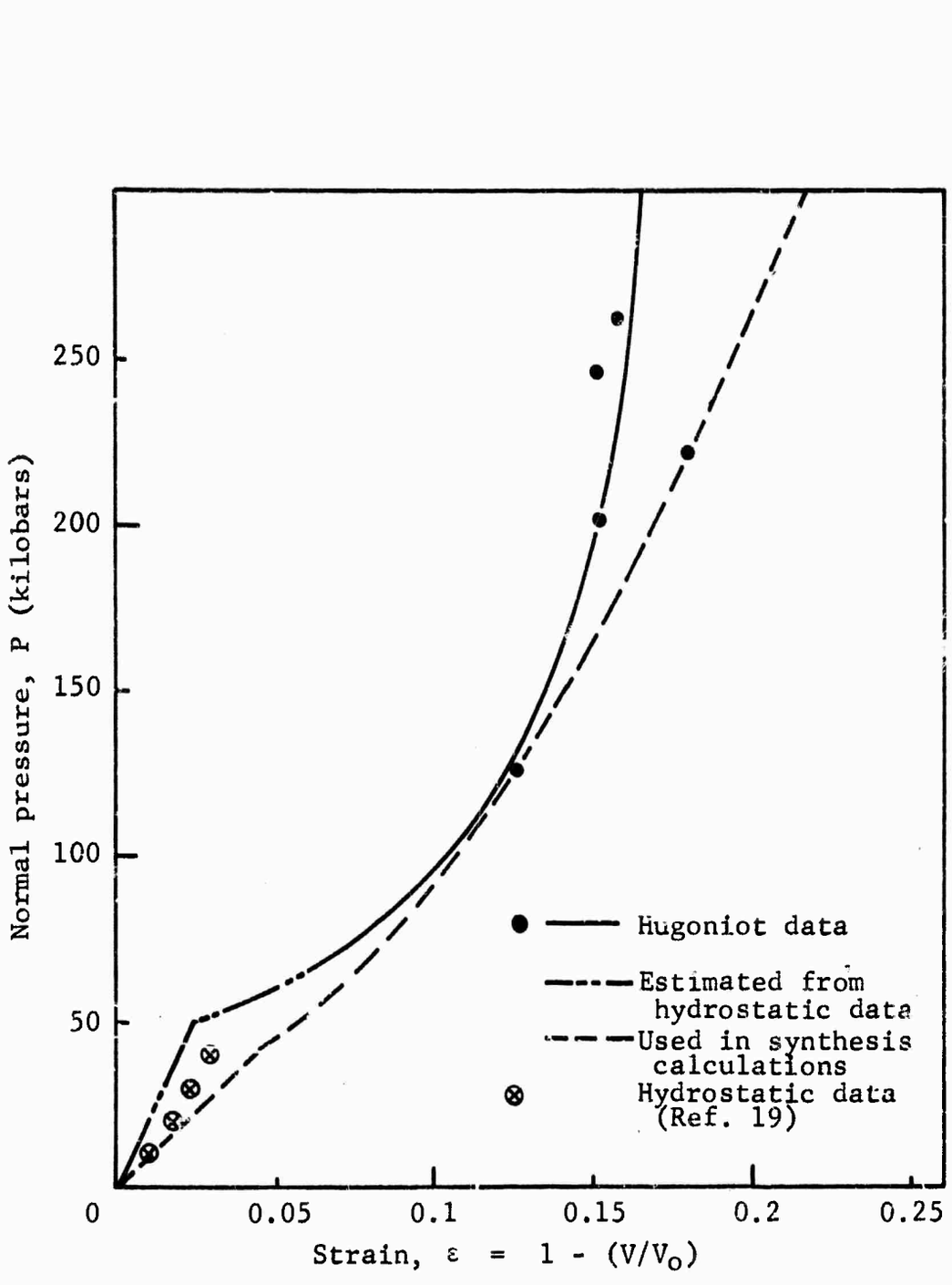

Figure 28 Hugoniot Data for Polycrystalline Olivine

computerized solution of the multiwave structure depicted by Figure 24. It is noted graphically that the Hugoniots in figures show yield at about 50 kilobars. This interpretation is the result of synthesis calculations on measured bulk compressibilities and shear moduli but not directly on the measured data.

2. Crystal Orientation

In Figure 29, a crystal of orthoclase is shown. Although orthoclase is monoclinic while the plagioclases are triclinic, the two are similar because the triclinic angles between the a and b and b and c crystal axes are close to 90 deg. Therefore, in defining orientation, Figure 28 may be considered applicable to all of the feldspars studied. All have good cleavage parallel to the c-pinicoid which lies in the plane of the a and b crystal axes. This cleavage plane was easily recognized in all of our samples. In addition, many of our orthoclase samples were cut from a single crystal of orthoclase in which all of the pinicoids and crystal directions were fairly easily determined. Consequently, all feldspar samples included those cut parallel to the c-pinicoid. These samples were mounted so that the shock propagation direction was perpendicular to the c-pinicoid, as shown on the left in Figure 29. All samples oriented in this way are listed in the data tables as the C-direction.

For orthoclase, samples were also cut parallel to the b-pinicoid (Figure 29): These are listed as B-orientations. Samples of labradorite and oligoclase were not of a size or crystal completeness that facilitated identification of any but the c-pinicoids. These numerals were cut and mounted, therefore, so

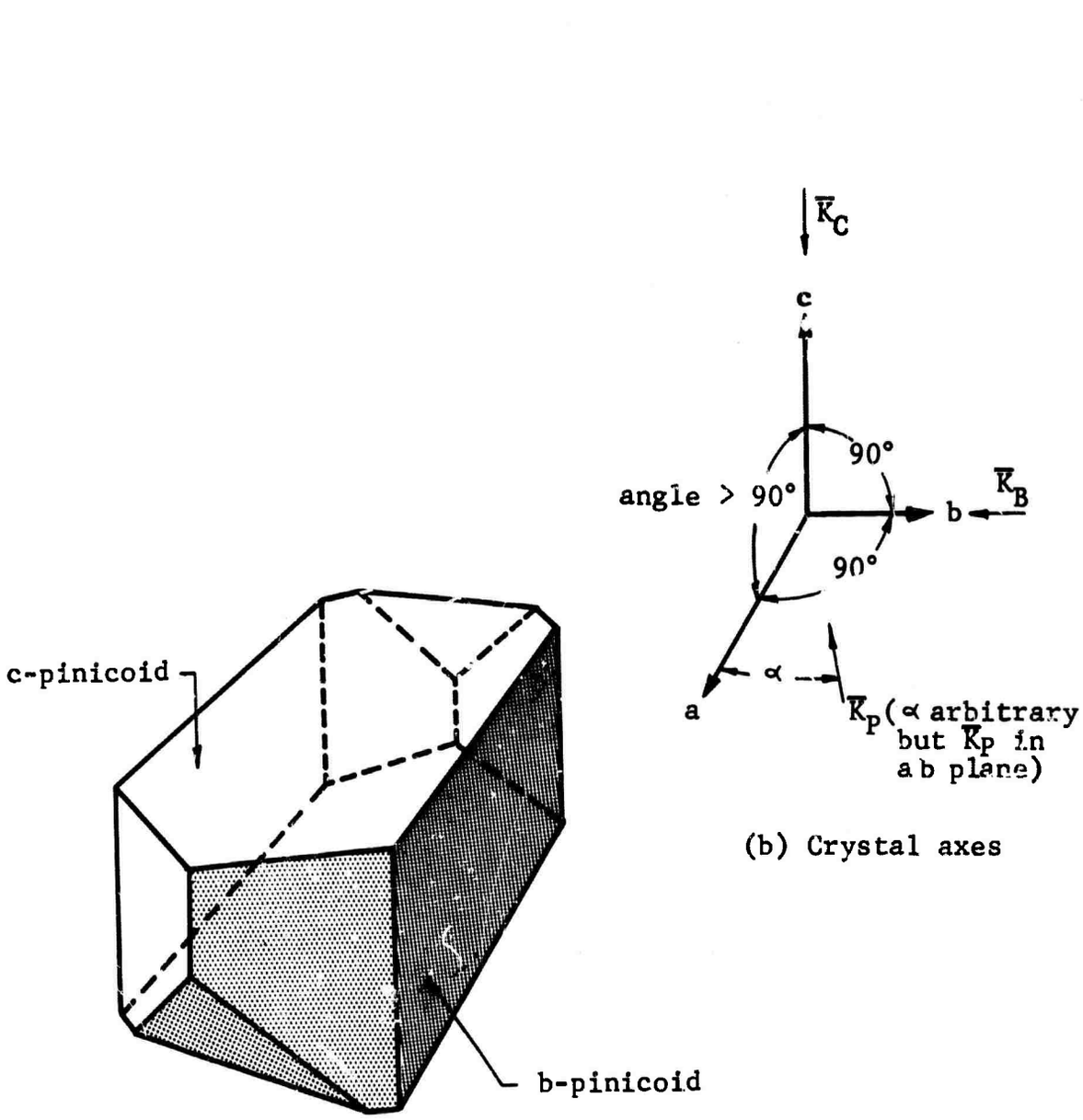

(b) Crystal axes

(a) Monoclinic crystal

Figure 29 Monoclinic Crystal (a) Showing b- and c-pinicoids and Monoclinic Axes (b) Showing Shock Propagation Directions $\overline{K}_C$, $\overline{K}_B$, and $\overline{K}_P$ for Crystal Orientations Listed in Tables II and III as C, B, and P Respectively

that the shock propagation direction was in the plane formed by the a and b crystal axes, but otherwise arbitrary. Such orientations are labeled with the symbol P to indicate the parallel direction. This arbitrariness may indeed be partially responsible for some of the scatter in the observed values of the elastic wave velocities in these samples. Ultrasonic measurements have shown that in crystals of labradorite and oligoclase the values of the longitudinal elastic velocities are significantly dependent on the crystal orientation (Ref. 21). Those values are not reproduced here because of difficulties in determining the meaning of the orientations used in that work.

3. Yield Point Approximation

The preceding discussion of the Hugoniot data and the interpretation of that data are not consistent with the location of the yield points shown in Figures 25, 26 and 27. Nevertheless, certain other factors must also be considered. The basic objective in obtaining these mineral data is to test the synthesis hypothesis. The feldspars and olivine chosen for investigation are all constituents of granite, which is believed to exhibit a dynamic yield point at about 50 kilobars (Figure 30). It is reasoned that this yield point must be manifested as a result of similar yielding of its mineral constituents, individually or in combination in the granite composite. Furthermore, the location of these yield points, which is somehow not apparent from the shock data, is implied from extrapolation of the hydrostatic compression data of Bridgman (Ref. 19) and ultrasonic measurements of the longitudinal velocities of several of the crystals (Ref. 21).

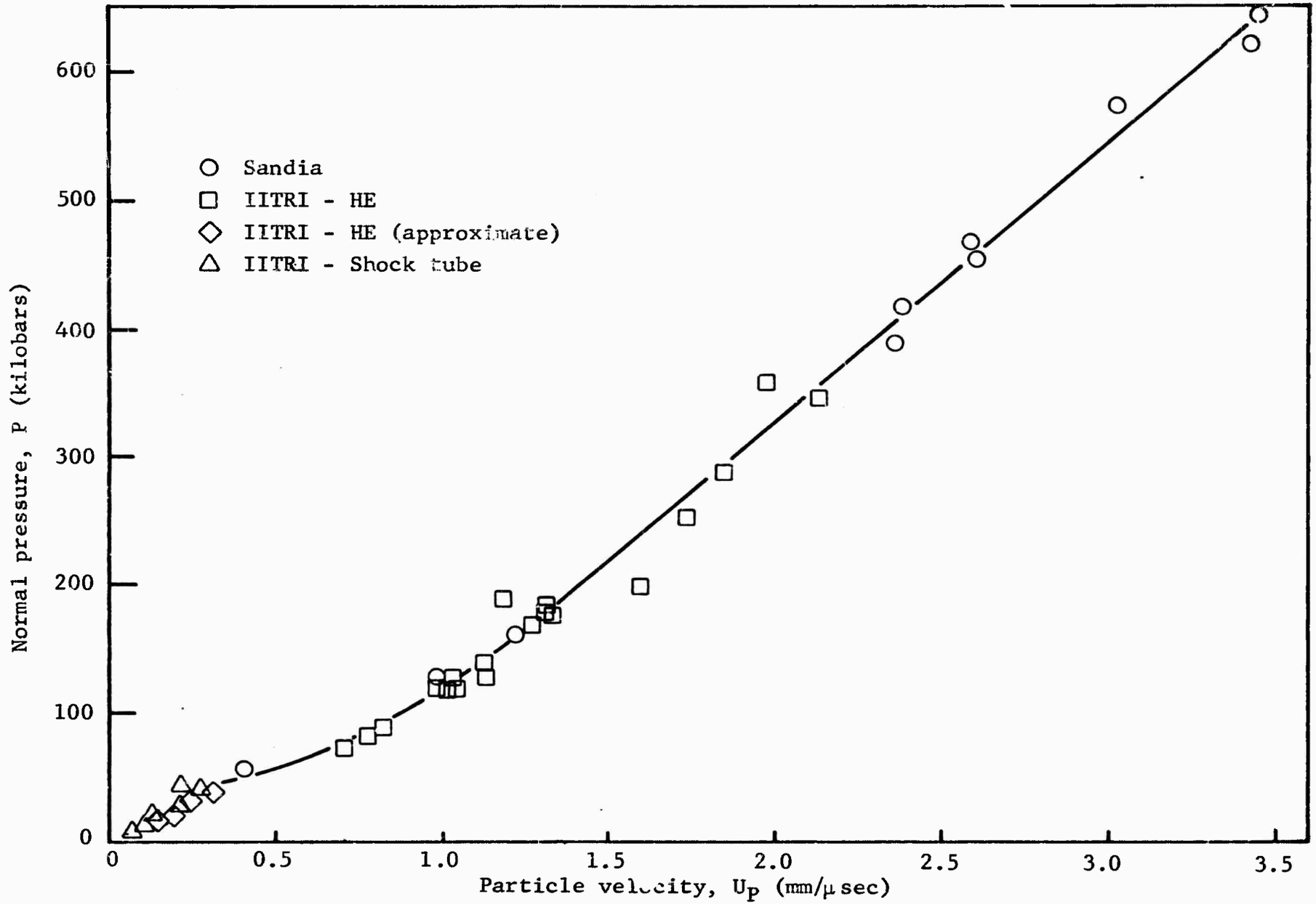

Figure 30 Granodiorite Hugoniot Data Taken from References 9 and 12

In reference 9 two viewing methods are listed. The side viewing method is less approximate at low pressure. The presence of dynamic yield at 50 kilobars is indicated.

The longitudinal velocity in a direction perpendicular to the c-pinicoid was found to be 7.53 mm per μsec for labradorite, and 6.8 mm per μsec for oligoclase (Ref. 21). In a direction perpendicular to the normal to the c-pinicoid, the average velocity was 6.90 mm per μsec for labradorite and 6.77 mm per μsec for oligoclase. These velocities are associated with linear elastic stress-strain lines in Figures 26 and 27. These lines are of slope $P/\varepsilon = \rho_o C^2$, where C is the appropriate elastic velocity. These lines of constant slope have then been extended to the extrapolated lower end of the experimental Hugoniot curve.

The hydrostatic compression data of Bridgman for orthoclase, labradorite and olivine have been plotted in Figures 25, 26 and 28. To roughly establish a yield point for these materials, these hydrostatic data were used as a basis for calculating the equivalent normal stress associated with shock or uniaxial strain. For further convenience this calculation was based on the isotropic stress-strain relationship (Ref. 1)

$$\tau_{ij} = 2\mu\varepsilon_{ij} + \lambda(\varepsilon_{11} + \varepsilon_{22} + \varepsilon_{33})\delta_{ij} \qquad (15)$$

where τ_{ij} is the stress tensor and ε_{ij} the strain tensor. Although the Lamé constants λ and μ can be associated with isotropic materials only, there is an equivalent λ and μ for a polycrystalline material of lower symmetry. As in reference 1, equation (15) may be used to establish the relationship between the hydrostatic and uniaxial compression states:

$$P_{1-d} = P_{hyd} + 2\mu \frac{\Delta V}{V} . \qquad (16)$$

For values of μ taken from Birch (Ref. 8) this correction has been applied to the hydrostatic data. The yield points estimated in this way are intended to give an average value of the Hugoniots of the minerals, and apply only to a quasi-isotropic material made up of many crystals in intimate contact and random orientation.

Each of the mineral Hugoniots in Figures 25, 26, 27 and 28 consists of two parts,

(1) an upper (dashed) portion representing the average between the two orientations investigated experimentally, and

(2) a lower portion representing the elastic zone estimated from either hydrostatic or ultrasonic measurements.

The Hugoniots made up of these two parts have been tabulated and used for the composite synthesis calculations.

Obviously, the question of yielding in these minerals is by no means settled. Additional experiments in the region close to the yield point, where the greatest difference between the plastic and elastic velocities might be found, are required. In addition, more detailed analysis of some of the optical records exhibiting "rounding" will be informative and especially so when more low pressure data are available.

One obvious question regarding the interpretation of the experimental records relates to the absence of the high pressures associated with the yield points. From optical records, such as those of Figure 20, it is implied that the upper shock state is connected by a single chord to a low-pressure state. Such a

situation is shown schematically in Figure 31. If such a representation pertained, one would expect the lower plastic velocity to be associated with the higher pressure state as is implied by shots 40 and 41 on Table II.

P_{YP} = Hypothetical yield point implied from hydrostatic and ultrasonic experiments

$P_2 + P_2'$ = High pressure states $P_2' > P_2$ (analogous to shots 41-44)

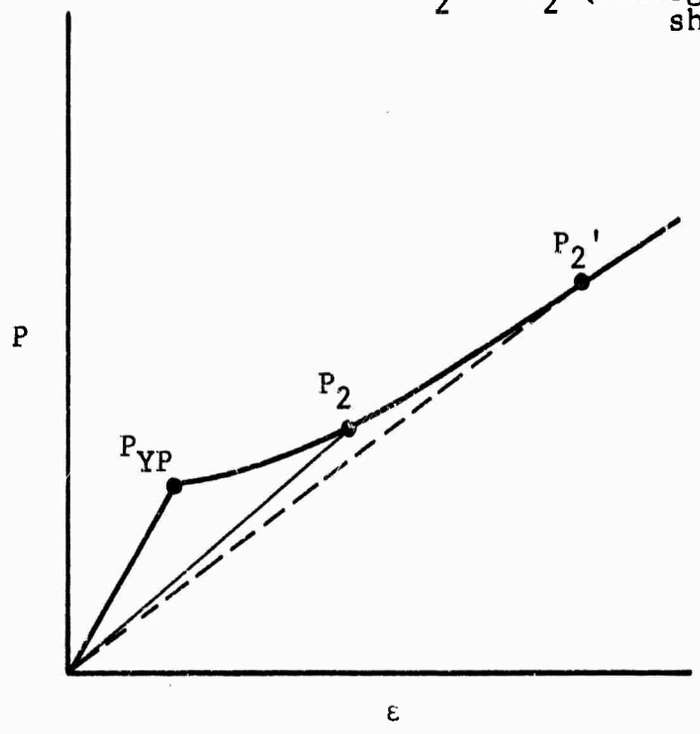

Figure 31 Schematic Representation of Shock Compression to State (P_2, ε_2), Where $P_2 > P_{YP}$, Indicating Dynamic Yield Pressure Is Very Low

IV SYNTHESIS OF COMPOSITE HUGONIOT

A. Advantages of the Synthesis Method

The usual methods for determining the shock-loading or Hugoniot characteristics of a material are quite extensive and costly. These methods involve laboratory and field experiments of the type described in the last section. Customarily, each material for which the dynamic properties are desired is analyzed. In some cases, although a new material is similar in composition to another material previously investigated, no real advantage is taken of this similarity. The over-all goal of the synthesis program is to devise a method by which the similarities of naturally occurring geological samples may be used to simplify the job of determining the dynamic properties.

As an example, consider the similarity in composition of the principal types of igneous rocks. Table V lists the mineral constituents (Ref. 24). Each of the rocks is made up of various percentages of the 14 minerals listed. Ideally, the synthesis method would be applied to this system as follows:

(1) Analyze a new rock to determine the mass percentages of the various minerals present.

(2) Use the known properties of the minerals--their Hugoniots--to synthesize the Hugoniot of the composite. The advantage of the synthesis scheme is that it would no longer be necessary to carry out the extensive experimentation for every new material.

Table V

APPROXIMATE MINERAL COMPOSITIONS OF PRINCIPAL TYPES OF IGNEOUS ROCKS (Ref. 24)

Constituent	Granite	Syenite	Grano-diorite	Quartz diorite	Diorite	Gabbro	Olivine diabase	Dia-base	Dunite
Quartz	25%		21	20	2				
Orthoclase and Microperthite	40	72	15	6	3				
Oligoclase	26	12							
Andesine			46	56	64				
Labradorite						65	63	62	
Biotite	5	2	3	4	5	1		1	
Amphibole	1	7	13	8	12	3		1	
Orthopyroxene				1	3	6			2
Clinopyroxene		4		3	8	14	21	29	
Olivine						7	12	3	95
Magnetite	2	2	1	2	2	2	2	2	3
Ilmenite	1	1				2	2	2	
Apatite	tr	tr	tr	tr	tr				
Sphene	tr	tr	1	tr	tr				

A major effort on this program was to generate sufficient mineral Hugoniot data to test the feasibility of the proposed synthesis method. Contrary to the earlier synthesis work of Porzel (Ref. 22) and Chabai (Ref. 23), it was intended here to use known dynamic properties of the mineral constituents to predict the properties of composites (here, igneous rocks) made up of these constituent minerals. The experimentally determined Hugoniots to be used in the synthesis are represented by the dashed lines in Figures 25-28. The Hugoniot of a fifth mineral studied, biotite, was incompletely determined and not useful in these synthesis calculations because of the low stress levels attained. The stress level or pressure attained in a given experiment is a function of the material itself. The properties of biotite are such that, for the loading method used in these experiments, only ~100 kilobars was reached, compared with pressures of ~300 kilobars reached in the other materials.

To test a synthesis method on rocks of known properties, the Hugoniot of quartz was also needed. The data for quartz from references 15 and 25 are plotted in Figure 32. Data were reported for three orientations of quartz and also for fused quartz. Only the average Hugoniot is shown in Figure 32. In this first attempt at synthesis, only one curve for each mineral was required; the dashed line in Figures 25, 26, 27, 28 and 32 represents the "average" Hugoniot for the various orientations.

B. Synthesis Methods

Two methods of synthesis were attempted in this analysis. The first, or "direct," method applies the known mineral Hugoniot

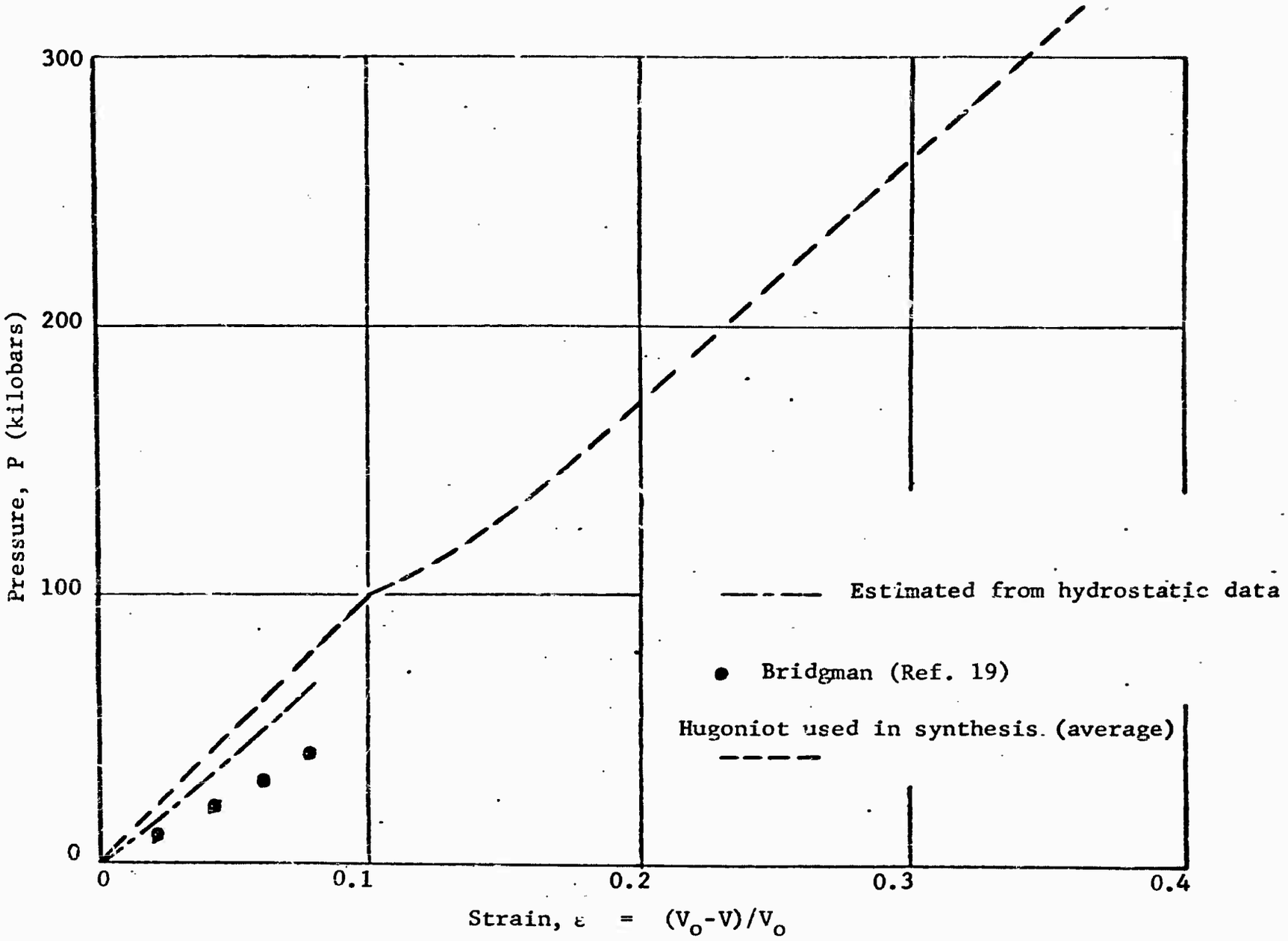

Figure 32 Hugoniot Curve for Quartz Showing Average Used in Synthesis

data to the determination of unknown composite Hugoniot determination. The equations used are those reflecting the law of partial volumes. In the synthesis relationship, the partial volume of a mineral is taken to be the final volume after shock loading to the high pressure state. A more detailed review of some of the differences between the static and dynamic multicomponent model are outlined in Appendix B. In the second, or "indirect," method, both known mineral and composite Hugoniot data are used to generate the Hugoniots of unknown composite materials. The same synthesis equations are used in this method.

1. Application of Law of Partial Volumes

For a series of N mineral constituents making up an igneous composite of volume V_c,

$$V_c = \sum_n^N V_n$$

where V_n is the volume of the n^{th} mineral constituent.
Since

$$V_c = M v_c$$

where M is the composite mass and v_c the specific volume of the composite, and

$$V_n = M_n v_n$$

where M_n is the mass of the n^{th} mineral in the composite and v_n its specific volume,

$$v_c = \sum_n^N \frac{M_n}{M} v_n = \sum_n^N a_n v_n \qquad (17)$$

where $a_n = M_n/M$ is the mass ratio of the n^{th} mineral contained in the rock. It is evident that $\sum_n^N a_n = 1$ and a_n are the percentages in Table V. Equation (17) may be applied at each pressure or stress level of interest, and may also be thought of as representing a mass-weighted averaging technique.

2. Direct Synthesis Method

As may be seen from equation (17), an adequate test of this simplified synthesis model requires a knowledge of the shock-loading characteristics of the rock, its mineral constituents, and the minerals' mass fractions, a_n. For many of the materials for which Hugoniot data have been published, mineral or petrographic analyses sufficient for our purposes have not been made. In some cases it is necessary to resort to the average listing of mineral percentages (Table V). Use of equation (17) requires Hugoniot data to be in terms of specific volume and pressure. Pressure-volume Hugoniot data are shown in Table VI for several composites and in Table VII for several minerals. The values of a_n used for the Shoal granite are taken from reference 26. These values of the mass fractions a_n specify granodiorite rather than granite.

A schematic representation of the synthesis of an arbitrary material is provided in the third figure of reference 27. The results of the synthesis method using equation (17) and the values of the compressed volumes from Table VII are shown in Figure 33. The mass fractions a_n used in the synthesis are based on those given in references 26 and 28 for granodiorite and basalt, respectively. These values were modified to include only those minerals

Table VI

HUGONIOT DATA (COMPRESSED SPECIFIC VOLUMES) FOR IGNEOUS ROCKS
(USED IN EQUATION 20 FOR RESULTS IN FIGURE 34)

Pressure (kilobars)	Granite (Ref. 10)	Granodiorite (Ref. 12)	Gabbro (Ref. 29)	Dunite (Ref. 29)
300	0.246	0.258	0.246	0.252
250	0.266	0.276	0.260	0.259
200	0.286	0.294	0.275	0.268
150	0.306	0.313	0.289	0.276
100	0.327	0.332	0.304	0.286
50	0.348	0.352	0.318	0.296
0	0.372	0.372	0.333	0.308

Table VII

HUGONIOT DATA (COMPRESSED SPECIFIC VOLUMES) FOR SEVERAL
MINERAL CONSTITUENTS OF IGNEOUS ROCKS
(USED IN EQUATIONS 17 AND 20 FOR RESULTS IN FIGURES 33 AND 34)

Pressure (kilobars)	Quartz (Ref.2,3)	Orthoclase*	Oligoclase*	Labradorite*	Olivine*
300	0.248	0.264	0.251	0.232	0.245
250	0.268	0.279	0.271	0.254	0.251
200	0.288	0.296	0.291	0.277	0.259
150	0.309	0.314	0.311	0.300	0.268
100	0.323	0.335	0.332	0.324	0.280
50	0.342	0.359	0.354	0.346	0.298
0	0.375	0.390	0.377	0.369	0.312

*Volumes for these materials were taken from the early results of experiments in this program

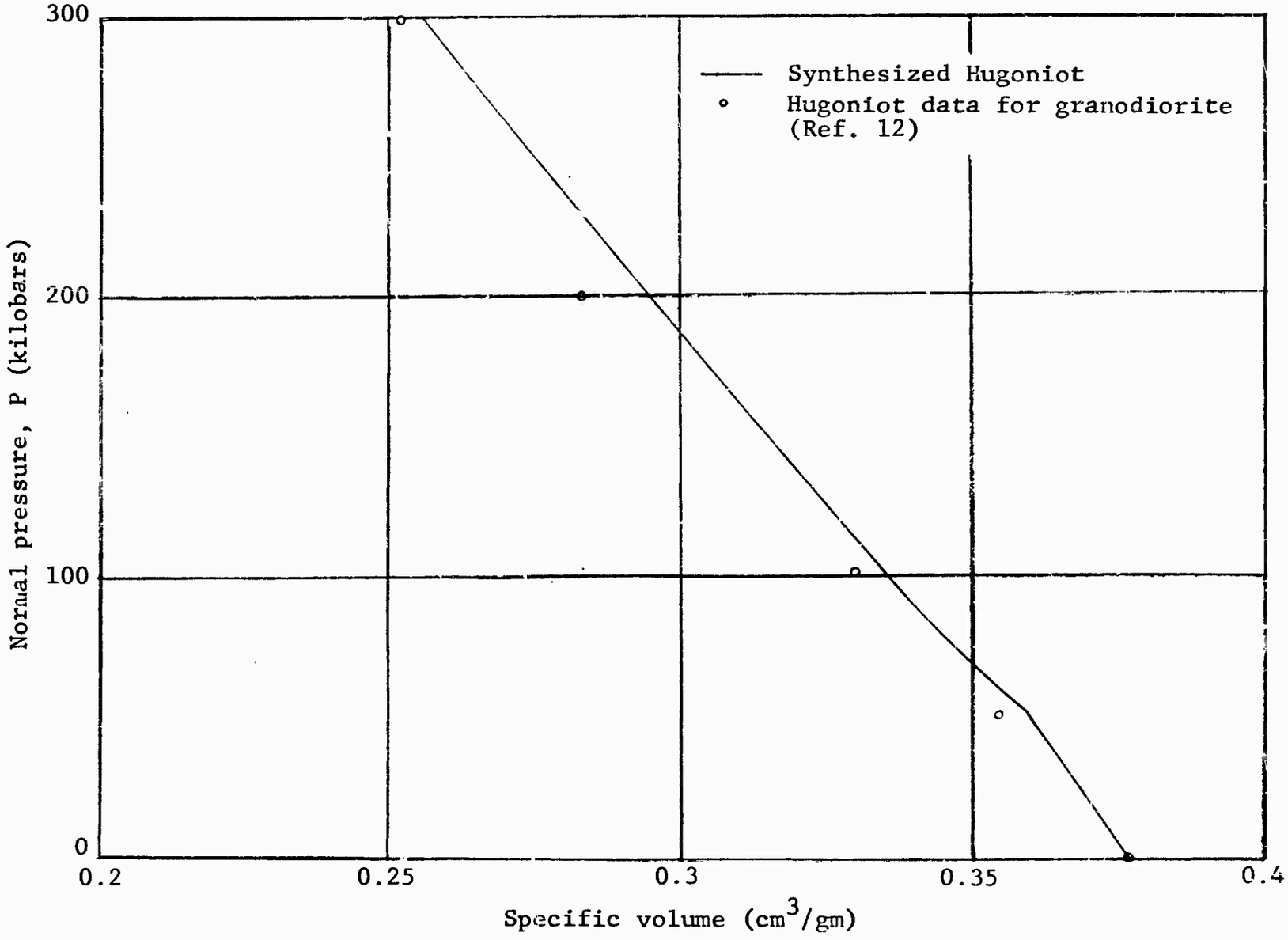

Figure 33(a) Comparison of Synthesized Hugoniot with Experimental Data for Granodiorite (Synthesis based on mineral Hugoniot data of quartz, labradorite and orthoclase)

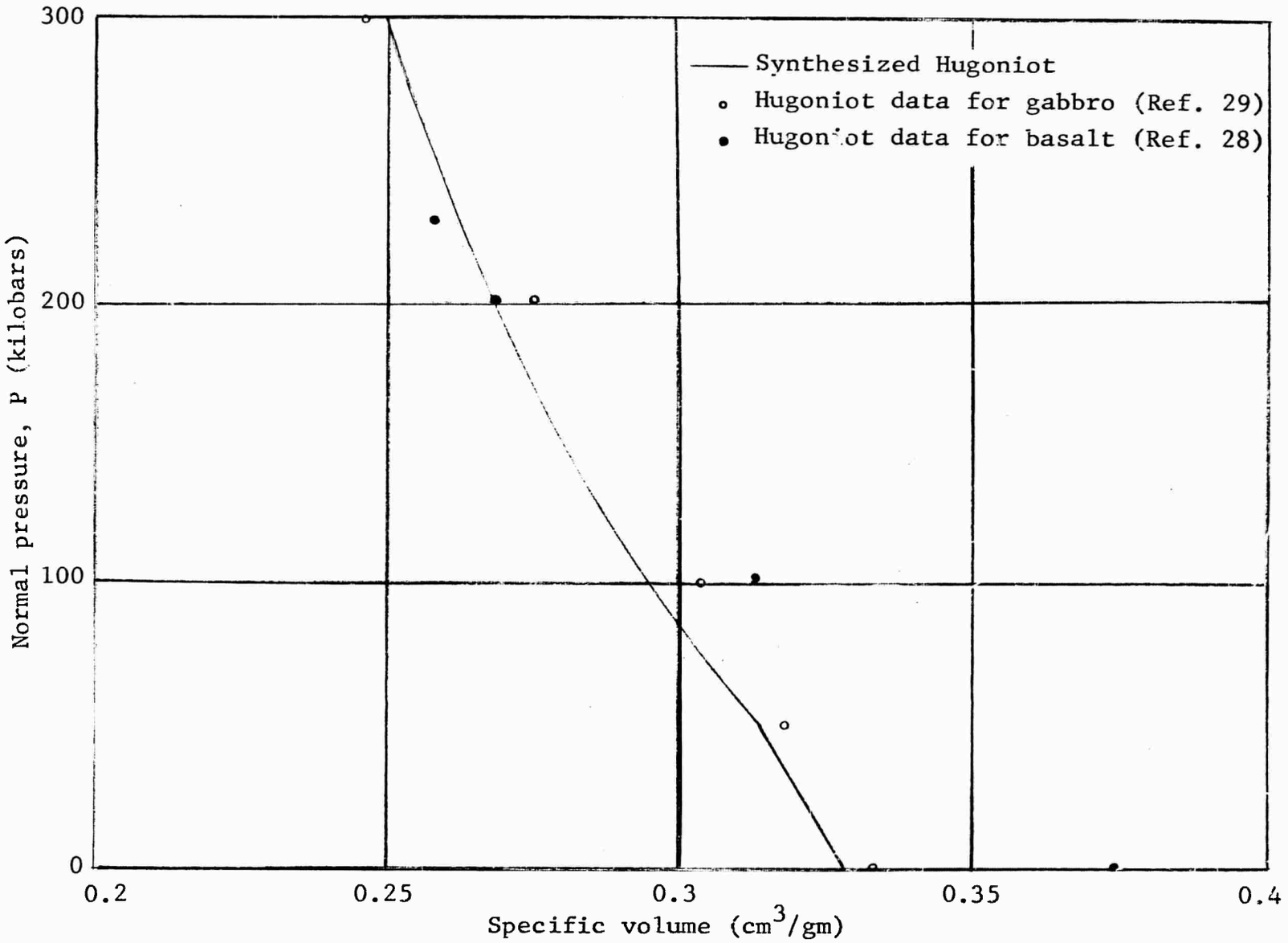

Figure 33(b) Comparison of Synthesized Hugoniot with Experimental Data for Gabbro and Basalt (Synthesis based on mineral Hugoniot data of labradorite and olivine)

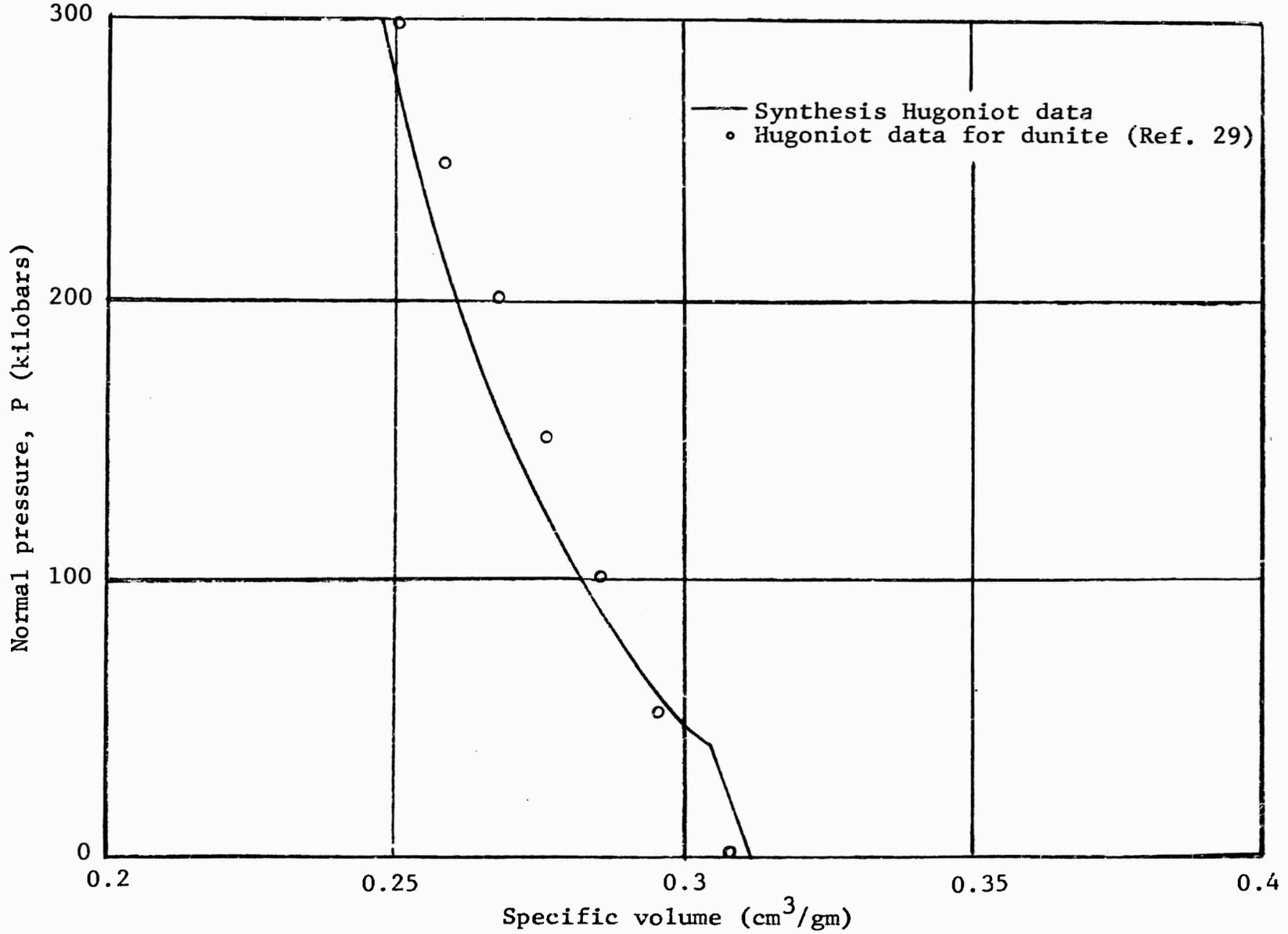

Figure 33(c) Comparison of Synthesized Hugoniot with Experimental Data for Dunite (Synthesis based on mineral Hugoniot data for olivine)

listed in Table VII for which Hugoniot data exist. In addition, the relationship $\Sigma a_n = 1.0$ was satisfied. The experimentally obtained Hugoniots for the composites synthesized are also shown in Figure 33. Two sets of Hugoniot data are shown for basalt and gabbro. One set corresponds to that of reference 28, the other to that of reference 29.

3. Indirect Synthesis Method

Hugoniot synthesis may be accomplished in a somewhat indirect manner in cases where only incomplete mineral data are available but partial composite data are also available. To take advantage of this partial knowledge, equation (17) may be generalized as follows:

$$V_{i(\text{composite})} = \sum_j a_{ij} v_j \qquad (18)$$

where V_i is the volume of the i^{th} composite and a_{ij} is the mass fraction of the j^{th} mineral in the i^{th} composite. The summation of the partial volumes is over the j minerals in the i^{th} composite. Equation (18) may be applied at any pressure so that, with further generalization,

$$V_{ik} = \sum_j a_{ij} v_{jk} \qquad (19)$$

where k refers to the k^{th} pressure so that V_{ik} refers to the volume of the i^{th} composite at the k^{th} pressure. Equation (19) may be expanded into matrix form for clarification.

In equation (20), each row represents a Hugoniot, the composites in the lefthand V-matrix and the minerals in the v-matrix.

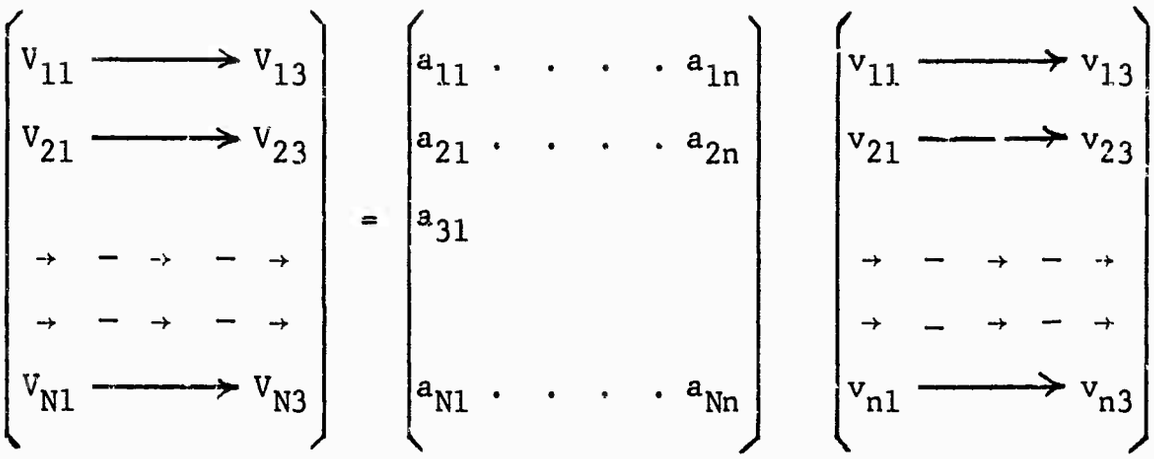

Composite Hugoniot Data | Mass Fraction Data | Mineral Hugoniot Data

(20)

Since some of each are known (solid arrows), and some unknown (dashed arrows), the equation is rewritten and solved for the unknown Hugoniots.

This procedure was carried out for the materials listed in Table V. The values of a_n were taken from Table V but modified as shown. The results of this calculation are shown in Figure 34. Since Hugoniot data for these materials do not exist, these indirect calculations cannot serve as a check or test for the synthesis method but rather as an illustration of its ultimate application.

4. Temperature Calculations

To gain insight into the question of the validity of the assignment of an average or effective temperature to a mineral composite, temperatures were calculated along the mineral Hugoniots and on several unloading isentropes. Details of this assignment and possible modifications to the synthesis method are included in Appendix B. The methods described in reference 18 were used

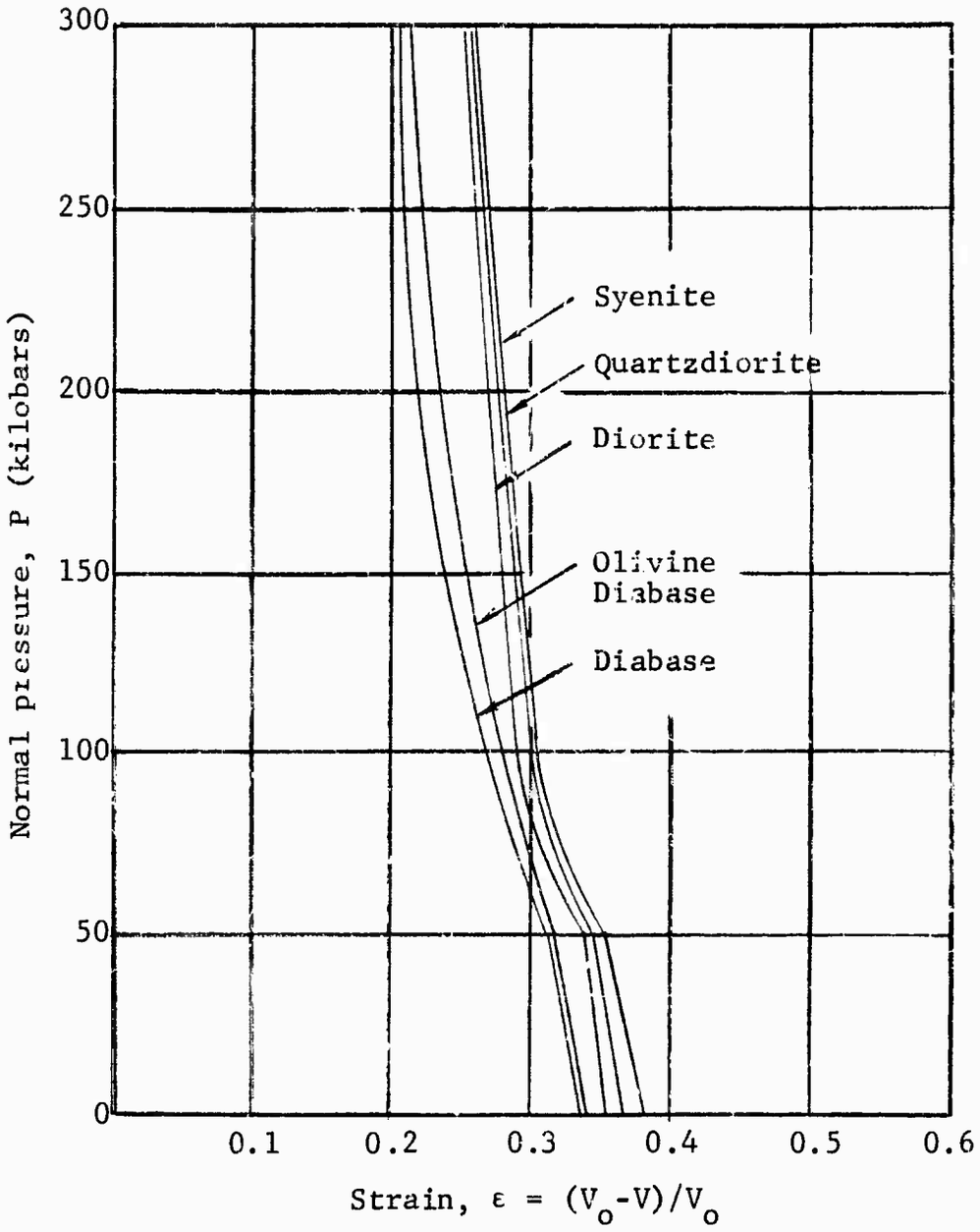

Figure 34 Synthesized Composite Hugoniot Curves Calculated from Equation 24 Using Data of Tables VI and VII and Modified Values of Table V

and will not be detailed here. A computer program was written to calculate the required temperatures. This calculation involved the solution of the equations given in reference 18 for any two of the four Hugoniot variables, P, V, U_S and U_p.

The results of the temperature calculation are given in Table VIII. These results are plotted in Figure 35. These calculations include results for granite. It is interesting to note that the granite results fall in the mid-range of temperatures for the higher pressures. The various granites listed are described in Figure 35. There are two reasons for the slight negative temperature change in one granite sample. First, the computer program utilized the rough rather than smoothed Hugoniot data. A line integral involved in the calculation is sensitive to abrupt or apparent changes in the slope of the input Hugoniot. Secondly, the method of reference 18 is best suited to Hugoniots having very low yield points, such as the metals for which it was used in reference 6, or to gas-like materials having Hugoniots with no cusps.

The temperature-volume Hugoniot data are shown in Figure 36. Unloading adiabats were also calculated. These unloading paths lie above the Hugoniots. Several such adiabats are listed in Table IX. The methods described in Appendix B may be more significant to the unloading process than to the loading process because of the longer times involved. The physical constants used in approximate temperature calculations are listed in Table X.

C. Summary of Synthesis Method

Comparison of the synthesized Hugoniots with those determined by direct experiment (Figure 33) indicates that the method, as

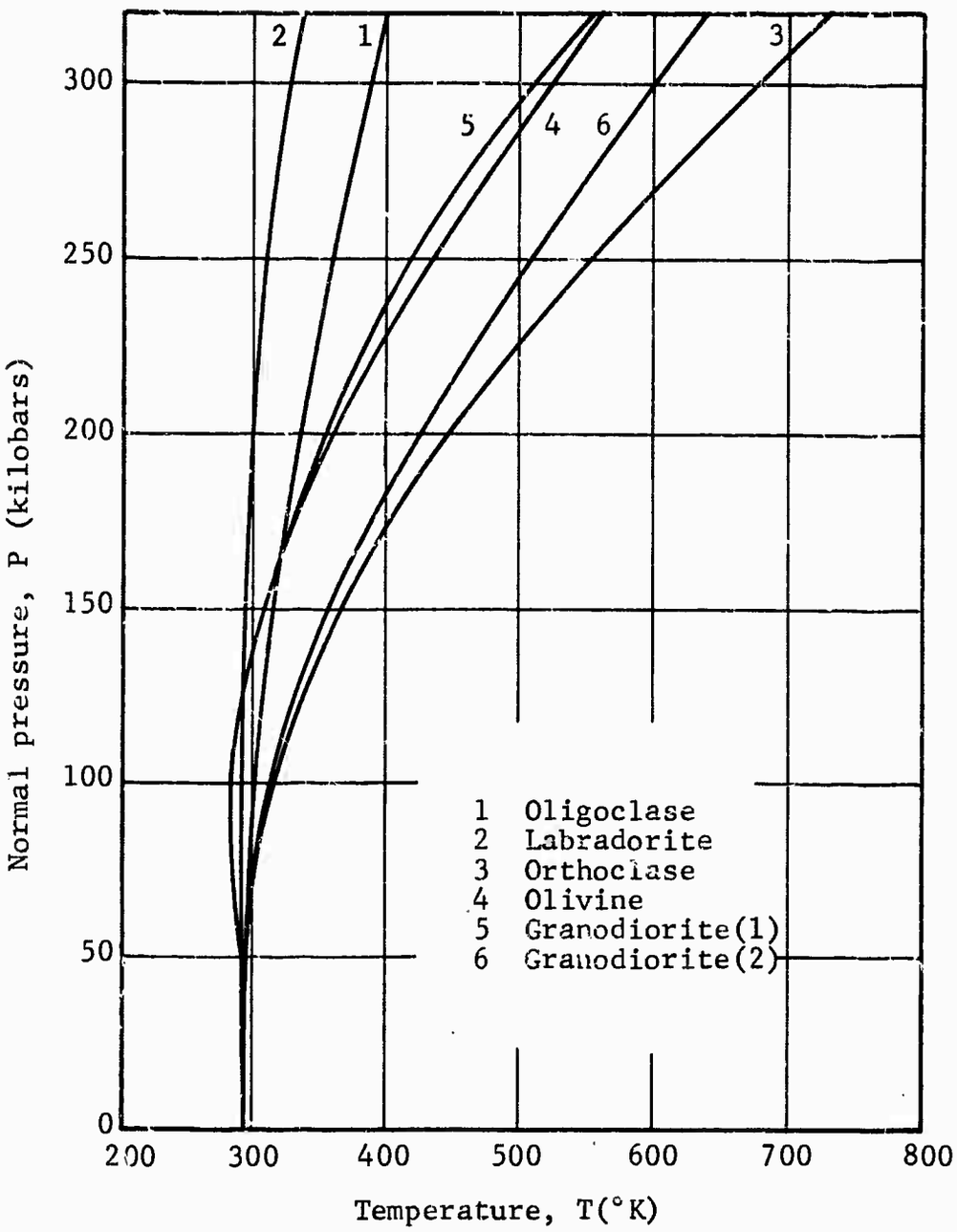

Figure 35 Temperatures on the Hugoniots of Granodiorite and its Major Mineral Constituents

Hugoniot data for granodiorite (1) are taken directly from reference 12, while data for granodiorite (2) are taken from Figure 30. The thermodynamic properties used in the calculation are listed in Table X.

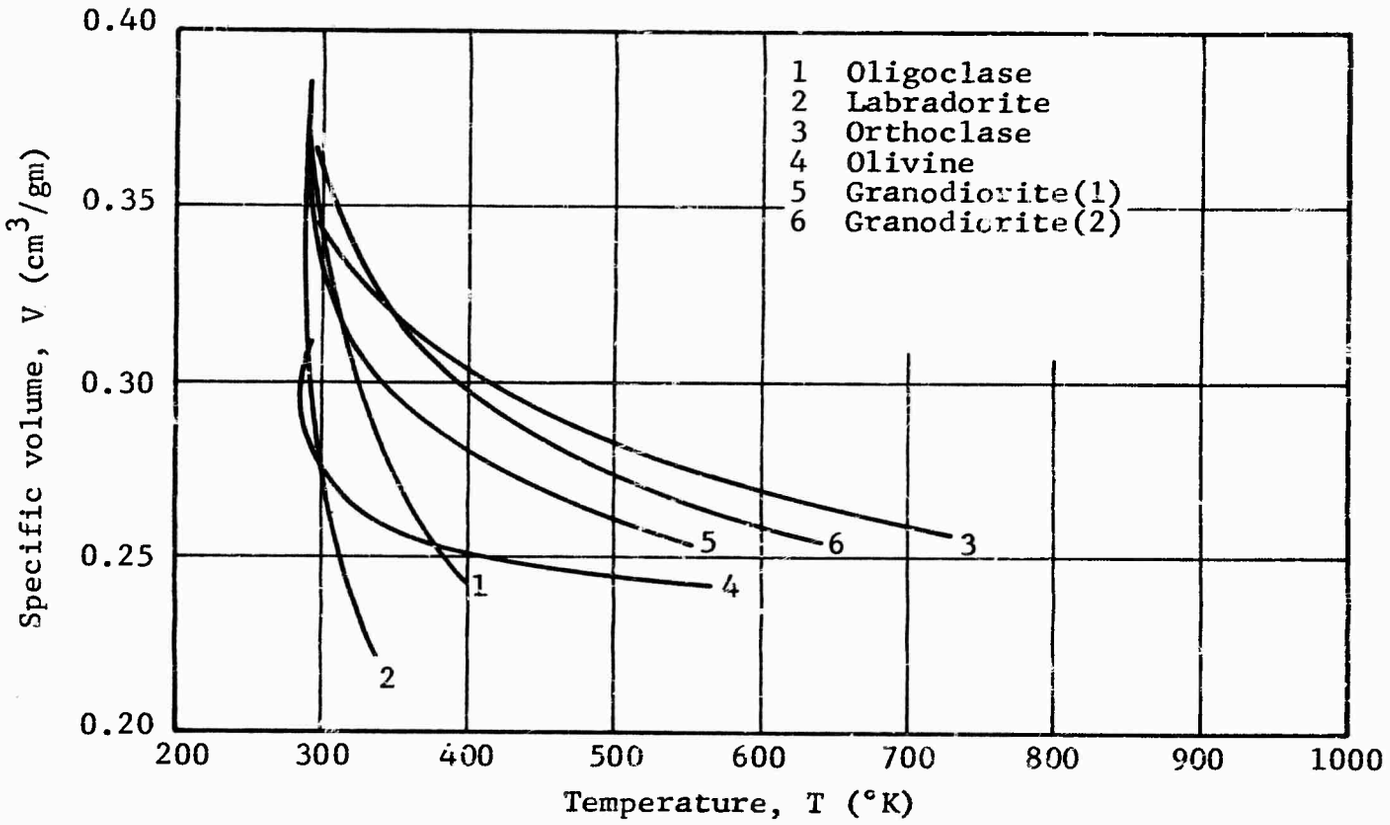

Figure 36 Temperature Volume Data for Granodiorite and its Major Mineral Constituents

applied, has promise. The results are somewhat inconclusive because of the uncertain values for the composite Hugoniot data as well as for the values of the mineral mass fractions a_n. Nevertheless, these results are perhaps as good as would be expected, considering that the synthesis equation used (equation (17)) is basically static in nature and that the mineral Hugoniot data are limited, incomplete and, in some cases, questionable.

The basalt curve as shown in Figure 33(b) was synthesized on the basis of the mineral analysis given in reference 28. Because of lack of Hugoniot data, it was not possible to base the synthesis on all the materials given in that analysis. In fact, the synthesis was based on only two (labradorite and olivine) of the five materials given. Furthermore, the data for this material show a relatively high initial volume, indicating the presence of voids, which are not taken into account in the analysis. It should be noted, however, that the Hugoniot data approach the synthesized curve at higher pressures; at these pressures, the voids are probably compressed out. The Hugoniot data for gabbro is also shown and seem to agree much better with the synthesized curve. The closer agreement in the initial density between these data and the synthesized curve indicates the importance of the initial density in the mechanical behavior. In Figure 33(c) the comparison is made for dunite, the major constituent of which is olivine. Dunite, synthesized on this basis (i.e., 100 per cent olivine), compares very well with the dunite Hugoniot data.

While the matrix method yielding additional composite data (Figure 34) cannot in any way be used as a test, it does serve

as an indication of one method of application of the method. The data presented in Figure 34 were determined without compensating for the difference in initial density brought about by the aforementioned adjustments in a_n. The initial composite density is, therefore, in error but the order is correct, i.e., the composite with the largest initial density remains so in the synthesis.

The fact that the yield point is the same in all new composites reflects the fact that the granodiorite curve with a yield point of about 50 kilobars was used. In this indirect method (equation (20)), input mineral Hugoniot data are incomplete and calculated (partially) from the composite input data.

It is somewhat reassuring that all of the curves in Figure 34 have the same familiar shape. To some degree this result is due to the use of a limited amount of similar mineral data. When a composite is made up of only two or three minerals, it is necessary to know the associated mass fractions fairly accurately as errors in a_n, for small a_n and n, can lead to large errors in the resulting calculated Hugoniots.

Table VIII(a)

TEMPERATURES ALONG HUGONIOT CALCULATED FROM SHOCK AND FREE SURFACE VELOCITIES SHOWN FOR ORTHOCLASE*

Shock Velocity, U_S, (mm/μsec)	Free Surface Velocity, U_{FS}, (mm/μsec)	Particle Velocity, U_P, (mm/μsec)	Specific Volume Ratio, V/V_o	Pressure, P, (dyne/cm^2)	Temperature, T, (°K)
0.	0.	0.	0.100000E 01	0.	0.293000E 03
0.694243E 01	0.108302E-00	0.541510E-01	0.992200E 00	0.100000E 11	0.293695E 03
0.562064E 01	0.267542E-00	0.133771E-00	0.976200E 00	0.200000E 11	0.293186E 03
0.561278E 01	0.401875E-00	0.200938E-00	0.964200E 00	0.300000E 11	0.294209E 03
0.561474E 01	0.535647E 00	0.267823E-00	0.952300E 00	0.400000E 11	0.295298E 03
0.561122E 01	0.669979E 00	0.334990E-00	0.940300E 00	0.500000E 11	0.296305E 03
0.560887E 01	0.804312E 00	0.402156E-00	0.928300E 00	0.600000E 11	0.297315E 03
0.560468E 01	0.938761E 00	0.469380E-00	0.917700E 00	0.700000E 11	0.300189E 03
0.560887E 01	0.107242E 01	0.536208E 00	0.904400E 00	0.800000E 11	0.298849E 03
0.564441E 01	0.119887E 01	0.599436E 00	0.893800E 00	0.900000E 11	0.302367E 03
0.567090E 01	0.132586E 01	0.662928E 00	0.883100E 00	0.100000E 12	0.305692E 03
0.566408E 01	0.146020E 01	0.730099E 00	0.871100E 00	0.110000E 12	0.306074E 03
0.566042E 01	0.159397E 01	0.796987E 00	0.859200E 00	0.120000E 12	0.306709E 03
0.567969E 01	0.172095E 01	0.860473E 00	0.848500E 00	0.130000E 12	0.310639E 03
0.569812E 01	0.184733E 01	0.923665E 00	0.837900E 00	0.140000E 12	0.314880E 03
0.571424E 01	0.197370E 01	0.986850E 00	0.827300E 00	0.150000E 12	0.319135E 03
0.572690E 01	0.210063E 01	0.105031E 01	0.816600E 00	0.160000E 12	0.323058E 03
0.571902E 01	0.223499E 01	0.111750E 01	0.804600E 00	0.170000E 12	0.322202E 03
0.573141E 01	0.236134E 01	0.118067E 01	0.794000E 00	0.180000E 12	0.326935E 03
0.574258E 01	0.248768E 01	0.124384E 01	0.783400E 00	0.190000E 12	0.331483E 03
0.575141E 01	0.261459E 01	0.130730E 01	0.772700E 00	0.200000E 12	0.335707E 03
0.576065E 01	0.274092E 01	0.137046E 01	0.762100E 00	0.210000E 12	0.340406E 03
0.576793E 01	0.286781E 01	0.143391E 01	0.751400E 00	0.220000E 12	0.344635E 03
0.577571E 01	0.299413E 01	0.149706E 01	0.740800E 00	0.230000E 12	0.349387E 03
0.578238E 01	0.312044E 01	0.156022E 01	0.730200E 00	0.240000E 12	0.354155E 03
0.578846E 01	0.324732E 01	0.162366E 01	0.719500E 00	0.250000E 12	0.358381E 03
0.579462E 01	0.337363E 01	0.168681E 01	0.708900E 00	0.260000E 12	0.363200E 03
0.579938E 01	0.350050E 01	0.175025E 01	0.698200E 00	0.270000E 12	0.367432E 03
0.581685E 01	0.361925E 01	0.180962E 01	0.688900E 00	0.280000E 12	0.380458E 03
0.582147E 01	0.374553E 01	0.187277E 01	0.678300E 00	0.290000E 12	0.385065E 03
0.582579E 01	0.387182E 01	0.193591E 01	0.667700E 00	0.300000E 12	0.389687E 03
0.582899E 01	0.399868E 01	0.199934E 01	0.657000E 00	0.310000E 12	0.393626E 03
0.583281E 01	0.412497E 01	0.206248E 01	0.646400E 00	0.320000E 12	0.398298E 03

*maximum accuracy: 3 significant figures

Table VIII(b)

TEMPERATURES ALONG HUGONIOT CALCULATED FROM SHOCK AND FREE SURFACE VELOCITIES SHOWN FOR LABRADORITE

Shock Velocity, U_S, (mm/μsec)	Free Surface Velocity, U_{FS}, (mm/μsec)	Particle Velocity, U_P, (mm/μsec)	Specific Volume Ratio, V/V_o	Pressure, P, (dyne/cm^2)	Temperature, T, (°K)
0.	0.	0.	0.100000E 01	0.	0.293000E 03
0.653832E 01	0.112459E-00	0.562296E-01	0.991400E 00	0.100000E 11	0.294070E 03
0.594564E 01	0.247339E-00	0.123669E-00	0.979200E 00	0.200000E 11	0.294730E 03
0.578122E 01	0.381560E-00	0.190780E-00	0.967000E 00	0.300000E 11	0.295394E 03
0.569766E 01	0.516208E 00	0.258104E-00	0.954700E 00	0.400000E 11	0.296002E 03
0.565414E 01	0.650226E 00	0.325113E-00	0.942500E 00	0.500000E 11	0.296697E 03
0.562165E 01	0.784782E 00	0.392391E-00	0.930200E 00	0.600000E 11	0.297287E 03
0.560219E 01	0.918759E 00	0.459379E-00	0.918000E 00	0.700000E 11	0.298012E 03
0.558773E 01	0.105273E 01	0.526364E 00	0.905800E 00	0.800000E 11	0.298741E 03
0.557394E 01	0.118725E 01	0.593624E 00	0.893500E 00	0.900000E 11	0.299294E 03
0.553279E 01	0.132898E 01	0.664488E 00	0.879900E 00	0.100000E 12	0.297200E 03
0.549979E 01	0.147064E 01	0.735322E 00	0.866300E 00	0.110000E 12	0.295095E 03
0.549893E 01	0.160459E 01	0.802295E 00	0.854100E 00	0.120000E 12	0.296506E 03
0.547403E 01	0.174621E 01	0.873107E 00	0.840500E 00	0.130000E 12	0.294059E 03
0.545294E 01	0.188781E 01	0.943905E 00	0.826900E 00	0.140000E 12	0.291598E 03
0.545389E 01	0.202230E 01	0.101115E 01	0.814600E 00	0.150000E 12	0.293341E 03
0.545610E 01	0.215625E 01	0.107812E 01	0.802400E 00	0.160000E 12	0.295441E 03
0.545805E 01	0.229020E 01	0.114510E 01	0.790200E 00	0.170000E 12	0.297551E 03
0.545855E 01	0.242469E 01	0.121234E 01	0.777900E 00	0.180000E 12	0.299276E 03
0.544393E 01	0.256627E 01	0.128313E 01	0.764300E 00	0.190000E 12	0.295546E 03
0.544618E 01	0.270022E 01	0.135011E 01	0.752100E 00	0.200000E 12	0.298018E 03
0.544718E 01	0.283471E 01	0.141736E 01	0.739800E 00	0.210000E 12	0.300034E 03
0.544908E 01	0.296866E 01	0.148433E 01	0.727600E 00	0.220000E 12	0.302553E 03
0.545082E 01	0.310261E 01	0.155130E 01	0.715400E 00	0.230000E 12	0.305085E 03
0.545150E 01	0.323710E 01	0.161855E 01	0.703100E 00	0.240000E 12	0.307090E 03
0.545301E 01	0.337105E 01	0.168552E 01	0.690900E 00	0.250000E 12	0.309670E 03
0.545355E 01	0.350554E 01	0.175277E 01	0.678600E 00	0.260000E 12	0.311674E 03
0.545487E 01	0.363949E 01	0.181974E 01	0.666400E 00	0.270000E 12	0.314302E 03
0.545610E 01	0.377344E 01	0.188672E 01	0.654200E 00	0.280000E 12	0.316942E 03
0.545648E 01	0.390793E 01	0.195396E 01	0.641900E 00	0.290000E 12	0.318937E 03
0.545757E 01	0.404188E 01	0.202094E 01	0.629700E 00	0.300000E 12	0.321625E 03
0.545788E 01	0.417637E 01	0.208818E 01	0.617400E 00	0.310000E 12	0.323620E 03
0.546852E 01	0.430267E 01	0.215133E 01	0.606600E 00	0.320000E 12	0.336602E 03

Table VIII(c)

TEMPERATURES ALONG HUGONIOT CALCULATED FROM SHOCK AND FREE SURFACE VELOCITIES SHOWN FOR ORTHOCLASE

Shock Velocity, U_S, (mm/μsec)	Free Surface Velocity, U_{FS}, (mm/μsec)	Particle Velocity, U_P, (mm/μsec)	Specific Volume Ratio, V/V_o	Pressure, P, (dyne/cm^2)	Temperature, T, (°K)
0.	0.	0.	0.100000E 01	0.	0.293000E 03
0.845577E 01	0.913223E-01	0.456612E-01	0.994600E 00	0.100000E 11	0.293677E 03
0.588454E 01	0.262451E-00	0.131225E-00	0.977700E 00	0.200000E 11	0.292354E 03
0.544280E 01	0.425627E-00	0.212813E-00	0.960900E 00	0.300000E 11	0.291068E 03
0.519615E 01	0.594440E 00	0.297220E-00	0.942800E 00	0.400000E 11	0.288762E 03
0.519615E 01	0.743050E 00	0.371525E-00	0.928500E 00	0.500000E 11	0.290541E 03
0.519919E 01	0.891140E 00	0.445570E-00	0.914300E 00	0.600000E 11	0.292468E 03
0.523288E 01	0.103297E 01	0.516485E 00	0.901300E 00	0.700000E 11	0.296422E 03
0.526094E 01	0.117424E 01	0.587120E 00	0.888400E 00	0.800000E 11	0.300596E 03
0.530872E 01	0.130913E 01	0.654565E 00	0.876700E 00	0.900000E 11	0.307526E 03
0.534938E 01	0.144340E 01	0.721699E 00	0.865100E 00	0.100000E 12	0.314747E 03
0.540647E 01	0.157112E 01	0.785560E 00	0.854700E 00	0.110000E 12	0.325450E 03
0.545502E 01	0.169869E 01	0.849347E 00	0.844300E 00	0.120000E 12	0.336200E 03
0.549883E 01	0.182560E 01	0.912800E 00	0.834000E 00	0.130000E 12	0.347345E 03
0.551532E 01	0.196014E 01	0.980072E 00	0.822300E 00	0.140000E 12	0.353274E 03
0.556959E 01	0.207969E 01	0.103984E 01	0.813300E 00	0.150000E 12	0.370189E 03
0.561699E 01	0.219961E 01	0.109981E 01	0.804200E 00	0.160000E 12	0.386734E 03
0.564196E 01	0.232675E 01	0.116337E 01	0.793800E 00	0.170000E 12	0.397305E 03
0.566575E 01	0.245327E 01	0.122663E 01	0.783500E 00	0.180000E 12	0.408418E 03
0.568604E 01	0.258032E 01	0.129016E 01	0.773100E 00	0.190000E 12	0.419055E 03
0.572017E 01	0.269992E 01	0.134996E 01	0.764000E 00	0.200000E 12	0.436933E 03
0.576809E 01	0.281137E 01	0.140568E 01	0.756300E 00	0.210000E 12	0.463033E 03
0.581156E 01	0.292321E 01	0.146161E 01	0.748500E 00	0.220000E 12	0.488608E 03
0.583750E 01	0.304250E 01	0.152125E 01	0.739400E 00	0.230000E 12	0.505944E 03
0.586267E 01	0.316115E 01	0.158058E 01	0.730400E 00	0.240000E 12	0.524017E 03
0.589884E 01	0.327268E 01	0.163634E 01	0.722600E 00	0.250000E 12	0.550546E 03
0.593283E 01	0.338409E 01	0.169204E 01	0.714800E 00	0.260000E 12	0.577164E 03
0.596585E 01	0.349479E 01	0.174740E 01	0.707100E 00	0.270000E 12	0.604627E 03
0.599631E 01	0.360600E 01	0.180300E 01	0.699300E 00	0.280000E 12	0.631395E 03
0.602451E 01	0.371712E 01	0.185856E 01	0.691500E 00	0.290000E 12	0.658252E 03
0.605243E 01	0.382756E 01	0.191378E 01	0.683800E 00	0.300000E 12	0.686042E 03
0.607797E 01	0.393852E 01	0.196926E 01	0.676000E 00	0.310000E 12	0.713050E 03
0.609029E 01	0.405735E 01	0.202867E 01	0.666900E 00	0.320000E 12	0.728431E 03

Table VIII(d)

TEMPERATURES ALONG HUGONIOT CALCULATED FROM SHOCK AND FREE SURFACE VELOCITIES SHOWN FOR OLIVINE

Shock Velocity, U_S, (mm/μsec)	Free Surface Velocity, U_{FS}, (mm/μsec)	Particle Velocity, U_P, (mm/μsec)	Specific Volume Ratio, V/V_o	Pressure, P, (dyne/cm^2)	Temperature, T, (°K)
0.	0.	0.	0.100000E 01	0.	0.293000E 03
0.127650E 02	0.485072E-01	0.242536E-01	0.998100E 00	0.100000E 11	0.293299E 03
0.858567E 01	0.144239E-00	0.721196E-01	0.991600E 00	0.200000E 11	0.293424E 03
0.716341E 01	0.259316E-00	0.129658E-00	0.981900E 00	0.300000E 11	0.292800E 03
0.710961E 01	0.348371E-00	0.174185E-00	0.975500E 00	0.400000E 11	0.293594E 03
0.629210E 01	0.492042E-00	0.246021E-00	0.960900E 00	0.500000E 11	0.289247E 03
0.597685E 01	0.621593E 00	0.310796E-00	0.948000E 00	0.600000E 11	0.286271E 03
0.585121E 01	0.740764E 00	0.370382E-00	0.936700E 00	0.700000E 11	0.284914E 03
0.570120E 01	0.868863E 00	0.434431E-00	0.923800E 00	0.800000E 11	0.281594E 03
0.569539E 01	0.978468E 00	0.489234E-00	0.914100E 00	0.900000E 11	0.282794E 03
0.569075E 01	0.108807E 01	0.544036E 00	0.904400E 00	0.100000E 12	0.284000E 03
0.573067E 01	0.118854E 01	0.594271E 00	0.896300E 00	0.110000E 12	0.288108E 03
0.576459E 01	0.128806E 01	0.644481E 00	0.888200E 00	0.120000E 12	0.292234E 03
0.579618E 01	0.138877E 01	0.694383E 00	0.880200E 00	0.130000E 12	0.296598E 03
0.582140E 01	0.148911E 01	0.744557E 00	0.872100E 00	0.140000E 12	0.300741E 03
0.587820E 01	0.158006E 01	0.790031E 00	0.865600E 00	0.150000E 12	0.309038E 03
0.593140E 01	0.167028E 01	0.835142E 00	0.859200E 00	0.160000E 12	0.317641E 03
0.597753E 01	0.176098E 01	0.880490E 00	0.852700E 00	0.170000E 12	0.325977E 03
0.605300E 01	0.184132E 01	0.920661E 00	0.847900E 00	0.180000E 12	0.339710E 03
0.612105E 01	0.192[illegible]1E 01	0.961004E 00	0.843000E 00	0.190000E 12	0.353143E 03
0.615585E 01	0.201173E 01	0.100587E 01	0.836600E 00	0.200000E 12	0.361309E 03
0.621536E 01	0.209209E 01	0.104605E 01	0.831700E 00	0.210000E 12	0.375094E 03
0.627280E 01	0.217164E 01	0.108582E 01	0.826900E 00	0.220000E 12	0.389307E 03
0.629665E 01	0.226176E 01	0.113088E 01	0.820400E 00	0.230000E 12	0.396578E 03
0.634781E 01	0.234107E 01	0.117054E 01	0.815600E 00	0.240000E 12	0.411180E 03
0.642150E 01	0.241063E 01	0.120532E 01	0.812300E 00	0.250000E 12	0.432541E 03
0.646651E 01	0.248961E 01	0.124480E 01	0.807500E 00	0.260000E 12	0.446941E 03
0.650994E 01	0.256847E 01	0.128423E 01	0.802700E 00	0.270000E 12	0.461378E 03
0.657374E 01	0.263738E 01	0.131869E 01	0.799400E 00	0.280000E 12	0.483418E 03
0.663736E 01	0.270539E 01	0.135269E 01	0.796200E 00	0.290000E 12	0.506018E 03
0.669845E 01	0.277316E 01	0.138658E 01	0.793000E 00	0.300000E 12	0.528658E 03
0.675554E 01	0.284138E 01	0.142069E 01	0.789700E 00	0.310000E 12	0.550777E 03
0.678662E 01	0.291960E 01	0.145980E 01	0.784900E 00	0.320000E 12	0.564266E 03

Table VIII(e)

TEMPERATURES ALONG HUGONIOT CALCULATED FROM SHOCK AND FREE SURFACE VELOCITIES SHOWN FOR GRANODIORITE(1)

Shock Velocity, U_S, (mm/μsec)	Free Surface Velocity, U_{FS}, (mm/μsec)	Particle Velocity, U_P, (mm/μsec)	Specific Volume Ratio, V/V_O	Pressure, P, (dyne/cm^2)	Temperature, T, (°K)
0.	0.	0.	0.100000E 01	0.	0.293000E 03
0.614295E 01	0.122859E-00	0.614295E-01	0.990000E 00	0.100000E 11	0.294731E 03
0.614295E 01	0.245718E-00	0.122859E-00	0.980000E 00	0.200000E 11	0.296473E 03
0.568727E 01	0.398109E-00	0.199054E-00	0.965000E 00	0.300000E 11	0.296503E 03
0.579163E 01	0.521247E 00	0.260623E-00	0.955000E 00	0.400000E 11	0.299556E 03
0.575340E 01	0.655888E 00	0.327944E-00	0.943000E 00	0.500000E 11	0.300901E 03
0.568727E 01	0.796217E 00	0.398109E-00	0.930000E 00	0.600000E 11	0.301132E 03
0.567570E 01	0.930814E 00	0.465407E-00	0.918000E 00	0.700000E 11	0.302749E 03
0.566706E 01	0.106541E 01	0.532704E 00	0.906000E 00	0.800000E 11	0.304377E 03
0.568727E 01	0.119433E 01	0.597163E 00	0.895000E 00	0.900000E 11	0.307918E 03
0.570359E 01	0.132323E 01	0.661616E 00	0.884000E 00	0.100000E 12	0.311482E 03
0.567255E 01	0.146352E 01	0.731759E 00	0.871000E 00	0.110000E 12	0.310231E 03
0.568727E 01	0.159243E 01	0.796217E 00	0.860000E 00	0.120000E 12	0.314330E 03
0.571878E 01	0.171563E 01	0.857816E 00	0.850000E 00	0.130000E 12	0.321392E 03
0.574620E 01	0.183879E 01	0.919393E 00	0.840000E 00	0.140000E 12	0.328496E 03
0.573665E 01	0.197341E 01	0.986704E 00	0.828000E 00	0.150000E 12	0.328742E 03
0.574396E 01	0.210229E 01	0.105114E 01	0.817000E 00	0.160000E 12	0.332701E 03
0.575043E 01	0.223117E 01	0.111558E 01	0.806000E 00	0.170000E 12	0.336686E 03
0.578449E 01	0.234850E 01	0.117425E 01	0.797000E 00	0.180000E 12	0.349142E 03
0.578825E 01	0.247737E 01	0.123868E 01	0.786000E 00	0.190000E 12	0.352712E 03
0.580454E 01	0.260044E 01	0.130022E 01	0.776000E 00	0.200000E 12	0.361041E 03
0.581941E 01	0.272340E 01	0.136174E 01	0.766000E 00	0.210000E 12	0.369418E 03
0.583302E 01	0.284651E 01	0.142326E 01	0.756000E 00	0.220000E 12	0.377845E 03
0.585707E 01	0.296368E 01	0.148184E 01	0.747000E 00	0.230000E 12	0.391821E 03
0.587939E 01	0.308080E 01	0.154040E 01	0.738000E 00	0.240000E 12	0.405870E 03
0.591106E 01	0.319197E 01	0.159599E 01	0.730000E 00	0.250000E 12	0.425993E 03
0.591950E 01	0.331492E 01	0.165746E 01	0.720000E 00	0.260000E 12	0.433711E 03
0.593759E 01	0.343193E 01	0.171596E 01	0.711000E 00	0.270000E 12	0.447982E 03
0.596455E 01	0.354294E 01	0.177147E 01	0.703000E 00	0.280000E 12	0.469084E 03
0.598999E 01	0.365389E 01	0.182695E 01	0.695000E 00	0.290000E 12	0.490284E 03
0.601403E 01	0.376478E 01	0.188239E 01	0.687000E 00	0.300000E 12	0.511585E 03
0.603678E 01	0.387561E 01	0.193781E 01	0.679000E 00	0.310000E 12	0.532985E 03
0.605835E 01	0.398639E 01	0.199320E 01	0.671000E 00	0.320000E 12	0.554487E 03

Table VIII(f)

TEMPERATURES ALONG HUGONIOT CALCULATED FROM SHOCK AND FREE SURFACE VELOCITIES SHOWN FOR GRANODIORITE(2)

Shock Velocity, U_S, (mm/μsec)	Free Surface Velocity, U_{FS}, (mm/μsec)	Particle Velocity, U_P, (mm/μsec)	Specific Volume Ratio, V/V_o	Pressure, P, (dyne/cm^2)	Temperature, T, (°K)
0.	0.	0.	0.100000E 01	0.	0.293000E 03
0.877564E 01	0.860013E-01	0.430007E-01	0.995100E 00	0.100000E 11	0.293845E 03
0.583063E 01	0.258880E-00	0.129440E-00	0.977800E 00	0.200000E 11	0.293630E 03
0.555398E 01	0.407662E-00	0.203831E-00	0.963300E 00	0.300000E 11	0.294381E 03
0.542436E 01	0.556539E 00	0.278270E-00	0.948700E 00	0.400000E 11	0.295078E 03
0.535081E 01	0.705237E 00	0.352618E-00	0.934100E 00	0.500000E 11	0.295781E 03
0.539464E 01	0.839407E 00	0.419703E-00	0.922200E 00	0.600000E 11	0.299530E 03
0.542663E 01	0.973537E 00	0.486768E-00	0.910300E 00	0.700000E 11	0.303305E 03
0.544831E 01	0.110819E 01	0.554093E 00	0.898300E 00	0.800000E 11	0.306943E 03
0.549931E 01	0.123515E 01	0.617573E 00	0.887700E 00	0.900000E 11	0.313265E 03
0.554117E 01	0.136202E 01	0.681009E 00	0.877100E 00	0.100000E 12	0.319626E 03
0.554918E 01	0.149606E 01	0.748029E 00	0.865200E 00	0.110000E 12	0.322891E 03
0.558066E 01	0.162286E 01	0.811428E 00	0.854600E 00	0.120000E 12	0.329651E 03
0.560772E 01	0.174961E 01	0.874805E 00	0.844000E 00	0.130000E 12	0.336453E 03
0.565333E 01	0.186899E 01	0.934496E 00	0.834700E 00	0.140000E 12	0.347433E 03
0.571674E 01	0.198028E 01	0.990140E 00	0.826800E 00	0.150000E 12	0.363281E 03
0.573145E 01	0.210688E 01	0.105344E 01	0.816200E 00	0.160000E 12	0.369251E 03
0.578332E 01	0.221848E 01	0.110924E 01	0.808200E 00	0.170000E 12	0.385508E 03
0.583209E 01	0.232934E 01	0.116467E 01	0.800300E 00	0.180000E 12	0.402261E 03
0.585707E 01	0.244826E 01	0.122413E 01	0.791000E 00	0.190000E 12	0.412873E 03
0.587984E 01	0.256714E 01	0.128357E 01	0.781700E 00	0.200000E 12	0.423542E 03
0.591889E 01	0.267771E 01	0.133885E 01	0.773800E 00	0.210000E 12	0.441200E 03
0.595381E 01	0.278876E 01	0.139438E 01	0.765800E 00	0.220000E 12	0.458470E 03
0.598747E 01	0.289913E 01	0.144957E 01	0.757900E 00	0.230000E 12	0.476265E 03
0.601763E 01	0.301002E 01	0.150501E 01	0.749900E 00	0.240000E 12	0.493624E 03
0.604696E 01	0.312023E 01	0.156012E 01	0.742000E 00	0.250000E 12	0.511659E 03
0.607327E 01	0.323096E 01	0.161549E 01	0.734000E 00	0.260000E 12	0.529157E 03
0.609906E 01	0.334107E 01	0.167053E 01	0.726100E 00	0.270000E 12	0.547383E 03
0.612221E 01	0.345170E 01	0.172585E 01	0.718100E 00	0.280000E 12	0.565024E 03
0.614507E 01	0.356168E 01	0.178084E 01	0.710200E 00	0.290000E 12	0.583443E 03
0.616560E 01	0.367223E 01	0.183612E 01	0.702200E 00	0.300000E 12	0.601227E 03
0.618650E 01	0.378212E 01	0.189106E 01	0.694300E 00	0.310000E 12	0.619840E 03
0.620433E 01	0.389260E 01	0.194630E 01	0.686300E 00	0.320000E 12	0.637769E 03

Table IX(a)

UNLOADING ADIABATS CALCULATED FROM PRESSURES LISTED FOR OLIGOCLASE

Unloading from 320 kilobars			Unloading from 250 kilobars		
Specific Volume Ratio V/V_o	Pressure, P, (kilobars)	Temperature, T, (°K)	Specific Volume Ratio V/V_o	Pressure, P, (kilobars)	Temperature, T, (°K)
0.646400E 00	0.320000E 12	0.398298E 03			
0.657000E 00	0.310022E 12	0.397024E 03			
0.667700E 00	0.300039E 12	0.395742E 03			
0.678300E 00	0.290060E 12	0.394476E 03			
0.688900E 00	0.280082E 12	0.393215E 03			
0.698200E 00	0.270158E 12	0.392111E 03			
0.708900E 00	0.260177E 12	0.390845E 03			
0.719500E 00	0.250200E 12	0.389594E 03			
0.730200E 00	0.240219E 12	0.388336E 03	0.719500E 00	0.250000E 12	0.358381E 03
0.740800E 00	0.230241E 12	0.387094E 03	0.730200E 00	0.240020E 12	0.357223E 03
0.751400E 00	0.220264E 12	0.385856E 03	0.740800E 00	0.230043E 12	0.356081E 03
0.762100E 00	0.210283E 12	0.384610E 03	0.751400E 00	0.220066E 12	0.354942E 03
0.772700E 00	0.200305E 12	0.383380E 03	0.762100E 00	0.210086E 12	0.353795E 03
0.783400E 00	0.190324E 12	0.382142E 03	0.772700E 00	0.200109E 12	0.352664E 03
0.794000E 00	0.180346E 12	0.380919E 03	0.783400E 00	0.190128E 12	0.351525E 03
0.804600E 00	0.170368E 12	0.379701E 03	0.794000E 00	0.180151E 12	0.350401E 03
0.816600E 00	0.160354E 12	0.378326E 03	0.804600E 00	0.170173E 12	0.349280E 03
0.827300E 00	0.150371E 12	0.377104E 03	0.816600E 00	0.160160E 12	0.348015E 03
0.837900E 00	0.140391E 12	0.375898E 03	0.827300E 00	0.150178E 12	0.346891E 03
0.848500E 00	0.130410E 12	0.374696E 03	0.837900E 00	0.140198E 12	0.345782E 03
0.859200E 00	0.120427E 12	0.373486E 03	0.848500E 00	0.130218E 12	0.344676E 03
0.871100E 00	0.110423E 12	0.372145E 03	0.859200E 00	0.120236E 12	0.343563E 03
0.883100E 00	0.100417E 12	0.370797E 03	0.871100E 00	0.110232E 12	0.342329E 03
0.893800E 00	0.904303E 11	0.369630E 03	0.883100E 00	0.100227E 12	0.341090E 03
0.904400E 00	0.804452E 11	0.368418E 03	0.893800E 00	0.902408E 11	0.339988E 03
0.917700E 00	0.704272E 11	0.366940E 03	0.904400E 00	0.802563E 11	0.338901E 03
0.928300E 00	0.604381E 11	0.365766E 03	0.917700E 00	0.702390E 11	0.337541E 03
0.940300E 00	0.504361E 11	0.364442E 03	0.928300E 00	0.602505E 11	0.336461E 03
0.952300E 00	0.404341E 11	0.363122E 03	0.940300E 00	0.502492E 11	0.335243E 03
0.964200E 00	0.304327E 11	0.361818E 03	0.952300E 00	0.402479E 11	0.334029E 03
0.976200E 00	0.204309E 11	0.360508E 03	0.964200E 00	0.302472E 11	0.332830E 03
0.992200E 00	0.104165E 11	0.358769E 03	0.976200E 00	0.202463E 11	0.331625E 03
0.100000E 01	0.415515E 09	0.357924E 03	0.992200E 00	0.102325E 11	0.330025E 03
0.100926E 01	-0.488014E 10	0.356924E 03	0.100000E 01	0.231986E 09	0.329248E 03
			0.101006E 01	-0.552506E 10	0.328248E 03

*maximum accuracy: 3 significant figures

Table IX(a) Continued

UNLOADING ADIABATS CALCULATED FROM PRESSURES LISTED FOR OLIGOCLASE

Unloading from 150 kilobars		
Specific Volume Ratio V/V_o	Pressure, P, (kilobars)	Temperature, T, (°K)
0.827300E 00	0.150000E 12	0.319135E 03
0.837900E 00	0.140021E 12	0.318114E 03
0.848500E 00	0.130041E 12	0.317096E 03
0.859200E 00	0.120060E 12	0.316073E 03
0.871100E 00	0.110057E 12	0.314938E 03
0.883100E 00	0.100052E 12	0.313797E 03
0.893800E 00	0.900667E 11	0.312784E 03
0.904400E 00	0.800828E 11	0.311784E 03
0.917700E 00	0.700662E 11	0.310533E 03
0.928300E 00	0.600782E 11	0.309539E 03
0.940300E 00	0.500775E 11	0.308419E 03
0.952300E 00	0.400768E 11	0.307302E 03
0.964200E 00	0.300767E 11	0.306199E 03
0.976200E 00	0.200762E 11	0.305090E 03
0.992200E 00	0.100635E 11	0.303618E 03
0.100000E 01	0.633800E 08	0.302903E 03
0.101094E 01	-0.619463E 10	0.301903E 03

Unloading from 50 kilobars		
Specific Volume Ratio V/V_o	Pressure, P, (kilobars)	Temperature, T, (°K)
0.940300E 00	0.500000E 11	0.296305E 03
0.952300E 00	0.399996E 11	0.295232E 03
0.964200E 00	0.299998E 11	0.294172E 03
0.976200E 00	0.199995E 11	0.293107E 03
0.992200E 00	0.998719E 10	0.291693E 03
0.100000E 01	-0.127629E 08	0.291036E 03
0.101139E 01	-0.652681E 10	0.290006E 03

Table IX(b)

UNLOADING ADIABATS CALCULATED FROM PRESSURES LISTED FOR LABRADORITE

Unloading from 320 kilobars		
Specific Volume Ratio V/V_o	Pressure, P, (kilobars)	Temperature, T, (°K)
0.606600E 00	0.320000E 12	0.336602E 03
0.617400E 00	0.310101E 12	0.335070E 03
0.629700E 00	0.300103E 12	0.333333E 03
0.641900E 00	0.290112E 12	0.331620E 03
0.654200E 00	0.280114E 12	0.329902E 03
0.666400E 00	0.270122E 12	0.328206E 03
0.678600E 00	0.260131E 12	0.326520E 03
0.690900E 00	0.250133E 12	0.324828E 03
0.703100E 00	0.240141E 12	0.323158E 03
0.715400E 00	0.230144E 12	0.321484E 03
0.727600E 00	0.220152E 12	0.319831E 03
0.739800E 00	0.210160E 12	0.318188E 03
0.752100E 00	0.200163E 12	0.316539E 03
0.764300E 00	0.190170E 12	0.314912E 03
0.777900E 00	0.180122E 12	0.313108E 03
0.790200E 00	0.170123E 12	0.311486E 03
0.802400E 00	0.160127E 12	0.309885E 03
0.814600E 00	0.150132E 12	0.308292E 03
0.826900E 00	0.140133E 12	0.306695E 03
0.840500E 00	0.130096E 12	0.304938E 03
0.854100E 00	0.120059E 12	0.303192E 03
0.866300E 00	0.110058E 12	0.301633E 03
0.879900E 00	0.100024E 12	0.299906E 03
0.893500E 00	0.899903E 11	0.298188E 03
0.905800E 00	0.799815E 11	0.296643E 03
0.918000E 00	0.699745E 11	0.295118E 03
0.930200E 00	0.599676E 11	0.293602E 03
0.942500E 00	0.499594E 11	0.292080E 03
0.954700E 00	0.399523E 11	0.290579E 03
0.967000E 00	0.299444E 11	0.289073E 03
0.979200E 00	0.199371E 11	0.287586E 03
0.991400E 00	0.992995E 10	0.286110E 03
0.100000E 01	-0.697642E 08	0.285072E 03
0.100832E 01	-0.562523E 10	0.284072E 03

Unloading from 250 kilobars		
Specific Volume Ratio V/V_o	Pressure, P, (kilobars)	Temperature, T, (°K)
0.693900E 00	0.250000E 12	0.309670E 03
0.703100E 00	0.240009E 12	0.308078E 03
0.715400E 00	0.230012E 12	0.306482E 03
0.727600E 00	0.220021E 12	0.304907E 03
0.739800E 00	0.210029E 12	0.303339E 03
0.752100E 00	0.200033E 12	0.301768E 03
0.764300E 00	0.190041E 12	0.300217E 03
0.777900E 00	0.179993E 12	0.298497E 03
0.790200E 00	0.169995E 12	0.296951E 03
0.802400E 00	0.160000E 12	0.295424E 03
0.814600E 00	0.150005E 12	0.293906E 03
0.826900E 00	0.140007E 12	0.292383E 03
0.840500E 00	0.129971E 12	0.290708E 03
0.854100E 00	0.119934E 12	0.289043E 03
0.866300E 00	0.109934E 12	0.287558E 03
0.879900E 00	0.999007E 11	0.285911E 03
0.893500E 00	0.898678E 11	0.284273E 03
0.905800E 00	0.798597E 11	0.282800E 03
0.918000E 00	0.698533E 11	0.281347E 03
0.930200E 00	0.598470E 11	0.279901E 03
0.942500E 00	0.498394E 11	0.278450E 03
0.954700E 00	0.398329E 11	0.277019E 03
0.967000E 00	0.298257E 11	0.275584E 03
0.979200E 00	0.198190E 11	0.274167E 03
0.991400E 00	0.981246E 10	0.272758E 03
0.100000E 01	-0.186829E 09	0.271769E 03
0.100873E 01	-0.601431E 10	0.270769E 03

Table IX(b) Continued

UNLOADING ADIABATS CALCULATED FROM PRESSURES LISTED FOR LABRADORITE

Unloading from 150 kilobars		
Specific Volume Ratio V/V_o	Pressure, P, (kilobars)	Temperature, T, (°K)
0.814600E 00	0.150000E 12	0.293341E 03
0.826900E 00	0.140002E 12	0.291821E 03
0.840500E 00	0.129966E 12	0.290149E 03
0.854100E 00	0.119929E 12	0.288487E 03
0.866300E 00	0.109929E 12	0.287005E 03
0.879900E 00	0.998958E 11	0.285361E 03
0.893500E 00	0.898630E 11	0.283726E 03
0.905800E 00	0.798549E 11	0.282256E 03
0.918000E 00	0.698486E 11	0.280806E 03
0.930200E 00	0.598423E 11	0.279362E 03
0.942500E 00	0.498347E 11	0.277915E 03
0.954700E 00	0.398283E 11	0.276486E 03
0.967000E 00	0.298210E 11	0.275054E 03
0.979200E 00	0.198144E 11	0.273640E 03
0.991400E 00	0.985784E 10	0.272234E 03
0.100000E 01	-0.191429E 09	0.271247E 03
0.100874E 01	-0.603018E 10	0.270247E 03

Unloading from 50 kilobars		
Specific Volume Ratio V/V_o	Pressure, P, (kilobars)	Temperature, T, (°K)
0.942500E 00	0.500000E 11	0.296697E 03
0.954700E 00	0.399927E 11	0.295172E 03
0.967000E 00	0.299846E 11	0.293642E 03
0.979200E 00	0.199771E 11	0.292133E 03
0.991400E 00	0.996974E 10	0.290632E 03
0.100000E 01	-0.301139E 08	0.289578E 03
0.100819E 01	-0.549912E 10	0.288578E 03

Table IX(c)

UNLOADING ADIABATS CALCULATED FROM PRESSURES LISTED FOR ORTHOCLASE

Unloading from 320 kilobars			Unloading from 250 kilobars		
Specific Volume Ratio V/V_o	Pressure, P, (kilobars)	Temperature, T, (°K)	Specific Volume Ratio V/V_o	Pressure, P, (kilobars)	Temperature, T, (°K)
0.666900E 00	0.320000E 12	0.728431E 03			
0.676000E 00	0.310089E 12	0.725611E 03			
0.683800E 00	0.300264E 12	0.723202E 03			
0.691500E 00	0.290444E 12	0.720831E 03			
0.699300E 00	0.280613E 12	0.718438E 03			
0.707100E 00	0.270791E 12	0.716053E 03			
0.714800E 00	0.260969E 12	0.713706E 03			
0.722600E 00	0.251142E 12	0.711337E 03	0.722600E 00	0.250000E 12	0.550546E 03
0.730400E 00	0.241313E 12	0.708976E 03	0.730400E 00	0.240175E 12	0.548718E 03
0.739400E 00	0.231422E 12	0.706260E 03	0.739400E 00	0.230289E 12	0.546617E 03
0.748500E 00	0.221526E 12	0.703526E 03	0.748500E 00	0.220397E 12	0.544500E 03
0.756300E 00	0.211691E 12	0.701190E 03	0.756300E 00	0.210566E 12	0.542693E 03
0.764000E 00	0.201860E 12	0.698892E 03	0.764000E 00	0.200738E 12	0.540914E 03
0.773100E 00	0.191968E 12	0.696186E 03	0.773100E 00	0.190850E 12	0.538820E 03
0.783500E 00	0.182021E 12	0.693106E 03	0.783500E 00	0.180909E 12	0.536436E 03
0.793800E 00	0.172079E 12	0.690069E 03	0.793800E 00	0.170971E 12	0.534085E 03
0.804200E 00	0.162132E 12	0.687016E 03	0.804200E 00	0.161029E 12	0.531723E 03
0.813300E 00	0.152231E 12	0.684356E 03	0.813300E 00	0.151132E 12	0.529664E 03
0.822300E 00	0.142332E 12	0.681735E 03	0.822300E 00	0.141238E 12	0.527635E 03
0.834000E 00	0.132350E 12	0.678343E 03	0.834000E 00	0.131261E 12	0.525010E 03
0.844300E 00	0.122408E 12	0.675371E 03	0.844300E 00	0.121324E 12	0.522710E 03
0.854700E 00	0.112463E 12	0.672383E 03	0.854700E 00	0.111384E 12	0.520397E 03
0.865100E 00	0.102518E 12	0.669408E 03	0.865100E 00	0.101444E 12	0.518095E 03
0.876700E 00	0.925459E 11	0.666106E 03	0.876700E 00	0.914769E 11	0.515539E 03
0.888400E 00	0.825716E 11	0.662792E 03	0.888400E 00	0.815079E 11	0.512974E 03
0.901300E 00	0.725754E 11	0.659156E 03	0.901300E 00	0.715175E 11	0.510160E 03
0.914300E 00	0.625776E 11	0.655513E 03	0.914300E 00	0.615256E 11	0.507341E 03
0.928500E 00	0.525632E 11	0.651557E 03	0.928500E 00	0.515175E 11	0.504279E 03
0.942800E 00	0.425477E 11	0.647597E 03	0.942800E 00	0.415084E 11	0.501214E 03
0.960900E 00	0.324960E 11	0.642619E 03	0.960900E 00	0.314647E 11	0.497361E 03
0.977700E 00	0.224543E 11	0.638032E 03	0.977700E 00	0.214353E 11	0.493811E 03
0.994600E 00	0.124124E 11	0.633452E 03	0.994600E 00	0.113958E 11	0.490266E 03
0.100000E 01	0.240687E 10	0.631995E 03	0.100000E 01	0.139259E 10	0.489139E 03
0.100371E 01	0.641640E 09	0.630995E 03	0.100480E 01	-0.886638E 09	0.488139E 03
0.100743E 01	-0.112637E 10	0.629995E 03			

Table IX(c) Continued

UNLOADING ADIABATS CALCULATED FROM PRESSURES LISTED FOR ORTHOCLASE

Unloading from 150 kilobars		
Specific Volume Ratio V/V_o	Pressure, P, (kilobars)	Temperature, T, (°K)
0.813300E 00	0.150000E 12	0.370189E 03
0.822300E 00	0.140110E 12	0.368771E 03
0.834000E 00	0.130139E 12	0.366936E 03
0.844300E 00	0.120207E 12	0.365328E 03
0.854700E 00	0.110272E 12	0.363712E 03
0.865100E 00	0.100336E 12	0.362103E 03
0.876700E 00	0.903748E 11	0.360317E 03
0.888400E 00	0.804113E 11	0.358524E 03
0.901300E 00	0.704270E 11	0.356558E 03
0.914300E 00	0.604410E 11	0.354587E 03
0.928500E 00	0.504395E 11	0.352447E 03
0.942800E 00	0.404369E 11	0.350305E 03
0.960900E 00	0.304015E 11	0.347612E 03
0.977700E 00	0.203747E 11	0.345131E 03
0.994600E 00	0.103477E 11	0.342653E 03
0.100000E 01	0.346944E 09	0.341865E 03
0.1006[illegible]E 01	-0.291254E 10	0.340865E 03

Unloading from 50 kilobars		
Specific Volume Ratio V/V_o	Pressure, P, (kilobars)	Temperature, T, (°K)
0.928500E 00	0.500000E 11	0.290541E 03
0.942800E 00	0.400001E 11	0.288775E 03
0.960900E 00	0.280680E 11	0.286555E 03
0.977700E 00	0.199445E 11	0.284510E 03
0.994600E 00	0.992041E 10	0.282468E 03
0.100000E 01	-0.793916E 08	0.281818E 03
0.100834E 01	-0.403309E 10	0.280818E 03

Table IX(d)

UNLOADING ADIABATS CALCULATED FROM PRESSURES LISTED FOR OLIVINE

Unloading from 320 kilobars		
Specific Volume Ratio V/V_o	Pressure, P, (kilobars)	Temperature, T, (°K)
0.784900E 00	0.320000E 12	0.564266E 03
0.789700E 00	0.310165E 12	0.562813E 03
0.793000E 00	0.300454E 12	0.561817E 03
0.796200E 00	0.290751E 12	0.560853E 03
0.799400E 00	0.281048E 12	0.559890E 03
0.802700E 00	0.271336E 12	0.558899E 03
0.807500E 00	0.261514E 12	0.557460E 03
0.812300E 00	0.251692E 12	0.556025E 03
0.815600E 00	0.241971E 12	0.555041E 03
0.820400E 00	0.232151E 12	0.553613E 03
0.826900E 00	0.222225E 12	0.551684E 03
0.831700E 00	0.212400E 12	0.550264E 03
0.836600E 00	0.202569E 12	0.548818E 03
0.843000E 00	0.192655E 12	0.546936E 03
0.847900E 00	0.182819E 12	0.545499E 03
0.852700E 00	0.172988E 12	0.544095E 03
0.859200E 00	0.163076E 12	0.542199E 03
0.865600E 00	0.153169E 12	0.540339E 03
0.872100E 00	0.143257E 12	0.538457E 03
0.880200E 00	0.133281E 12	0.536120E 03
0.888200E 00	0.123310E 12	0.533823E 03
0.896300E 00	0.113335E 12	0.531506E 03
0.904400E 00	0.103359E 12	0.529200E 03
0.914100E 00	0.933381E 11	0.526451E 03
0.923800E 00	0.833171E 11	0.523716E 03
0.936700E 00	0.732221E 11	0.520102E 03
0.948000E 00	0.631604E 11	0.516956E 03
0.960900E 00	0.530707E 11	0.513388E 03
0.975500E 00	0.429563E 11	0.509379E 03
0.981900E 00	0.329432E 11	0.507632E 03
0.991600E 00	0.228985E 11	0.504995E 03
0.998100E 00	0.128761E 11	0.503236E 03
0.100000E 01	0.287329E 10	0.502723E 03
0.100371E 01	0.724209E 09	0.501723E 03
0.100742E 01	0.142806E 10	0.500723E 03

Unloading from 250 kilobars		
Specific Volume Ratio V/V_o	Pressure, P, (kilobars)	Temperature, T, (°K)
0.812300E 00	0.250000E 12	0.432541E 03
0.815600E 00	0.240282E 12	0.431776E 03
0.820400E 00	0.230467E 12	0.430654E 03
0.826900E 00	0.220546E 12	0.429164E 03
0.831700E 00	0.210726E 12	0.428059E 03
0.836600E 00	0.200899E 12	0.426935E 03
0.843000E 00	0.190991E 12	0.425470E 03
0.847900E 00	0.181160E 12	0.424352E 03
0.852700E 00	0.171333E 12	0.423260E 03
0.859200E 00	0.161427E 12	0.421786E 03
0.865600E 00	0.151525E 12	0.420339E 03
0.872100E 00	0.141618E 12	0.418874E 03
0.880200E 00	0.131650E 12	0.417057E 03
0.888200E 00	0.121686E 12	0.415269E 03
0.896300E 00	0.111717E 12	0.413467E 03
0.904400E 00	0.101749E 12	0.411673E 03
0.914100E 00	0.917364E 11	0.409535E 03
0.923800E 00	0.817236E 11	0.407407E 03
0.936700E 00	0.716396E 11	0.404595E 03
0.948000E 00	0.615875E 11	0.402148E 03
0.960900E 00	0.515087E 11	0.399373E 03
0.975500E 00	0.414064E 11	0.396254E 03
0.981900E 00	0.313987E 11	0.394895E 03
0.991600E 00	0.213621E 11	0.392844E 03
0.998100E 00	0.113450E 11	0.391475E 03
0.100000E 01	0.134364E 10	0.391076E 03
0.100477E 01	-0.141509E 10	0.390076E 03

Table IX(d) Continued

UNLOADING ADIABATS CALCULATED FROM PRESSURES LISTED FOR OLIVINE

Unloading from 150 kilobars		
Specific Volume Ratio V/V_o	Pressure, P, (kilobars)	Temperature, T, (°K)
0.865600E 00	0.150000E 12	0.309038E 03
0.872100E 00	0.140099E 12	0.307961E 03
0.880200E 00	0.130137E 12	0.306625E 03
0.889200E 00	0.120179E 12	0.305311E 03
0.896300E 00	0.110218E 12	0.303986E 03
0.904400E 00	0.100256E 12	0.302667E 03
0.914100E 00	0.902507E 11	0.301094E 03
0.923800E 00	0.802457E 11	0.299530E 03
0.936700E 00	0.701719E 11	0.297463E 03
0.948000E 00	0.601287E 11	0.295664E 03
0.960900E 00	0.500600E 11	0.293623E 03
0.975500E 00	0.399699E 11	0.291331E 03
0.981900E 00	0.299662E 11	0.290331E 03
0.991600E 00	0.199379E 11	0.288823E 03
0.998100E 00	0.992489E 10	0.287817E 03
0.100000E 01	-0.750278E 08	0.287524E 03
0.100649E 01	-0.382413E 10	0.286524E 03

Unloading from 50 kilobars		
Specific Volume Ratio V/V_o	Pressure, P, (kilobars)	Temperature, T, (°K)
0.960900E 00	0.500000E 11	0.289247E 03
0.975500E 00	0.399099E 11	0.286988E 03
0.981900E 00	0.299[illegible]E 11	0.286004E 03
0.991600E 00	0.1[illegible]E 11	0.284518E 03
0.998100E 00	0.986[illegible]E 10	0.283527E 03
0.100000E 01	-0.133743E 09	0.283238E 03
0.100659E 01	-0.393946E 10	0.282238E 03

Table IX(e)

UNLOADING ADIABATS CALCULATED FROM PRESSURES LISTED FOR GRANODIORITE (1)

Unloading from 320 kilobars		
Specific Volume Ratio V/V_o	Pressure, P, (kilobars)	Temperature, T, (°K)
0.671000E 00	0.320000E 12	0.554487E 03
0.679000E 00	0.310214E 12	0.551891E 03
0.687000E 00	0.300426E 12	0.549307E 03
0.695000E 00	0.290638E 12	0.546736E 03
0.703000E 00	0.280849E 12	0.544176E 03
0.711000E 00	0.271058E 12	0.541629E 03
0.720000E 00	0.261187E 12	0.538777E 03
0.730000E 00	0.251239E 12	0.535626E 03
0.738000E 00	0.241438E 12	0.533119E 03
0.747000E 00	0.231565E 12	0.530312E 03
0.756000E 00	0.221691E 12	0.527520E 03
0.766000E 00	0.211752E 12	0.524435E 03
0.776000E 00	0.201812E 12	0.521368E 03
0.786000E 00	0.191871E 12	0.518319E 03
0.797000E 00	0.181874E 12	0.514985E 03
0.806000E 00	0.171984E 12	0.512274E 03
0.817000E 00	0.161992E 12	0.508980E 03
0.828000E 00	0.152000E 12	0.505706E 03
0.840000E 00	0.141962E 12	0.502159E 03
0.850000E 00	0.132009E 12	0.499223E 03
0.860000E 00	0.122056E 12	0.496303E 03
0.871000E 00	0.112057E 12	0.493111E 03
0.884000E 00	0.102010E 12	0.489365E 03
0.895000E 00	0.920148E 11	0.486218E 03
0.906000E 00	0.820195E 11	0.483091E 03
0.918000E 00	0.719996E 11	0.479703E 03
0.930000E 00	0.619798E 11	0.476339E 03
0.943000E 00	0.519416E 11	0.472720E 03
0.955000E 00	0.419193E 11	0.469405E 03
0.965000E 00	0.319228E 11	0.466659E 03
0.980000E 00	0.218769E 11	0.462572E 03
0.990000E 00	0.118660E 11	0.459867E 03
0.100000E 01	0.185520E 10	0.457177E 03
0.100373E 01	0.861362E 08	0.456177E 03
0.100747E 01	-0.168679E 10	0.455177E 03

Unloading from 250 kilobars		
Specific Volume Ratio V/V_o	Pressure, P, (kilobars)	Temperature, T, (°K)
0.730000E 00	0.250000E 12	0.425993E 03
0.738000E 00	0.240235E 12	0.423099E 03
0.747000E 00	0.230338E 12	0.421766E 03
0.756000E 00	0.220471E 12	0.419546E 03
0.766000E 00	0.210539E 12	0.417092E 03
0.776000E 00	0.200606E 12	0.414653E 03
0.786000E 00	0.190673E 12	0.412228E 03
0.797000E 00	0.180683E 12	0.409577E 03
0.806000E 00	0.170799E 12	0.407420E 03
0.817000E 00	0.160815E 12	0.404830E 03
0.828000E 00	0.150830E 12	0.402197E 03
0.840000E 00	0.140801E 12	0.399376E 03
0.850000E 00	0.130855E 12	0.397040E 03
0.860000E 00	0.120908E 12	0.394718E 03
0.871000E 00	0.110926E 12	0.392180E 03
0.884000E 00	0.100878E 12	0.389201E 03
0.895000E 00	0.908902E 11	0.386698E 03
0.906000E 00	0.809021E 11	0.384211E 03
0.918000E 00	0.708921E 11	0.381516E 03
0.930000E 00	0.608781E 11	0.378840E 03
0.943000E 00	0.508482E 11	0.375963E 03
0.955000E 00	0.408336E 11	0.373326E 03
0.965000E 00	0.308434E 11	0.371142E 03
0.980000E 00	0.208070E 11	0.367891E 03
0.990000E 00	0.108024E 11	0.365740E 03
0.100000E 01	0.797769E 09	0.363601E 03
0.100373E 01	-0.142427E 10	0.362601E 03

Table IX(e) Continued

UNLOADING ADIABATS CALCULATED FROM PRESSURES LISTED FOR GRANODIORITE (1)

Unloading from 150 kilobars			Unloading from 50 kilobars		
Specific Volume Ratio V/V_o	Pressure, P, (kilobars)	Temperature, T, (°K)	Specific Volume Ratio V/V_o	Pressure, P, (kilobars)	Temperature, T, (°K)
0.828000E 00	0.150000E 12	0.328742E 03			
0.840000E 00	0.139977E 12	0.326437E 03			
0.850000E 00	0.130035E 12	0.324528E 03			
0.860000E 00	0.120094E 12	0.322630E 03			
0.871000E 00	0.110117E 12	0.320555E 03			
0.884000E 00	0.100075E 12	0.318120E 03			
0.895000E 00	0.900922E 11	0.316074E 03			
0.906000E 00	0.801092E 11	0.314041E 03			
0.918000E 00	0.701027E 11	0.311839E 03			
0.930000E 00	0.600963E 11	0.309651E 03			
0.943000E 00	0.500723E 11	0.307299E 03	0.943000E 00	0.500000E 11	0.307931E 03
0.955000E 00	0.400631E 11	0.305144E 03	0.955000E 00	0.399914E 11	0.298790E 03
0.965000E 00	0.300775E 11	0.303359E 03	0.965000E 00	0.300061E 11	0.297043E 03
0.980000E 00	0.200478E 11	0.300702E 03	0.980000E 00	0.199770E 11	0.294441E 03
0.993000E 00	0.100475E 11	0.298944E 03	0.993000E 00	0.997726E 10	0.292719E 03
0.100000E 01	0.474070E 08	0.297195E 03	0.100000E 01	-0.225179E 08	0.291037E 03
0.100575E 01	-0.266947E 10	0.296195E 03	0.100587E 01	-0.277703E 10	0.290037E 03

Table IX(f)

UNLOADING ADIABATS CALCULATED FROM PRESSURES LISTED FOR GRANODIORITE (2)

Unloading from 320 kilobars		
Specific Volume Ratio V/V_o	Pressure, P, (kilobars)	Temperature, T, (°K)
0.686300E 00	0.320000E 12	0.637769E 03
0.694300E 00	0.310169E 12	0.634784E 03
0.702200E 00	0.300346E 12	0.631849E 03
0.710200E 00	0.290514E 12	0.628891E 03
0.718100E 00	0.280689E 12	0.625984E 03
0.726100E 00	0.270855E 12	0.623053E 03
0.734000E 00	0.261028E 12	0.620173E 03
0.742000E 00	0.251193E 12	0.617270E 03
0.749900E 00	0.241365E 12	0.614416E 03
0.757900E 00	0.231529E 12	0.611540E 03
0.765800E 00	0.221698E 12	0.608713E 03
0.773800E 00	0.211861E 12	0.605863E 03
0.781700E 00	0.202029E 12	0.603062E 03
0.791000E 00	0.192112E 12	0.599782E 03
0.800300E 00	0.182195E 12	0.596519E 03
0.808200E 00	0.172353E 12	0.593761E 03
0.816200E 00	0.162506E 12	0.590982E 03
0.826800E 00	0.152532E 12	0.587319E 03
0.834700E 00	0.142680E 12	0.584604E 03
0.844000E 00	0.132768E 12	0.581423E 03
0.854600E 00	0.122804E 12	0.577820E 03
0.865200E 00	0.112840E 12	0.574238E 03
0.877100E 00	0.102832E 12	0.570244E 03
0.887700E 00	0.928639E 11	0.566710E 03
0.898300E 00	0.828957E 11	0.563197E 03
0.910300E 00	0.728921E 11	0.559247E 03
0.922200E 00	0.628908E 11	0.555357E 03
0.934100E 00	0.528896E 11	0.551494E 03
0.948700E 00	0.428444E 11	0.546792E 03
0.963300E 00	0.327996E 11	0.542129E 03
0.977800E 00	0.227562E 11	0.537538E 03
0.995100E 00	0.126924E 11	0.532111E 03
0.100000E 01	0.268470E 10	0.530584E 03
0.100322E 01	0.115906E 10	0.529584E 03
0.100644E 01	-0.369447E 09	0.528584E 03

Unloading from 250 kilobars		
Specific Volume Ratio V/V_o	Pressure, P, (kilobars)	Temperature, T, (°K)
0.742000E 00	0.250000E 12	0.511658E 03
0.749900E 00	0.240177E 12	0.509293E 03
0.757900E 00	0.230346E 12	0.506909E 03
0.765800E 00	0.220521E 12	0.504565E 03
0.773800E 00	0.210689E 12	0.502203E 03
0.781700E 00	0.200863E 12	0.499882E 03
0.791000E 00	0.190952E 12	0.497162E 03
0.800300E 00	0.181042E 12	0.494458E 03
0.808200E 00	0.171205E 12	0.492172E 03
0.816200E 00	0.161363E 12	0.489868E 03
0.826800E 00	0.151396E 12	0.486832E 03
0.834700E 00	0.141550E 12	0.484581E 03
0.844000E 00	0.131644E 12	0.481945E 03
0.854600E 00	0.121687E 12	0.478958E 03
0.865200E 00	0.111730E 12	0.475989E 03
0.877100E 00	0.101729E 12	0.472679E 03
0.887700E 00	0.917683E 11	0.469749E 03
0.898300E 00	0.818068E 11	0.466837E 03
0.910300E 00	0.718109E 11	0.463563E 03
0.922200E 00	0.618171E 11	0.460339E 03
0.934100E 00	0.518233E 11	0.457137E 03
0.948700E 00	0.417872E 11	0.453239E 03
0.963300E 00	0.317514E 11	0.449374E 03
0.977800E 00	0.217169E 11	0.445569E 03
0.995100E 00	0.116636E 11	0.441070E 03
0.100000E 01	0.165889E 10	0.439804E 03
0.100388E 01	-0.179684E 09	0.438804E 03

Table IX(f) Continued

UNLOADING AIDABATS CALCULATED FROM PRESSURES LISTED FOR GRANODIORITE (2)

Unloading from 150 kilobars		
Specific Volume Ratio V/V_o	Pressure, P, (kilobars)	Temperacure, T (°K)
0.826800E 00	0.150000E 12	0.363281E 03
0.834700E 00	0.140160E 12	0.361601E 03
0.844000E 00	0.130262E 12	0.359634E 03
0.854600E 00	0.120314E 12	0.357405E 03
0.865200E 00	0.110365E 12	0.355190E 03
0.877100E 00	0.100374E 12	0.352720E 03
0.887700E 00	0.904211E 11	0.350533E 03
0.898300E 00	0.804680E 11	0.348361E 03
0.910300E 00	0.704815E 11	0.345917E 03
0.922200E 00	0.604973E 11	0.343511E 03
0.934100E 00	0.505124E 11	0.341122E 03
0.948700E 00	0.404874E 11	0.338213E 03
0.963300E 00	0.304627E 11	0.335329E 03
0.977800E 00	0.204391E 11	0.332490E 03
0.995100E 00	0.103988E 11	0.329133E 03
0.100000E 01	0.397627E 09	0.328188E 03
0.100520E 01	-0.206335E 10	0.327188E 03

Unloading from 50 kilobars		
Specific Volume Ratio V/V_o	Pressure, P, (kilobars)	Temperature, T, (°K)
0.934100E 00	0.500000E 11	0.295781E 03
0.948700E 00	0.399704E 11	0.293259E 03
0.963300E 00	0.299591E 11	0.290759E 03
0.977800E 00	0.199397E 11	0.288296E 03
0.995100E 00	0.990441E 10	0.285386E 03
0.100000E 01	-0.952982E 08	0.284567E 03
0.100600E 01	-0.293245E 10	0.283567E 03

Table X

THERMODYNAMIC PROPERTIES OF GEOLOGICAL MATERIALS USED IN TEMPERATURE CALCULATIONS

Material	Specific Heat, $c_v = C_p$*, (joules/gm)	Thermal Expansion Coefficient α* (per °C)	Low Pressure Compressibility β_o** (cm^2/dyne)	$\left(\frac{\partial P}{\partial T}\right)_v$* $\left(\frac{dyne}{cm^2\ °C}\right)$	Density ρ_o (gm/cm^3)
Oligoclase	0.796×10^7	11.2×10^{-6}	1.74×10^{-12}	6.4×10^6	2.66
Labradorite	0.766	13.2	1.50	8.8	2.72
Orthoclase	0.643	15.0	2.12	7.1	2.59
Olivine	0.79	23.8	1.74	13.7	3.23
Granodiorite(1)&(2)	0.727	24.0	2.12	11.3	2.65

*Reference 8
**Reference 8,19

V CONCLUSIONS AND RECOMMENDATIONS

The synthesis methods, the work leading to the application of these methods and the results of the application were detailed in the earlier sections of this report. In this section, the complete work of this program is summarized briefly. Some of the possible conclusions, both optimistic and otherwise, regarding the feasibility of applying synthesis methods are listed. The discussion of the synthesis method is divided into two categories;

(1) that involving what was or might have been done on this and other, related past programs,

(2) that involving what might be done in any future program.

These are best considered in that order.

This program was actually considered to be somewhat of a feasibility study of the methods suggested in the excellent work of Chabai (Ref. 30) but applied using mineral rather than elemental Hugoniot data. The necessity for gathering only a minimal amount of mineral Hugoniot data, coupled with the uncertainties in these data, especially those related to the yield behavior of these materials, required that the synthesis calculations lack the luxury of great detail. Even a casual look at the synthesis methods employed here reveals that the main features of the dynamic loading process, as outlined in Appendix B, are entirely absent. Nevertheless the results of even these calculations are very promising <u>but</u> <u>not</u> conclusive evidence of ultimate feasibility.

It must again be emphasized that much of the composite Hugoniot data that presently exist are not actually available for detailed comparison, in this or future synthesis work. This is due to the unfortunate circumstance that it has not been customary to perform a detailed mineral analysis on geological samples before testing. It is probably worth noting that much of the past Hugoniot work on composites was done to determine the behavior of a particular composite and, in addition, to do this on a "crash program" basis. Since there is every evidence that there will be continuing interest in Hugoniot data, the need and desirability of a dependable synthesis method seems apparent and especially so for crash programs.

It is believed to be worthwhile to recommend, then, the steps necessary in the development of an ultimate synthesis model. In general, the development of such a model must be based on the dynamic characteristics of the physical problem rather than the quasistatic ideas considered here. Such an analysis is very probably amenable to computerized averaging or synthesis techniques. One of the more promising aspects of the problem is that composites may be expected to be characterized by bulk isotropy even when made up of anisotropic minerals. In fact, in similar elastic problems Lamé constants have been developed for mixtures of anisotropic materials (Ref. 31). Such bulk isotropy might be expected to greatly simplify the over-all problem. In addition, if the method is to be extended to lighter, more porous materials, such factors as saturation and porosity must be included. Some consideration must also be given to grain size

in an ultimate theory and application. Remarks concerning grain size in Appendix B are believed to be appropriate. Even without these significant features of an ultimate model, useful predictions may be expected over a limited range of material properties. Thus, by considering the quasistatic problem, as was done here, the use of mineral weighting factors may be extended to other composite materials.

Before the development of the ultimate problem is undertaken, several more immediate steps are believed to be necessary. These were suggested above previously and are listed as follows:

(1) A better understanding of the behavior of the feldspars and other minerals in the neighborhood of the dynamic yield point is required. Low-pressure experiments, probably in shock tubes with pressures below 100 kilobars, are best. Even before such experiments are continued the records such as those discussed in Section III should be re-evaluated on the basis of a continuous loading process as demonstrated in Appendix A. This type of loading would occur as a result of a compression fan or by the elastic reverberations discussed in Section III. These elastic reverberations should be reconciled to the sharp transitions found by other investigators.

Unfortunately neither time nor funding was available to carry out this envisioned (computer) analysis of the experimental records obtained in this program. In several cases, limited analysis indicated that much more

Hugoniot information is available from these records than has presently evolved. It is hoped that this phase may be completed in the near future.

(2) The synthesis techniques developed here should then be applied to this re-evaluated mineral Hugoniot data. Some consideration should be given to the development or use of thermo gradients and conduction in the unloading adiabat calculations and an attempt to synthesize the unloading process should be made.

(3) As a rather direct requirement in a slightly more advanced program, Hugoniot data should be obtained for composites, fabricated or natural but containing only minerals of known properties.

Many of the details of these steps and others of a more complete analysis have been detailed previously (Ref. 31) and will not be repeated. These three specific recommendations are included here because they are direct consequences of the work reported here.

Appendix A

Appendix A

INDEFINITE TIME RESOLUTION

Appendix A

INDEFINITE TIME RESOLUTION

The determination of the Hugoniot depends on measurements of the velocities of one or more shock waves. In cases where two waves are transmitted, it is necessary to determine the free-surface velocity change associated with the arrival and velocity of the second wave. Assuming the simple t-x diagram illustrated in Figure 7(a), this velocity change occurs abruptly.

Several methods have been used to determine the arrival time of the second wave by continuous or quasicontinuous monitoring of the free-surface motion. Two continuous recording optical methods were considered for use in this investigation; the reflecting wire method of Wackerly (Ref. 15) and the inclined mirror method of Fowles (Ref. 14).

In an effort to compare these methods an optical mock-up of these experimental configurations was set up in the laboratory. Results of these simulation experiments and of several field experiments using the inclined mirror configuration indicated that considerable difficulty would be associated with the exact location of the transition time in either method. It, therefore, became of interest to determine the sensitivity of the experimental Hugoniot determination to errors in the location of the transition time, and to determine if records with indefinite transition times could be analyzed. The graphical method used to make the latter determination and the optical simulation experiments are discussed.

Optical Simulation Experiments

The simulation set-up is shown schematically in Figure A-1. The free surface motion of a sample was simulated by a reflecting surface driven by an electric motor. The change in reflectance of the inclined mirror, which occurs as the free surface of the sample comes into contact with the mirror, is simulated by the reflector's being driven into an optical mask. The image of the reflector mask interface was then focussed onto the adjustable entrance slit of the recording camera. An Avco 360 deg rotating mirror camera with rotor driven by a slow-speed synchronous motor was used. The combination of camera rotor speed and reflector drive speed was sufficient to result in angles of about those obtained in some early field experiments. In addition, the geometric arrangement between the light source reflector and recording camera was approximately that of the field experiments.

A series of runs was made in which the angles α and β (Figure A-1), as well as the light intensity and slit width, were varied. A sample record is shown in Figure A-2. In this run, the reflector drive motor was switched to a higher speed midway in the run. The change in speed is analogous to an instantaneous change in velocity of the free surface caused by the arrival of a second wave.

In each run a wire stretched across the reflector a few millimeters from the free surface was used to simulate the reflecting wire method. The wire trace is shown below the mask-reflector interface in Figure A-2. As described in reference 15, there are two images of the wire seen on the film record. One is

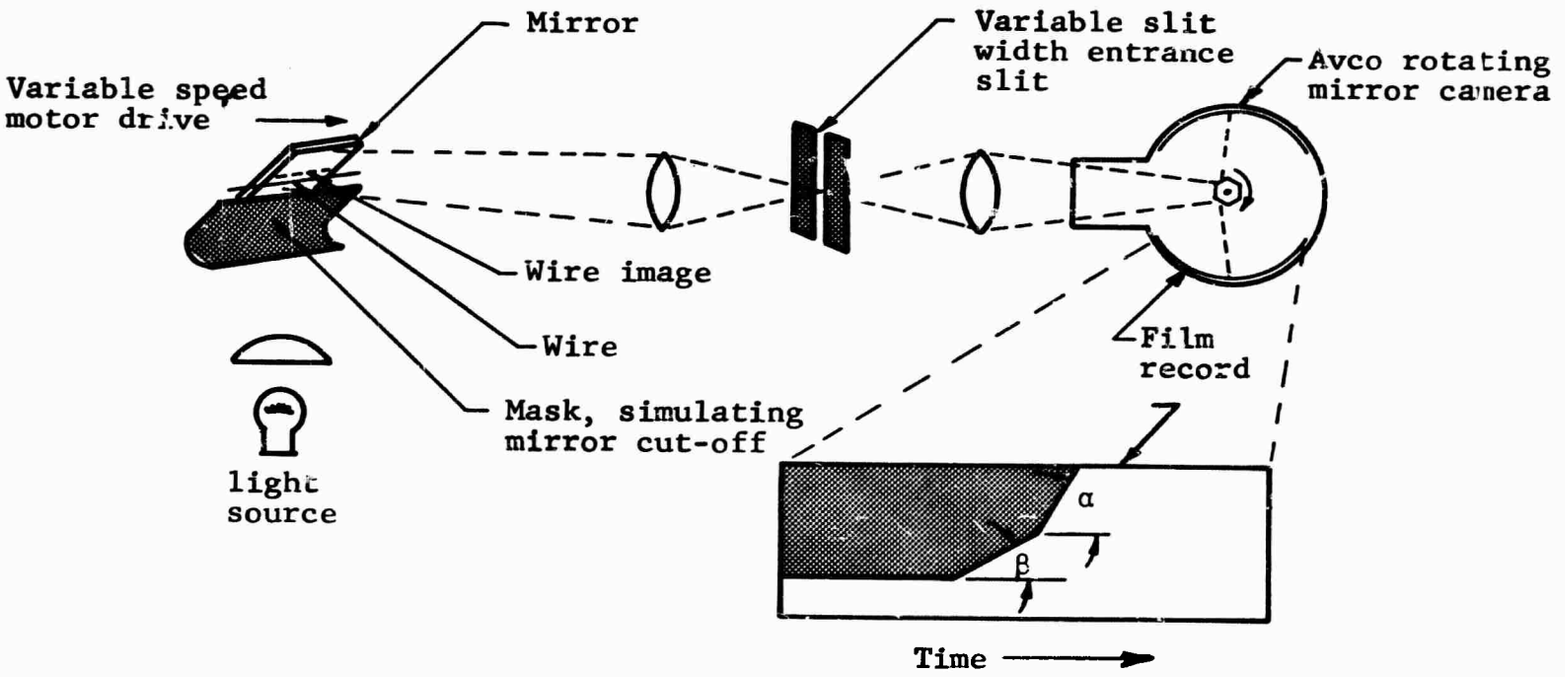

Figure A-1 Optical Simulation Setup for Comparing Wire Reflection and Inclined Mirror Experiments

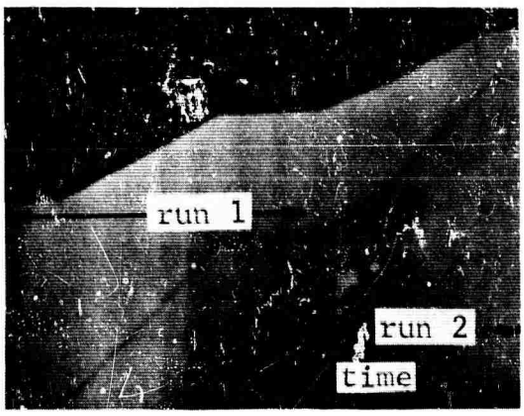

(a) Change in free surface velocity not determinable (see Figure A-1)

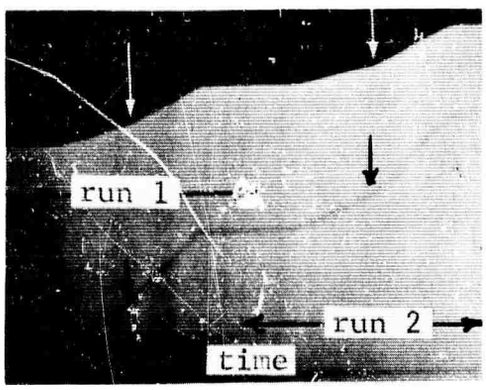

(b) Change in free surface velocity indicated by arrows in run 3 and run 4

Figure A-2 Sample Records from Mock-up Optical Experiments Showing Inclined Mirror Cutoff, Top of (a) and (b), and Reflecting Wire and Image Separation, Bottom of (a) and (b) (In (a) the free surface motion and geometric variables are such that the change in free surface motion (corresponding to arrival of second wave) is not determinable by either method; in (b) change may be seen in both traces)

due to the wire itself; the other to its virtual image from the reflector. The relative motion between these images corresponds to twice the free surface velocity of the reflector in these experiments, or of the sample in actual field experiments.

The records were compared for these idealized cases of very good reflection for the wire method and distinct reflector-mask interface for the inclined mirror method. There was little difference between the two methods in the difficulty of locating the transition in free surface velocity, and it was decided to continue the experimental program using the inclined mirror method since that method does not require a reflecting sample surface.

Graphical Analysis Method

A graphical method was used to determine the sensitivity of calculated Hugoniot data to the accuracy in location of any transition times in free-surface sample motion. It consisted of constructing a t-x or free-surface motion diagram from an assumed Hugoniot. The Hugoniot used corresponded roughly to that of granite but was approximated by two straight-line segments, as shown in Figure A-3(a).

To construct the t-x diagram, the following equations were used. The indefiniteness in the location of the transition

$$U_{S2} = \sqrt{\frac{P_2 - P_1}{\rho_o(\varepsilon_2 - \varepsilon_1)}} + \left(U_{P1} = \sqrt{\frac{P_1\varepsilon_1}{\rho_o}}\right)$$

$$U_{P2} - U_{P1} = \sqrt{\frac{(P_2 - P_1)(\varepsilon_2 - \varepsilon_1)}{\rho_o}} \quad (\varepsilon_2 - 1)$$

(a) Assumed Hugoniot

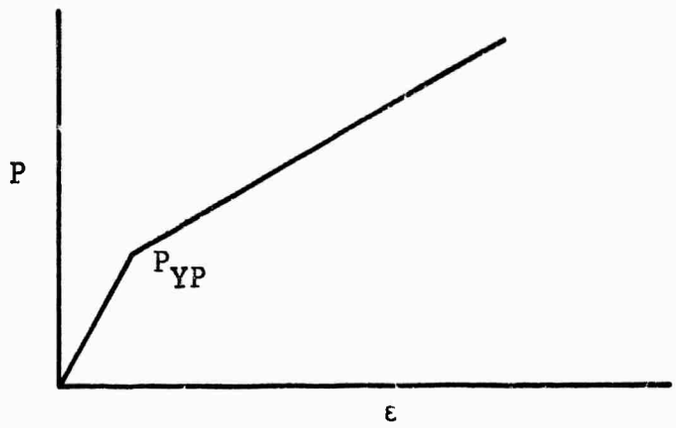

(b) t-x diagram calculated from (a)

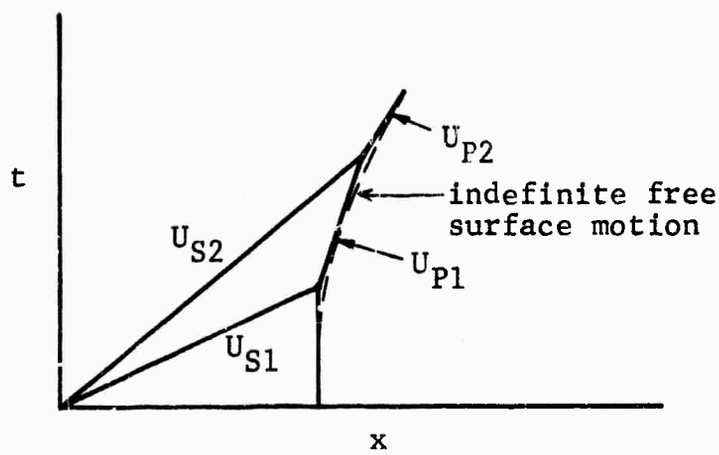

(c) Approximate t-x diagram showing arbitrarily chosen segments

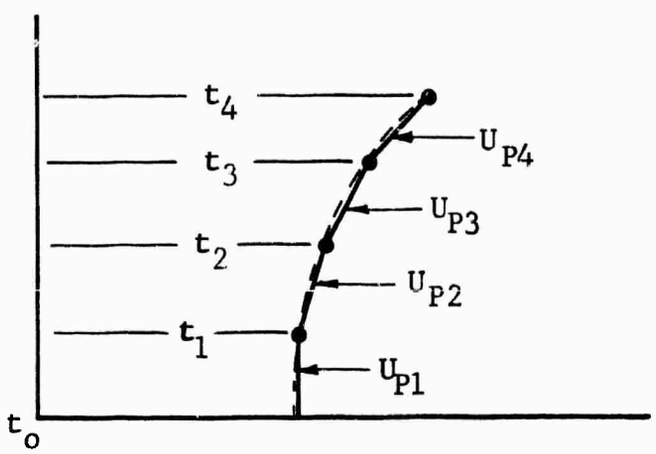

Figure A-3 Schematic Representation of Graphical Method Used to Test Sensitivity of Data Analysis Method When Time Resolution Is Insufficient or for Rounded Records

time, i.e., the arrival of the second shock wave at the free surface, was imposed by replacing the calculated segmented free surface motion by the curved line (shown dotted in Figure A-3(b)). The new free surface curve was then approximated by n segments of equal time increments. The related free surface and shock velocities were then measured graphically, and the P-ε states calculated using the equations

$$P_N = P_{N-1} + \frac{P_o(U_{SN} - U_{P,N-1})(U_{PN} - U_{P,N-1})}{1 - \varepsilon_{N-1}}$$

$$1 - \varepsilon_N = \prod_{i=1}^{i=N} \frac{(U_{Si} - U_{Pi})}{(U_{Si} - U_{P,i-1})} \quad .$$

A comparison of the various n line approximations is shown in Figure A-4. The construction indicates that the calculation process is convergent and that, for indefinite transitions, analysis could be made on this basis.

There are several approximations involved in the calculation: Perhaps the most serious is the inherent construction error associated with establishing the curved free surface diagram of Figure A-3(b). Since this construction error would not be a source of error in actual record analysis, application of this method seems desirable for indefinite or rounded records.

It is interesting to test the method in cases where the material properties are such that the t-x diagram would be curved with no sharp transitions. Such a curved Hugoniot is shown in

Figure A-5. The resulting n segmented approximations were calculated as before and are also shown in Figure A-5.

Convergence to the actual Hugoniot is more rapid than before; thus, the analysis method is apparently applicable to rounded records as well. In the second example it was necessary to approximate the Hugoniot by several segments in order to construct the t-x diagram. In this example 16 segments were used.

When many lines are used, analysis becomes tedious and quite inaccurate. If many records are involved, the equations may be programmed for electronic computation, thereby eliminating considerable construction and iteration error.

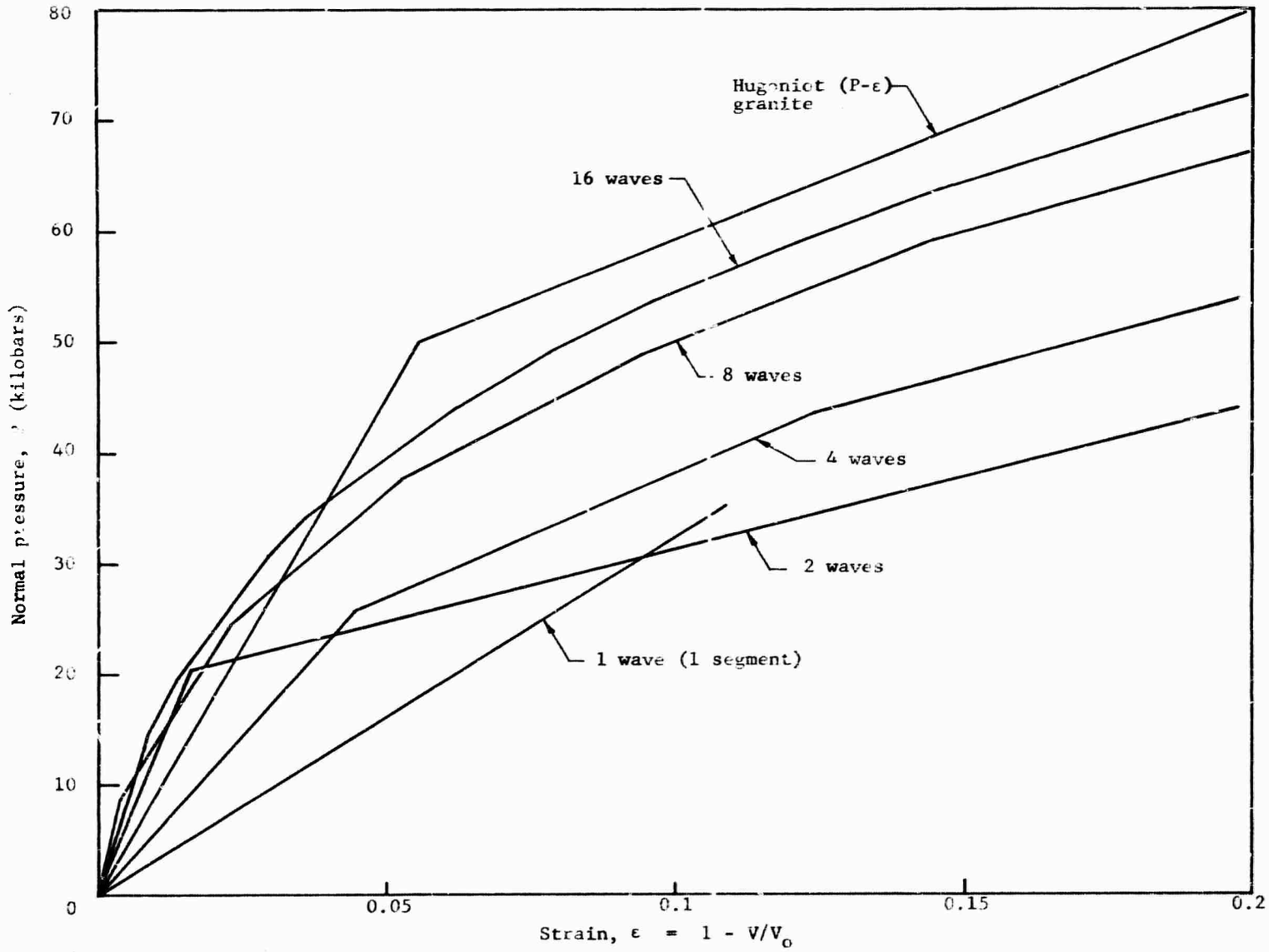

Figure A-4 Results of Calculation Procedure of Figure A-3 Showing Convergence of Calculated (P-ε) States to Assumed (P-ε) States (in this case, granite) as the Degree of Segments and Shock Waves Involved Are Increased

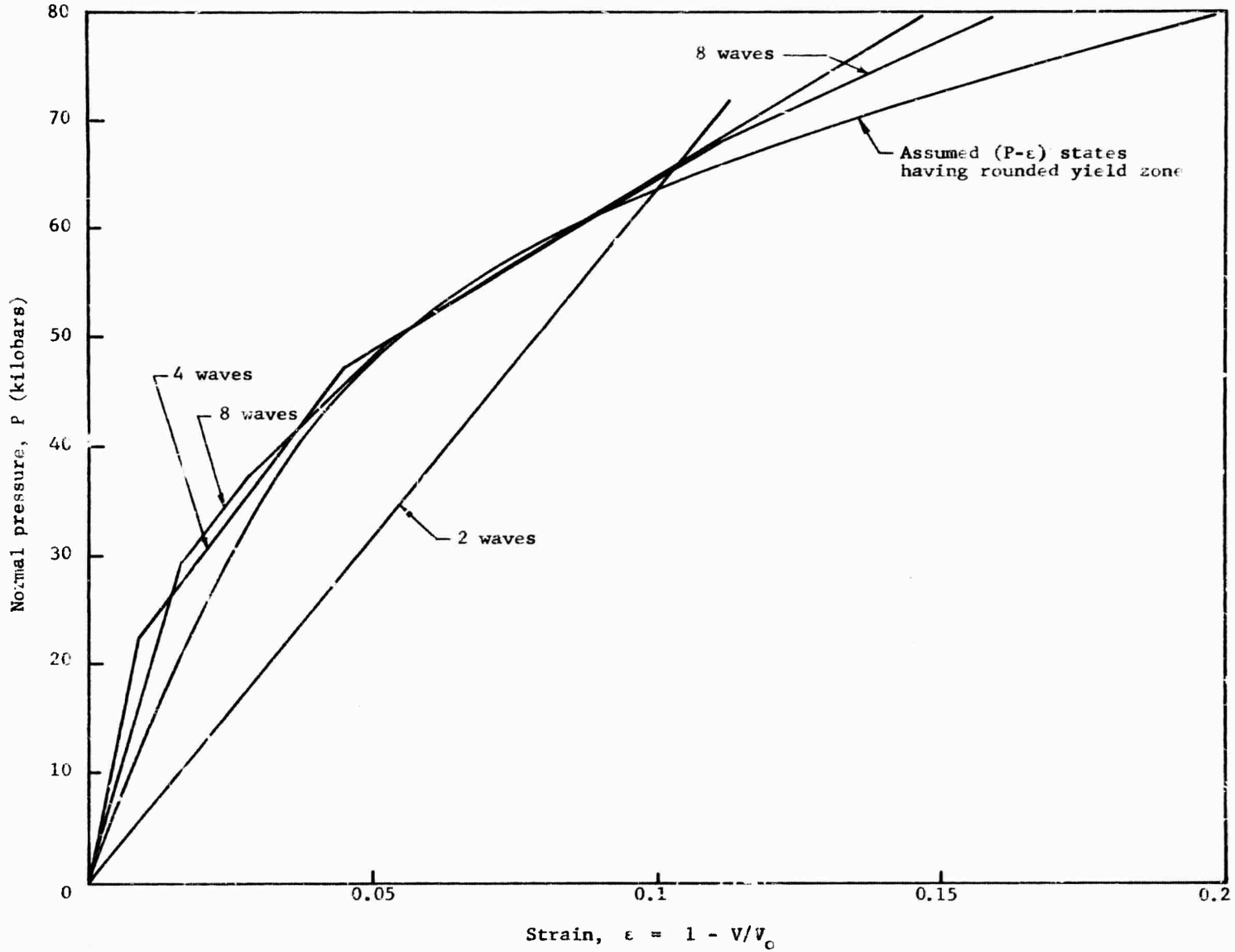

Figure A-5 Results of Calculations for Material Having Rounded Yield Zone Showing Convergence of Calculated (P-ε) States to Assumed (P-ε) States with the Number of Segments or Waves Assumed in the Calculation

Appendix B

THEORETICAL MODEL STUDIES

Appendix B

THEORETICAL MODEL STUDIES

Dynamic Loading

The simplified analysis leading to the equation

$$v_c = \sum_n^N \frac{M_n}{M} v_n = \sum_n^N a_n v_n \qquad \text{(B-1)}$$

is based on the assumption that the pressure on all mineral constituents is the same. This is essentially a static rather than dynamic view of the process. Even if an equation such as (B-1) is considered an averaging equation where the a_n are unspecified weighting terms to be determined from experiments, it is necessary to assign an effective pressure which characterizes the composite material. The existence of such an effective or average pressure is, in fact, necessary to describe the Hugoniot state of the material.

To clarify the differences between static and dynamic loading processes, it is helpful to consider the layered material of Figure B-1. Here, we are considering the one-dimensional case where it is assumed that the strain in a direction perpendicular to the applied force is zero. In Figure B-1(b), both materials A and b experience the same pressure. The total strain is equal to the sum of the contributions of the two materials. This is completely analogous to the discussion leading to equation (B-1). The composite state would be represented by P and ε_T, where ε_T is

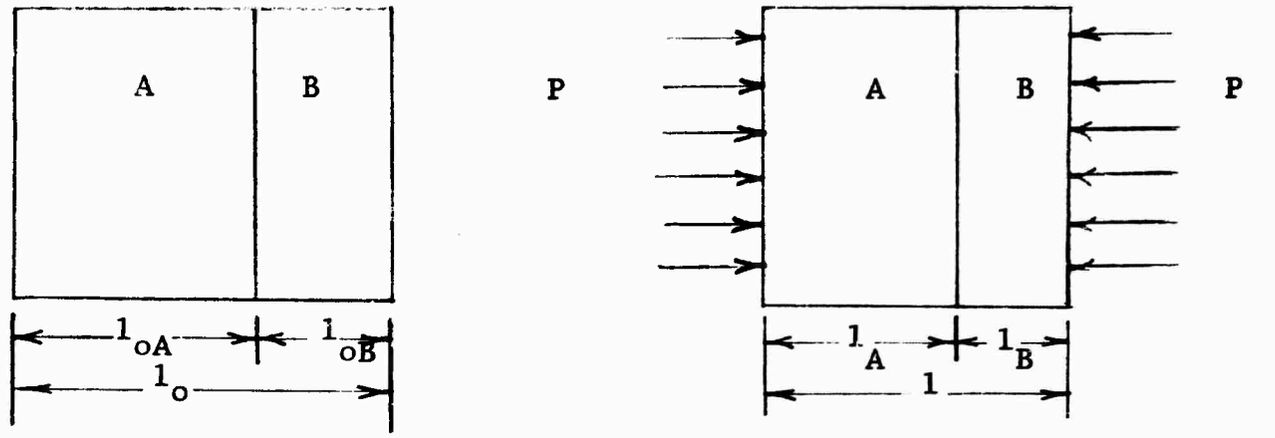

$\varepsilon_T = 0$

$\varepsilon_A = \varepsilon_B = \varepsilon_o$

$\varepsilon = \frac{1-l_o}{l_o}$

(a) P = 0

$\varepsilon_T = \frac{l_{oA}}{l_o}\varepsilon_A + \frac{l_{oB}}{l_o}\varepsilon_B$

$\varepsilon_A \neq 0 \quad \varepsilon_B \neq 0$

(b) $P \neq 0$

Figure B-1 Composite Sample in State of Zero Stress (a) and in State of Uniaxial Compression (b) Showing Relationship of Total Strain ε_T to ε_A and ε_B

$$\varepsilon_T = \sum_{i=A,B} \frac{V_{oi}}{V_o} \varepsilon_i$$

the total strain of the composite material, and V_{oi}/V_o is the initial volume ratio for the layered constituents. For the one-dimensional case considered here, the area perpendicular to the direction of the applied stress is constant so that the volume ratio may be replaced by the length ratio.

$$\varepsilon_T \text{ (one-dimensional)} = \sum_i \frac{l_{oi}}{l_o} \varepsilon_i$$

and $$\varepsilon_i \frac{V_{oi} - V_i}{V_{oi}} = \frac{l_{oi} - l_i}{l_{oi}}$$

Even for this relatively simple geometry, the case of shock loading is very much complicated by the multiple shock wave reflections. In Figure B-2(a) and (b) the shock-loading case is considered. Here it is assumed that a projectile is being used to impose the initial shock loading conditions on material A. The resulting loading conditions are transmitted by the shock and unloading waves as they reverberate through the sample. The wave and particle velocities are best described on a phase or t-x diagram. Such a diagram combined with a pressure particle velocity (P, U_p) plot depicting the possible loading (Hugoniot) and unloading states of materials A and B is shown in Figure B-2(a) and B-2(b), respectively. To facilitate the discussion and diagrams, the following simplifying assumptions have been made:

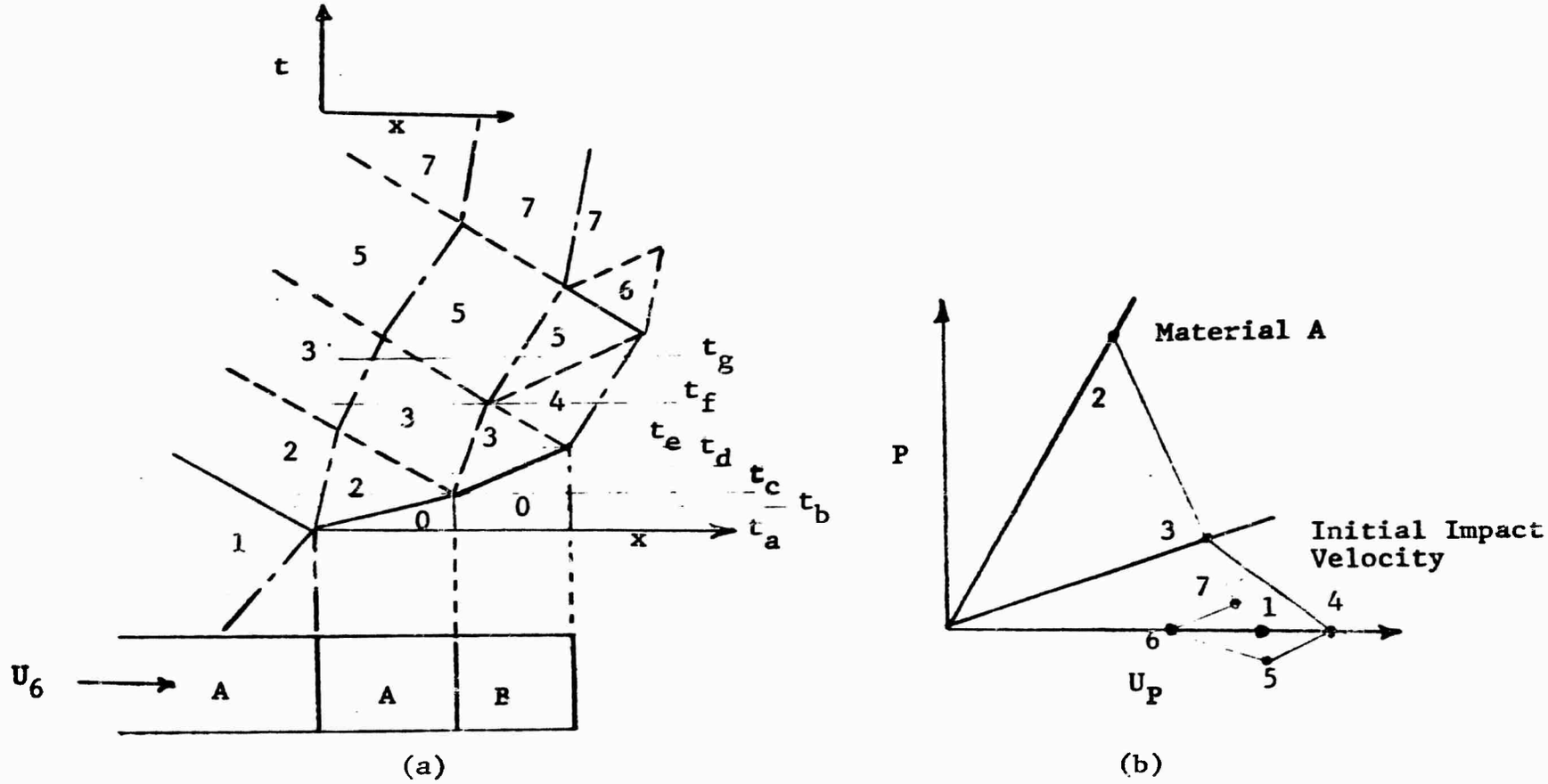

Figure B-2 t-x Diagram Showing Shock and Particle Motions (a) and the Associated Pressure-Particle Velocity (P-U_p) States (b)

(1) The projectile material is also material A.

(2) The (P,U_p) loading Hugoniot is a straight line, corresponding to the case where all loading is below the dynamic elastic limit.

(3) Unloading occurs along the reflected Hugoniot (i.e., Hugoniot reflected through a vertical line).

On the t-x diagram the lines represent velocities either particle (broken lines) or wave (solid for loading, dashed for unloading). Each time is represented by a horizontal line, so that the loading state can be seen at a particular time from the numbered regions. These states are shown schematically on the (P,U_p) diagram. In Figure B-3(a) to B-3(g), the pressure pulse is shown at the various times corresponding to the horizontal time intercepts of Figure B-2(a). As may be seen from Figure B-3, the pressure state is neither uniform in space nor constant in time. As in the static one-dimensional case, however, the volume is represented by the lengths; the corresponding values of l_{oA}, l_{oB}, l_o, l_A and l_B are shown on the diagram.

The first phase of the loading process is complete at the time t_e. At the time, t_e, the first shock loading wave completes its passage through the sample (i.e., arrives at the right edge of material B). At this time the pressure (state 3) is relieved at the free surface. This is represented in Figure B-2(a) by a release or unloading wave (leftward-sloping dashed line separating states 3 and 4). After t_e, the average stress (either compression or tension) decreases toward zero. As may be seen from Figure B-2(b),

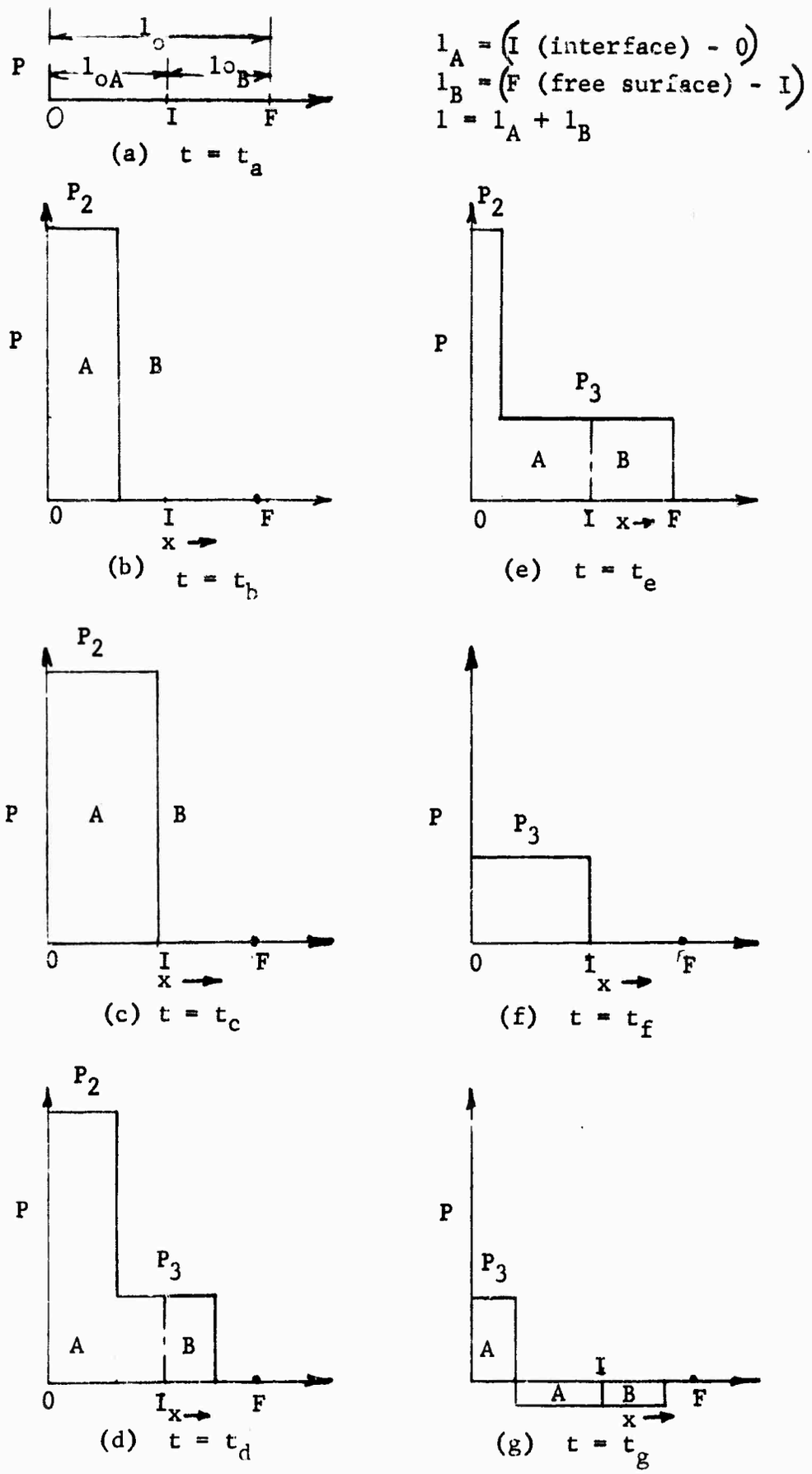

Figure B-3 Pressure Pulse in Material of Figure B-2(b) at Various Times Shown in Figure B-2(a)

and takes on many of the characteristics of a simple one component material. Although the final state in this case is a state of zero pressure (State 1, Figure B-2(b)), this is not necessarily the case but depends on the boundary conditions.

Temperature Differences

In most static determinations of the equations of state or pressure-volume states, the temperature is held constant. Since the temperature along the Hugoniot varies, it becomes another parameter which should be considered in Hugoniot synthesis. The quasistatic derivation of equation (B-1) neglected the temperature variation along the Hugoniot.

As seen in Section III, the temperatures of all the minerals at any given pressure are not the same. If, as was assumed in the synthesis, all constituents are at the same pressure, some thermal conductivity will occur. The resulting temperature change of any constituent subsequent to its initial loading may cause some thermal expansion or contraction. The variation in the thermal properties of the various constituents may cause an over-all change in the volume of the composite. These volume changes have been neglected but it is of interest to see how they might be considered. In addition it is of interest to consider the validity or meaning of the assignment of a composite temperature.

The Hugoniots of a three-component composite are considered in Figure B-4. An average temperature might be calculated simply by averaging the temperatures of the constituents suitably weighted, by their mass ratios, as represented by the dashed line. A slightly more physically meaningful calculation might involve

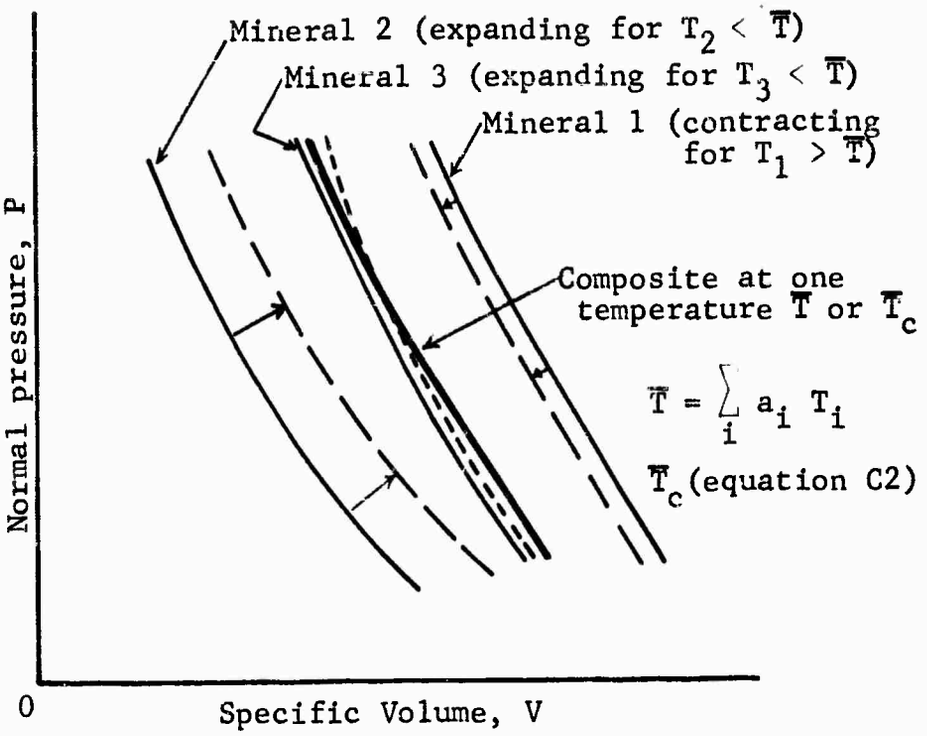

Figure B-4 Schematic Representation of Changes in Volume of Three Minerals in Intimate Contact but Shocked to Different Temperatures As Thermodynamic Equilibrium Is Approached

Solid curve for minerals are those immediately after shock loading; dashed curves represent a later time.

an energy balance between the internal energy increase of the composite and its constituents; thus

$$M\Delta E_c = \sum_i m_i \Delta E_i \qquad \text{(B-2)}$$

where ΔE_c and ΔE_i are the internal energy increases of the composite and i^{th} constituent respectively.

From equation (B-2), an effective or potential composite temperature might be defined by

$$\overline{T}_c \equiv \sum_i a_i \frac{c_i}{c_c} T_i + T_o\left(1 - \sum_i a_i \frac{c_i}{c_c}\right) \qquad \text{(B-3)}$$

where T_c is the effective composite temperature, c_i and c_c the specific heat at constant pressure for the i^{th} mineral and the composite, respectively, and T_o is the ambient temperature. To establish thermal equilibrium, the minerals having temperature $T_i > \overline{T}_c$ would tend to cool; those with $T_i < \overline{T}_c$ would tend to be heated. A corresponding change in the volumes could also be expected.

$$\Delta V_i = \alpha_i \Delta T_i \qquad \text{(B-4)}$$

where $$\Delta V_i = V_i' - V_i(H),$$

$V_i(H)$ is the initial shocked volume on the Hugoniot of the i^{th} mineral at the pressure P, V_i' is the thermally expanded or contracted volume, and α_i is the i^{th} thermal expansion coefficient. The situation is schematically represented in Figure B-4 where the various minerals' Hugoniots have been shifted through ΔV_i.

Such "corrections" have not been taken into account in the synthesis. Physically, such volume corrections represent an idealized situation where sufficient time is available for heat transfer to occur. Although no calculations have been made, it is unlikely that the thermal conductivities of the minerals are sufficiently high or the times involved sufficiently long to justify these calculations.

REFERENCES

1. M. H. Rice, R. G. McQueen, and J. M. Walsh, Solid State Physics Volume 6, p. 12, Academic Press Inc., New York, London (1958)

2. G. E. Duvall, Bulletin of Seismological Society of America 52, 869 (1962)

3. H. Napadensky, CRREL Research Report 119, March 1964

4. R. G. McQueen and S. P. Marsh, J. Appl. Phys. 31, 1253 (1960)

5. M. A. Cook and L. A. Rogers, J. Appl. Phys. 34, 2330 (1963)

6. V. G. Gregson, T. J. Ahrens, C. F. Peterson, Dynamic Properties of Rocks, AFCRL-63-662, Stanford Research Institute, Aug 1963

7. N. F. Mott and H. Jones, Theory of Metals, Dover(1936)

8. Geol Soc of Am Special Papers No. 36, Jan 1942 (P-58) Handbook of Physical Constants, Editor F. Birch

9. R. S. Dennen, Final Report IITRI A6040-1 (Sept 1963)

10. D. B. Lombard, U. of Calif. Lawrence Radiation Laboratory Report UCRL-6311

11. M. H. Rice, J. Chem. Phys. 26, 824 (1957)

12. R. C. Bass, H. L. Hawk, A. J. Chabai, Sandia Corp. SC-4903(RR), Jun 1963

13. F. S. Minshall, J. Appl. Phys. 26, 463 (1955)

14. G. R. Fowles, Poulter Labs Tech. Report 003-61, Stanford Research Institute

15. J. Wackerle, J. Appl. Phys. 33, 922 (1962)

16. J. M. Walsh, M. H. Rice, R. G. McQueen and F. L. Yarger, Phys. Rev. 108, 196 (1957)

17. M. H. Rice, R. G. McQueen, and J. M. Walsh, Solid State Physics Volume 6, p. 30, Academic Press Inc., New York, London (1958)

18. J. M. Walsh and R. H. Christian, Phys. Rev. 97, 1544 (1955)

Security Classification

DOCUMENT CONTROL DATA - R&D

(Security classification of title, body of abstract and indexing annotation must be entered when the overall report is classified)

1. ORIGINATING ACTIVITY (Corporate author) IIT Research Institute 10 West 35th Street Chicago, Illinois 60616	2a. REPORT SECURITY CLASSIFICATION U 2b GROUP ---

3. REPORT TITLE

SYNTHESIS OF ROCK HUGONIOTS

4. DESCRIPTIVE NOTES (Type of report and inclusive dates)

Final Report

5. AUTHOR(S) (Last name, first name, initial)

Dennen, Robert S.

6. REPORT DATE	7a. TOTAL NO. OF PAGES	7b. NO. OF REFS
October, 1965	140	31

8a. CONTRACT OR GRANT NO.	9a. ORIGINATOR'S REPORT NUMBER(S)
DA49-146-XZ-237	
b. PROJECT NO.	DASA 1652
c. 8100	9b. OTHER REPORT NO(S) (Any other numbers that may be assigned this report)
d.	T6056 FR

10. AVAILABILITY/LIMITATION NOTICES

Qualified requestors may obtain copies of this report from DDC.

11. SUPPLEMENTARY NOTES	12. SPONSORING MILITARY ACTIVITY
None	Advanced Research Projects Agency DEFENSE ATOMIC SUPPORT AGENCY Washington, D.C. 20301

13. ABSTRACT

Methods of obtaining the Hugoniot equation of state were investigated. Several of these, employing high explosive devices, were used to obtain Hugoniot data for mineral samples common to many igneous rocks. Hugoniot data were found for orthoclase, oligoclase, labradorite and olivine in the pressure range from 50 to 300 kilobars. Analytical synthesis models were constructed and used to determine the synthesized Hugoniot equations of state for granodiorite, gabbro and dunite. These compared favorably with existing Hugoniot data for similar materials. Methods were also developed and used to predict, roughly, Hugoniot curves for other geological composites for which no experimental data are presently available. These materials included syenite, quartzdiorite, diorite, olivine diabase, and diabase. Estimates of temperatures along the Hugoniots and along several selected unloading adiabats were calculated for several minerals and igneous rocks.

DD FORM 1 JAN 64 1473

Security Classification

SUPPLEMENTARY

INFORMATION

AD-474 687 IIT Research Inst., Chicago, Ill. Final rept. 30 Jun 63-31 Mar 65. Rept. no. DASA-1652 31 Mar 65 Contract DA-49-146-XZ-237	No Foreign without approval of Advanced Research Projects Agency, Defense Atomic Support Agency, Washington, D. C.	No limitation	ARPA memo, 19 May 69